1977

Cross field current instabilites in a vlasov plasma

Don S. Lemons
College of William & Mary - Arts & Sciences

INFORMATION TO USERS

This material was produced from a microfilm copy of the original document. While the most advanced technological means to photograph and reproduce this document have been used, the quality is heavily dependent upon the quality of the original submitted.

The following explanation of techniques is provided to help you understand markings or patterns which may appear on this reproduction.

1. The sign or "target" for pages apparently lacking from the document photographed is "Missing Page(s)". If it was possible to obtain the missing page(s) or section, they are spliced into the film along with adjacent pages. This may have necessitated cutting thru an image and duplicating adjacent pages to insure you complete continuity.

2. When an image on the film is obliterated with a large round black mark, it is an indication that the photographer suspected that the copy may have moved during exposure and thus cause a blurred image. You will find a good image of the page in the adjacent frame.

3. When a map, drawing or chart, etc., was part of the material being photographed the photographer followed a definite method in "sectioning" the material. It is customary to begin photoing at the upper left hand corner of a large sheet and to continue photoing from left to right in equal sections with a small overlap. If necessary, sectioning is continued again — beginning below the first row and continuing on until complete.

4. The majority of users indicate that the textual content is of greatest value, however, a somewhat higher quality reproduction could be made from "photographs" if essential to the understanding of the dissertation. Silver prints of "photographs" may be ordered at additional charge by writing the Order Department, giving the catalog number, title, author and specific pages you wish reproduced.

5. PLEASE NOTE: Some pages may have indistinct print. Filmed as received.

University Microfilms International
300 North Zeeb Road
Ann Arbor, Michigan 48106 USA
St. John's Road, Tyler's Green
High Wycombe, Bucks, England HP10 8HR

CROSS FIELD CURRENT INSTABILITIES IN A VLASOV PLASMA

A Thesis

Presented to

The Faculty of the Department of Physics

The College of William and Mary in Virginia

In Partial Fulfillment

Of the Requirements for the Degree of

Doctor of Philosophy

---

by

Don S. Lemons

August 1977

APPROVAL SHEET

This dissertation is submitted in partial fulfillment of

the requirements for the degree of

Doctor of Philosophy

Don S. Lemons
Author

Approved, August 1977

S. Peter Gary
S. Peter Gary

Hans von Baeyer
Hans von Baeyer

David Montgomery
David Montgomery

George Vahala
George Vahala

Frank Hohl
Frank Hohl
NASA

TABLE OF CONTENTS

ACKNOWLEDGMENTS

I wish to express my gratitude to the following people:

Peter Gary for his expert direction of this research problem and for the energy and generosity with which he encouraged me by word and example in the study of plasma physics;

J. J. Sanderson for his interest and the help he gave to this undertaking during his stay at the College of William and Mary;

George Vahala for his suggestions during the course of this research and for his reading of this dissertation;

Tom Cayton for his friendship and encouragement;

Paul Cisterino for his earnest friendship in graduate school one token of which was the many hours given to mutual conversations about science and philosophy;

The professors and students of the Department of Physics of the College of William and Mary whose knowledge and enthusiasm provided a good environment for studying physics;

Bill Feldman, Jeremiah Brackbill, and Jeffrey Freidberg of the Los Alamos Scientific Laboratory who made possible extended visits to the laboratory during which much of this work was done;

and Yvonne Johnson for helping with the preparation of the final manuscript of this dissertation.

LIST OF FIGURES

ABSTRACT

The linear stability of an infinite inhomogeneous Vlasov plasma containing a current flowing perpendicular to a straight magnetic field is investigated.

Time independent solutions to the Vlasov-Maxwell equations are constructed which model two physical situations: a shock in which density and magnetic field gradients point in the same direction and a sheath in which the magnetic field and density gradients point in opposite directions. These solutions are used as the zero order around which the equations are linearized. The linear equations imply a dispersion relation connecting the frequency, growth rate, and wavenumber of the first order perturbations. In the course of this derivation the local approximation was used, the ions were cosidered to be unmagnetized, while the effect of the magnetic field and ExB and gradient drifts were concentrated in the electrons. In contrast to previous work the full contribution of transverse fields is included in the dispersion relation and arbitrary direction of wave propagation in the plane formed by the direction of the magnetic field and the current is allowed. The dispersion relation is solved numerically for a variety of limiting cases as well as for the shock and and sheath configurations.

Solutions representing the lower hybrid drift and modified two stream instability were found and studied in detail.

It was demonstrated that transverse fields effect the dispersion properties of these instabilities only when the ratio $\beta_e/(ka_e)^2$ is greater than one where β_e is the electron beta and ka_e is the wave number normalized with the electron cyclotron radius. In this case wave growth rates are generally reduced and their direction of propagation is shifted away from the direction of the crossfield current. Also discovered was the fact that the shock configuration results in maximum growth rates for waves propagating at an angle of several degrees from the perpendicular to the magnetic field, while the sheath configuration has maximum growth rates for perpendicular propagation. The possible contribution of these and other dispersion properties of cross field drift instabilities to the earth's bow shock and other physical shocks and sheaths is discussed.

CROSS FIELD CURRENT INSTABILITIES IN A VLASOV PLASMA

I. INTRODUCTION

In recent years there has been much interest in the stability properties of a plasma in a spatially varying magnetic field. One reason for this interest is that the heating and confinement of thermonuclear plasmas with magnetic fields require the creation of sheaths containing inhomogenous plasmas and magnetic fields. Another reason is the increasing number of measurements made by satellites and space probes within the various inhomogenous plasma structures of our solar system. One widely studied example is that of the earth's bow shock, the region of interaction of the supersonic solar wind and the dipole magnetic field of the earth.

These and other similiar physical situations contain plasma and field configurations which are neither in thermodynamic equilibrium nor are able to relax to equilibrium by way of binary collisions because of the relatively large collision times and mean free paths involved. Typically the mean free path of charged particles in the earth's bow shock is many times greater than the shock width, and in many laboratory experiments and projected fusion reactors it exceeds the transverse dimensions of the apparatus. The behavior of such collisionless plasmas are dominated by collective oscillations which can be described by the collisionless Boltzman or Vlasov equation. These waves are important not only because nonlinear growth may disrupt a confined plasma but because they also contribute to wave turbulence

which takes the place of collisions in a classical plasma, scattering charged particles and determining its transport properties.

In a magnetized inhomogeneous plasma there are a number of waves which may be driven unstable by the current necessary to support a magnetic inhomogeneity. Among them are several waves with periods less than an ion cyclotron period and wave lengths less than an ion Larmor radius. These waves are studied in this dissertation by performing a normal mode analysis of the linearized Vlasov-Maxwell set of equations using a steady state configuration characteristic of a hot plasma in a magnetic field gradient. This analysis will reveal not only what configurations will be unstable but also the wave spectrum and growth rates of the unstable modes, and will constitute the main result of this dissertation.

A self consistent and more complete analysis of shocks and magnetic confinement sheaths requires including the effect of the unstable wave spectra upon the initial plasma configuration via anamolous transport coefficients due to wave particle interactions. For example, when studying resistive shocks the anamolous resistivity would be calculated and used in a macroscopic equation to determine shock widths, while for confinement sheaths the anamolous particle diffusion rate and hear flux are quantities of more interest. However, in this dissertation the construction of a self consistent picture of either a shock or sheath is not attempted. Rather, that piece of the picture encompassed by the linear theory of unstable waves is studied in detail.

The field and plasma steady state configuration used and their relationship to certain physical situations will be discussed below in

Chapter II, Steady State. Here it is described in qualitive terms sufficient for introducing the nature and delineating the boundaries of this work. The steady state fields consist of a unidirectional mangetic field with a small gradient in the magnitude perpendicular to it. Antiparallel to the magnetic gradient is a uniform electric field. These fields are used to calculate the orbits and constants of motion of a charged particle responding to them, which in turn allows the specification of the relevant electron and ion distribution functions, including electron drifts and density gradient. The steady state configuration can then be uniquely described with a few parameters. In this work there are five: m_e/m_i, the ratio of the electron and ion masses, ω_{pe}/Ω_e, the ratio of the electron plasma frequency to the electron cyclotron frequency, T_e/T_i, the ratio of elctron and ion temperatures, β_e, the ratio of the electron thermal to magnetic field pressures and any two of the drift speeds v_o, v_n, and $\langle v_B \rangle$ which are respectively the electron ExB drift, the density gradient drift, and the average magnetic field gradient drift.

Chapter III, The Dispersion Relation, presents the details of the normal mode analysis. The Vlasov-Maxwell set of equations is linearized by separating the fields and distributions into a zero-order, steady state part specified by the above five parameters and a first order fluctuating part whose quantities have a space-time dependence of $e^{i(\underline{k}\cdot\underline{x}-\omega t)}$ where $\underline{k}$ is the wave number vector and ω is the complex frequency, the imaginary part of which represents temporal wave growth or decay. The first order equations imply a dispersion relation which, in contrast to previous work, has been derived in a general form including all terms due to transverse fields and allowing

for wave propagation in the plane defined by the magnetic field and cross field drifts. Solution of this dispersion relation for an infinite plasma yields ω as a continuous function of $\underline{k}$ and the parameters describing the steady state. In the context of the present analysis the specification of the steady state or zero order parameters completely determines all the physics to be derived from the dispersion relation.

Several linear instabilities in this parameter space have already been identified and studied by others. The scope and physical relevance of these studies will outlined and related to the present work in Chapter IV, Review of Linear Instabilities. Because two of them, the modified two stream and the lower hybrid drift instabilities propagate at relatively long wavelengths they are sensitive to electromagnetic effects. Therefore these have been chosen for special study in this dissertation.

Chapter V, Numerical Methods, presents the dispersion relation prepared for computation and outlines the numerical methods used to solve it, while Chapter VI, Solutions, presents these solutions. Their relationship to both observed and derived parameters, including shock thickness, anomalous transport coefficients, and magnitude and polarization of fluctuating fields are discussed. Special attention is given to the effect of terms due to electromagnetic fields, density and magnetic field gradients and their alteration of the dispersion properties of crossfield drift instabilities known from less complete dispersion relations. A variety of values for steady state parameters are used including those appropriate to both stationary sheaths and

moving shocks. The latter case is emphasized since it has previously been less well studied than the former.

These results are summarized and discussed in the last chapter, Chapter VII, Summary and Conclusions.

II. STEADY STATE

The steady state field and plasma configuration is constructed with two examples of inhomogeneous plasma structures in mind, the earth's bow shock and the implosion and post implosion sheaths created in laboratory pinches.

For phenomenological purposes observations of the earth's bow shock have been categorized according to the values of the plasma beta, β, and the magnetosonic Mach number, M:

$$\beta = \frac{8\pi n_0 (T_e + T_i)}{B^2} \qquad M = \frac{V_{sw}}{\sqrt{C_A^2 + C_S^2}}$$

where V_{sw} is the solar wind speed perpendicular to the magnetic field direction, B the steady state magnetic field, and C_A and C_S are the Alfven and sound speeds, n the plasma density and T_e and T_i the electron and ion temperatures. These values show wide variations, but a 'typical' shock configuration of interest is the quasi perpendicular laminar shock characterized by low Mach numbers, $M \lesssim 3$, low beta, $\beta < 1$, and angles between the magnetic field and magnetic field gradient directions, θ_{nB}, of $50^\circ < \theta_{nB} < 88^\circ$ (Greenstadt,1975). In this case the bow shock appears as a simple monotonic magnetic profile possibly with some periodic downstream variations. Its width is the

same order of magnitude as the ion Larmor radius but appears to be primarily determined by dissipation due to turbulence created by cross field drift instabilities present in the shock (Morse and Greenstadt,1976). There is also an electric potential jump across the shock.

Many of the gross features of the earth's bow shock are reproduced in experimentally produced magnetic shocks and implosion sheaths. The shocks in magnetic pinches are nearly perpendicular by design, the contain potential barriers (Paul et. al.,1965), and their widths can also be determined by the properties of cross field drift instabilities (Manheimer and Boris,1972; Hamasaki and Krall,1974).

The main difference between the two situations is that laboratory shocks and stationary sheaths are used to compress and confine hot plasma, while the solar wind plasma is slowed down as it meets the bow shock but still passes through it. The plasma in a pinch is reflected from the magnetic gradient and builds up in front of it, during the implosion phase, then is confined by the magnetic gradient during the relatively stationary post implosion phase (e.g. Commisso and Griem,1977). In contrast, the density of the solar wind plasma increases with the magnetic field strength toward the downstream region of the bow shock and is consistent with changes in other plasma parameters as described by conservation laws (Morse and Greenstadt,1976; Sanderson,1977).

Actually the two configurations are not always distinguished from one another, especially in implosion sheaths where plasma is partially reflected by and partially passes through the magnetic gradient. However in referring to this distinction we will use the following

definitions. A shock is an inhomogeneous magnetic structure with plasma flowing through it and magnetic field and density gradients pointing in the same direction, while a sheath is one with no relative flow of plasma and fields, and magnetic field and density gradients pointing in opposite directions.

The field configuration and geometry used is that of the slab model of Krall and Liewer (1971), illustrated in Figure 1, which consists of crossed $\underline{B}$ and $\underline{E}$ fields pointing respectively in the positive z and negative x directions. The coordinate x corresponds to the radial coordinate in a cylindrical pinch while the B field in the z direction corresponds to either the azimuthal or axial magnetic field in respectively a Z or theta pinch. When applied to the earth's bow shock x corresponds to the coordinate along a line connecting the sun and earth. Within a shock there is an additional electric field in the positive y direction which causes the plasma to move in the positive x direction though the shock This field is not shown because it is assumed that it can be removed from consideration by transforming to an inertial frame which is moving with the plasma. In actual fact there is no inertial reference frame embedded in a plasma as it moves through a shock with a density gradient, since according to conservation requirements in one dimension the density and velocity of a fluid element, $n(x)$ and $v(x)$, must change so as to keep their product constant. Therefore one should keep in mind that the use of the above field configuration to describe a shock is possible only when the acceleration of the plasma in the x direction is ignored.

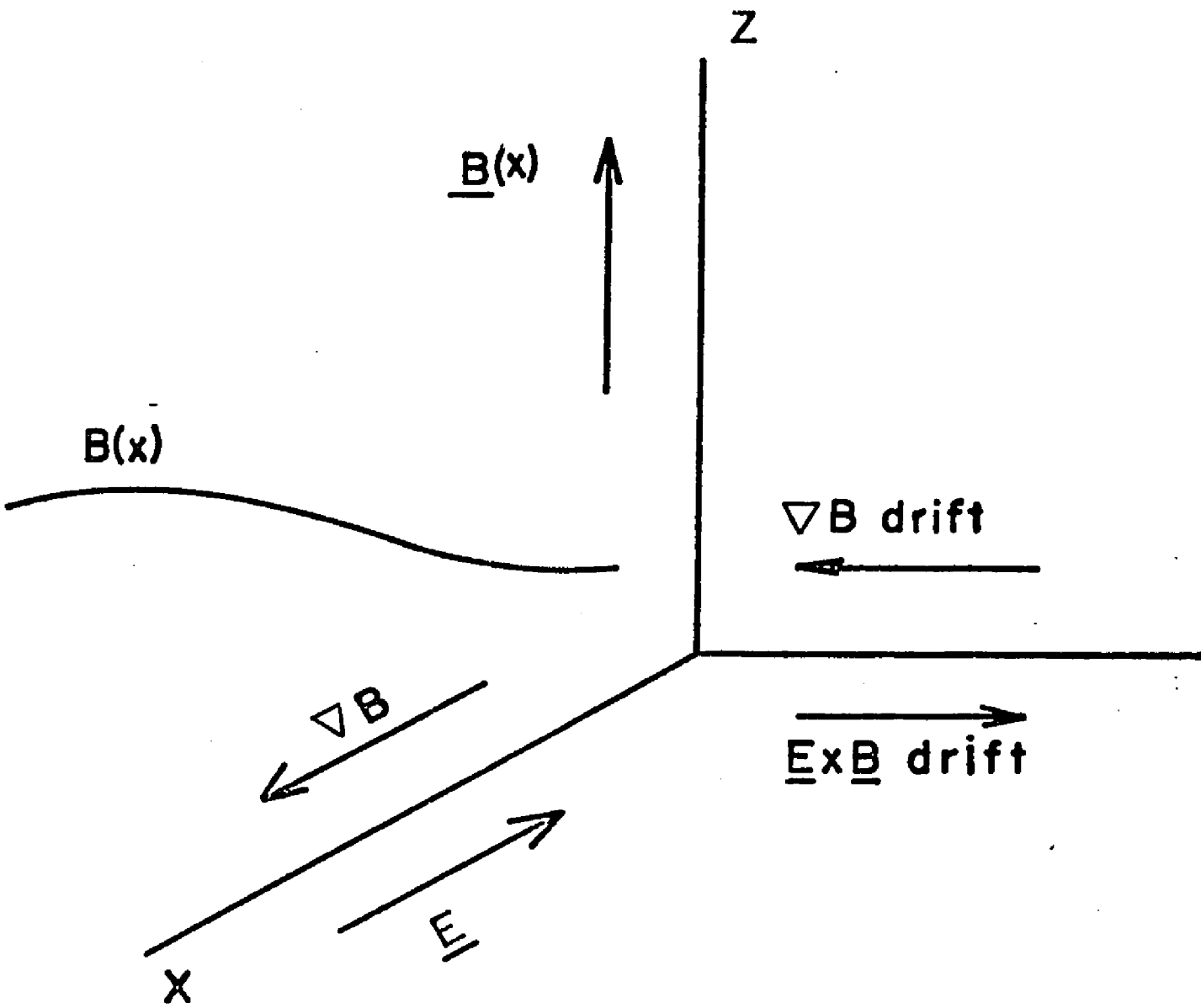

Fig. 1. Field configuration for slab geometry.

Drift wave theory seeks to represent all effects of field and plasma inhomogeneities with gradient and ExB drifts. This is done by employing the local approximation in deriving the dispersion relation (cf. Chapter 3) and using the following simple functional forms for the fields:

$$\underline{E} = -E_o \hat{x}$$

$$\underline{B} = B_o(1 + \varepsilon_B x)\hat{z} \qquad \text{(II-1)}$$

where ε_B, the inverse magnetic field gradient scale length, serves to introduce the gradient drifts. Any function of the constants of motion of a particle with charge q under the influence of these fields will be a solution of the Vlasov equation. Here we choose one based upon two constants which are easily integrable: the total energy, E, and the generalized momenta conjugate to coordinate, y, P_y. In terms of velocity space coordinates they are:

$$E = \frac{m}{2}\left(v_x^2 + v_y^2 + v_z^2\right) + qE_o x$$

$$P_y = m(x + v_y/\Omega)$$

Where $\Omega = qB/mc$. By combining P_y and E another useful constant is formed:

$$E - \Omega V_o P_y = \frac{m}{2}\left\{ V_x^2 + (V_y - V_o)^2 + V_z^2 \right\}$$

where $v_o = cE_o/B_o$.

Using these constants we construct an electron distribution function consisting of a drifting Maxwellian with a density gradient of scale length, ϵ_n:

$$f_o^e(x,\underline{v}) = n_o\left(\frac{m_e}{2\pi T_e}\right)^{3/2}\left[1 + \epsilon_n\left\{x - \frac{(V_y - V_o)}{\Omega_e}\right\}\right] x$$
$$\exp\left[-\frac{m_e}{2T_e}\left\{V_x^2 + (V_y - V_o)^2 + V_z^2\right\}\right] \qquad \text{(II-2)}$$

Here $\Omega_e = eB_o/m_e c$, $e = |q_e|$, and subsequent subscripts and superscripts "e" and "i" refer respectively to electron and ion. A temperature gradient may also be in included in $f_o^e(x,\underline{v})$ (Priest and Sanderson, 1972) but would complicate the resulting dispersion relation. Here it is left out; later its possible effects upon the results will be discussed.

The zeroth and first velocity moments of this distribution

function yield expressions for the electron density, n(x), and macroscopic electron velocity $\underline{v}_d$,

$$n(x) = n_o(1+\epsilon_n x)$$
$$\underline{V_d} = V_d\,\hat{y} = (V_o - V_n)\,\hat{y} \qquad \text{(II-3)}$$

where $v_n = \epsilon_n v_e^2/\Omega_e$ and v_e is the electron thermal velocity given by $v_e=(T_e/m_e)^{1/2}$. Equation II-3 has contributions from an $\underline{E}x\underline{B}$ drift,

$$c\,\frac{\underline{E}\times\underline{B}}{B^2} = \frac{cE_o}{B_o} = V_o\,\hat{y}$$

and an electron density gradient drift

$$\frac{T_e c}{n_o e}\,\frac{\underline{B}\times\nabla n}{B^2} = V_n\,\hat{y}$$

In deriving the expression for the constant $E-\Omega v_{o p_y}$ and the above distribution function we have implicitly assumed the quantities v_o/v_e and v_n/v_e are small by dropping terms which contain their products. Later it will be shown that Ampere's law linearly relates v_o, v_n, and

$\langle v_B \rangle$, the velocity averaged magnetic field gradient drift, requiring them to be the same order of magnitude Through first order in these quantities the distribution function of equation II-2 is a solution to the steady state Vlasov equation.

The functional form in equation II-2 could be used for both the electron and ion distribution functions. Then the relevant ion and electron parameters could be made consistent with the fields through Ampere's Law and Poisson's equation. Instead it is assumed that the ions can be represented with a Maxwellian distribution function

$$f_o^i(\underline{V}) = n_o\left(\frac{m_i}{2\pi T_i}\right)^{3/2} \exp\left[-\frac{m_i}{2T_i}\left\{V_x^2+V_y^2+V_z^2\right\}\right] \qquad \text{(II-4)}$$

This assumption is common in the theory of crossfield current instabilities and is usually based on the relatively large length and time scales of the ion cyclotron orbits. Here a further distinction should be made between a shock in which the ion spends only a fraction of its cyclotron period because of the supersonic speeds at which it is moving and a broad sheath with a width large compared to an ion Larmor radius. The ions can be only weakly influenced by the electric field and magnetic gradient associated with a shock. In the limit of no influence by the fields the ions may be represented by a simple Maxwellian. However within a broad sheath the ions may be expected to have a distribution similiar to that of the electrons. That is:

$$f_o^i(x,\underline{V}) = n_o\left(\frac{m_i}{2\pi T_i}\right)^{3/2}\left[1+\epsilon_n\left\{x+\frac{(V_y-V_0)}{\Omega_i}\right\}\right] \times \qquad \text{(II-5)}$$
$$\exp\left[-\frac{m_i}{2T_i}\left\{V_x^2+(V_y-V_0)^2+V_z^2\right\}\right]$$

Here the ion and electron density gradients are required to have an equal value of ε_n in order that the electric field of equation II-1 may satisfy Poisson's equation.

Krall and McBride (1977) have pointed out the fact that by using the local approximation, which ignores gradients but keeps gradient drifts by expanding the distribution function around the point x=0 and keeping only the first term in the expansion, and by disregarding terms involving products of the small quantities v_o/v_e and v_n/v_e distribution functions of the form used in equations II-2 and II-5 are equivalent to drifting Maxwellians of the form

$$f_o(\underline{v}) = n_o\left(\frac{m}{2\pi T}\right)^{3/2} \exp\left[-\frac{m}{2T}\left\{v_x^2 + (v_y - U_y)^2 + v_z^2\right\}\right]$$

where

$$U_y = v_o + \frac{\epsilon_n}{\Omega}\left(\frac{T}{m}\right)^{1/2} \qquad \text{(II-6)}$$

Therefore the use of a simple Maxwellian for the ion distribution implies that the ions are stationary in the frame of the fields of equation II-1, $U_{yi}=0$. This condition is known as 'electrostatic confinement of ions' and establishes a relationship between the ion ExB and density gradient drifts

When equations II-2 and II-4 are used as the electron and ion distribution functions the total drift velocity is related to the magnetic field gradient through Ampere's law

$$\nabla \times \underline{B} = \frac{4\pi \underline{J}}{c} = -\frac{4\pi n_o e V_d \hat{y}}{c}$$

which implies

$$\langle V_B \rangle = \frac{\beta_e}{2}(V_o - V_n) = \frac{\beta_e}{2} V_d \qquad \text{(II-8)}$$

Where $\langle v_B \rangle$ is defined as the velocity average of the microscopic electron ∇B drift, $\underline{v}_B$,

$$\underline{V_B} = -\frac{(V_x^2 + V_y^2)}{2\Omega_e} \frac{\underline{B} \times \nabla B}{B^2} = -\frac{(V_x^2 + V_y^2)\epsilon_B \hat{y}}{2\Omega_e}$$

$$\langle \underline{V_B} \rangle = -\langle V_B \rangle \hat{y} = -\frac{\epsilon_B V_c^2}{\Omega_e} \hat{y}$$

Equations II-2, II-4 and II-8 constitute the basic steady state configuration of this dissertation.

We also will make use of two additional conditions characterizing the physics of shocks and sheaths. In a perpenducular shock the magnetic field and density gradients increase by the same factor across the shock (Boyd and Sanderson,1969). When one assumes linear gradients in both B(x) and n(x) through the shock, this implies $\epsilon_n = \epsilon_B$. We refer to this as the "shock condition"; it may be written as

$$V_o = \langle V_B \rangle \qquad \text{(II-9)}$$

In contrast, the sheath of a stationary plasma confined by a strong magnetic field (e.g. the post implosion phase of a theta pinch) is characterized by magnetic field and density gradients pointing in opposite directions. When the expression for the ExB drift required by the electrostatic confinement of ions, eq. II-7, is substituted into Ampere's Law, eq. II-8, this condition is met. Consequently we call equation II-7 the "sheath condition". Equations II-7 and II-9 will be used as constraints on the basic steady state configuration.

The preceding construction of the steady state configuration proceeded from expressions for the steady state fields seen by the plasma within a magnetic inhomogeneity. Constants of the motion of a charged particle within these fields were found and used to construct reasonable distribution functions. Arguments were then made to motivate different treatments of ions and electrons. Finally the distribution functions were integrated to obtain expressions for macroscopic drifts and auxiliary conditions distinguishing shocks and sheaths were invoked.

An alternative approach to the derivation of the electron and ion drifts, equations II-3 and II-6 , and conditions characteristic of sheaths and shocks, equations II-7 and II-9, is presented in Appendix A. There the one fluid equations are presented, assumptions concerning the physics of supersonic shocks and stationary sheaths are made, and the relevant equations are derived. In this way the assumptions underlying the steady state configuration presented in this chapter are developed from another point of view.

III. THE DISPERSION RELATION

The dispersion relation for wave propagation in a steady state plasma described in the previous chapter can be derived by linearizing the Vlasov-Maxwell set of equations, and solving the linearized Vlasov equation by the method of "integration over unperturbed orbits". This procedure is well known and much used (Stix, Chapters 8 and 9,1962; Krall and Trivelpiece, Chapter 8,1973). Therefore only its major steps will outlined below.

In general the distribution functions, $f(\underline{x},\underline{v},t)$, and the electric and magnetic fields, $\underline{E}(\underline{x},t)$ and $\underline{B}(\underline{x},t)$, in a collisionless plasma are governed by The Vlasov and Maxwell equations.

$$\frac{\partial}{\partial t} f_\alpha + \underline{v} \cdot \frac{\partial}{\partial \underline{x}} f_\alpha + \frac{q_\alpha}{m_\alpha}\left(\underline{E} + \frac{\underline{v} \times \underline{B}}{c}\right) \cdot \frac{\partial}{\partial \underline{v}} f_\alpha$$

$$\frac{\partial}{\partial \underline{x}} \cdot \underline{E} = 4\pi\rho \qquad \frac{\partial}{\partial \underline{x}} \times \underline{E} = -\frac{1}{c}\frac{\partial \underline{B}}{\partial t}$$

$$\frac{\partial}{\partial \underline{x}} \times \underline{B} = \frac{4\pi \underline{J}}{c} + \frac{1}{c}\frac{\partial \underline{E}}{\partial t} \qquad \frac{\partial}{\partial \underline{x}} \cdot \underline{B} = 0$$

where $\underline{J}$ and , the current and charge density, are defined by

$$\underline{J} = \sum_\alpha n_\alpha q_\alpha \int d^3v f_\alpha \underline{v} \qquad \rho = \sum_\alpha n_\alpha q_\alpha \int d^3v f_\alpha$$

here d^3v denotes an integration over all of velocity space

$$\int_{-\infty}^{\infty}\int_{-\infty}^{\infty}\int_{-\infty}^{\infty} dv_x\, dv_y\, dv_z$$

and α the particle species of the distribution function.

The Vlasov equation is linearized by dividing $f(\underline{x},\underline{v},t)$, $\underline{E}(\underline{x},t)$, and $\underline{B}(\underline{x},t)$ into a zero order steady state part and a small first order fluctuating part

$$f(\underline{x},\underline{v},t) = f^{(0)}(\underline{x},\underline{v}) + f^{(1)}(\underline{x},\underline{v},t)$$

$$\underline{E}(\underline{x},t) = \underline{E}^{(0)}(\underline{x}) + \underline{E}^{(1)}(\underline{x},t)$$

$$\underline{B}(\underline{x},t) = \underline{B}^{(0)}(\underline{x}) + \underline{B}^{(1)}(\underline{x},t)$$

The steady state fields and distribution functions of equations II-1, II-2, and II-4 in Chapter II are used as zero order quantities.

The resulting zero order equations are, with the exception of Poisson's equation, satisfied. The violation of Poisson's equation is a consequence of using a homogeneous distribution to represent the ions. The first order equations are

$$\left(\frac{d}{dt}\right)_0 = \left(\frac{\partial}{\partial t} + \underline{v}\cdot\frac{\partial}{\partial \underline{x}} + \frac{q_\alpha}{m_\alpha}\left(\underline{E}^{(0)} + \frac{\underline{v}\times\underline{B}^{(0)}}{c}\right)\right) f_\alpha^{(1)} =$$

$$\frac{q_\alpha}{m_\alpha}\left(\underline{E}^{(1)} + \frac{\underline{v}\times\underline{B}^{(1)}}{c}\right)\cdot\frac{\partial}{\partial \underline{v}} f_\alpha^{(0)} \qquad \text{(III-1)}$$

$$\frac{\partial}{\partial \underline{x}}\cdot\underline{E}^{(1)} = 4\pi\rho^{(1)} \qquad \frac{\partial}{\partial \underline{x}}\times\underline{E}^{(1)} = -\frac{1}{c}\frac{\partial \underline{B}^{(1)}}{\partial t}$$

$$\frac{\partial}{\partial \underline{x}}\times\underline{B}^{(1)} = \frac{4\pi \underline{J}^{(1)}}{c} + \frac{1}{c}\frac{\partial \underline{E}^{(1)}}{\partial t} \qquad \frac{\partial}{\partial \underline{x}}\cdot\underline{B}^{(1)} = 0$$

Equation III-1, the first order Vlasov equation, has been expressed in terms of the time derivative of the distribution function $f^{(1)}$ as the particles move along their zero order orbits, $(d/dt)_0$, in order to motivate the method of "integration over unperturbed orbits".

Equation III-1 may then be formally solved by integrating it along a path in the six dimensional phase space $(\underline{x},\underline{v})$ defined by the orbit of a charged particle in the fields $\underline{E}^{(0)}$ and $\underline{B}^{(0)}$

$$f_\alpha^{(1)}(\underline{x},\underline{v},t) - f_\alpha^{(1)}(\underline{x}(-\infty),\underline{v}(-\infty),-\infty) =$$

$$-\frac{q_\alpha}{m_\alpha}\int_{-\infty}^{t} dt'\left\{\underline{E}^{(1)}(x',t') + \frac{\underline{v}'\times\underline{B}^{(1)}}{c}\right\}\cdot\frac{\partial f_\alpha^{(0)}}{\partial \underline{v}'}(\underline{x}',\underline{v}') \qquad \text{(III-2)}$$

where $\underline{x}'$ and $\underline{v}'$ are the zero order orbits defined by

$$\frac{d\underline{v}'}{dt'} = \frac{q}{m}\left(\underline{E}^{(0)} + \frac{\underline{v}'\times\underline{B}^{(0)}}{c}\right) \qquad \underline{v}' = \frac{d\underline{x}'}{dt'} \qquad \text{(III-3)}$$

with boundary conditions

$$\underline{X}'(t'=t)=\underline{X} \qquad \underline{V}'(t'=t)=\underline{V} \tag{III-4}$$

Whenever the wavelength of interest associated with the first order fluctuating fields and distributions is much shorter than the scale length of the magnetic field and density gradients it has been suggested that the local approximation may be used in solving equations such as III-2 (Krall, 1968). In this approximation the x dependence of the steady state distribution function is ignored so that

$$f^{(0)}(\underline{x},\underline{v}) \longrightarrow f^{(0)}(\underline{v})$$

Then a local wave space-time dependence of the first order fluctuating fields and distributions may be used

$$\underline{E}^{(1)}(\underline{x},t)=\underline{E}^{(1)}(\underline{K},\omega)\,e^{i(\underline{K}\cdot\underline{x}-\omega t)}$$

$$\underline{B}^{(1)}(x,t)=\underline{B}^{(1)}(\underline{K},\omega)\,e^{i(\underline{K}\cdot\underline{x}-\omega t)} \tag{III-5}$$

$$f_a^{(1)}(\underline{x},\underline{v},t)=f_\alpha^{(1)}(\underline{K},\underline{v},\omega)\,e^{i(\underline{K}\cdot\underline{x}-\omega t)}$$

with

$$\underline{K} = K_z \hat{z} + K_y \hat{y}$$

The only remnant of gradient effects in the local approximation is contained in the gradient drifts.

Although the local approximation in the general form stated above has not been rigorously justified, it has been shown to be valid in certain cases for electrostatic dispersion relations based upon distribution functions of wnich II-2 and II-4 are special cases (Davidson,1976). In this work a nonlocal linear dispersion relation for electrostatic waves in an inhomogeneous magnetized plasma with cylindrical geometry was derived and solved. It was found that when $(\omega_{pe}/\Omega_e)^2 >> 1$ the nonlocal dispersion relation for the lower hybrid drfit instability reduced to the local dispersion relation except for the fact that values of the wave number, k_y, were limited to integral values of the inverse radius of the plasma column. Since $(\omega_{pe}/\Omega_e)^2$ is satisfied throughout this work except in one parameter study (Figure 16), the local approximation is employed with some although not complete justification without further comment.

When $\mathrm{Im}\omega > 0$, $f^{(1)}(x'(-\infty),v'(-\infty),-\infty) = 0$ is implied and equation III-2 becomes

$$f_\alpha^{(1)}(\underline{K},\underline{V},\omega) = -\frac{q}{m}\int_{-\infty}^{0} d\tau\; e^{i\underline{K}\cdot(\underline{x}'-\underline{x})-i\omega\tau} \times \left\{\underline{E}^{(1)}(\underline{K},\omega) + \frac{\underline{v}'\times\underline{B}^{(1)}(\underline{K},\omega)}{c}\right\} \cdot \frac{\partial f_\alpha^{(0)}(\underline{V}')}{\partial \underline{V}'} \qquad \text{(III-6)}$$

where $\tau = t'-t$. The restriction on $\mathrm{Im}\,\omega$ corresponding to allowing only wave growth may now be relaxed by analytically continuing $f^{(1)}(\underline{k},\underline{v},t)$ into regions of $\underline{k},\omega$ space where $\mathrm{Im}\,\omega < 0$. Equations III-5 are also used to reduce the first order Maxwell equations to

$$i\underline{K}\cdot\underline{E}^{(1)} = 4\pi\rho^{(1)} \tag{III-7}$$

$$K \times E^{(1)} = \frac{\omega}{c}\underline{B}^{(1)} \tag{III-8}$$

$$i\underline{K}\times\underline{B}^{(1)} = \frac{4\pi J^{(1)}}{c} - i\frac{\omega \underline{E}^{(1)}}{c} \tag{III-9}$$

$$\underline{K}\cdot\underline{B}^{(1)} = 0 \tag{III-10}$$

Here and in the rest of this chapter the arguments $\underline{k}$ and ω are suppressed in the field amplitudes $\underline{E}^{(1)}(\underline{k},\omega)$ and $\underline{B}^{(1)}(\underline{k},\omega)$.

Equation III-8 is now used to eliminate $\underline{B}^{(1)}$ from equation III-6 and equation III-9

$$f_\alpha^{(1)}(\underline{k},\underline{v},\omega) = \int_{-\infty}^{0} d\tau\, e^{i(\underline{k}\cdot\underline{x}-\omega\tau)-i(\underline{k}\cdot\underline{x}')} \times \left\{\underline{E}^{(1)} + \frac{\underline{v}\times(\underline{k}\times\underline{E}^{(1)})}{\omega}\right\}\cdot\frac{\partial f_\alpha^{(0)}(\underline{v}')}{\partial \underline{v}'} \tag{III-11}$$

$$\frac{ic}{\omega}\underline{k}\times(\underline{k}\times\underline{E}^{(1)}) = \frac{4\pi J^{(1)}}{c} - i\frac{\omega \underline{E}^{(1)}}{c} \tag{III-12}$$

When $\underline{E}^{(1)}$ is expressed in the Cartesian coordinate system used in Chapter II

$$\underline{E}^{(1)} = E_x^{(1)}\hat{x} + E_y^{(1)}\hat{y} + E_z^{(1)}\hat{z}$$

equations III-3, III-11, and III-12 form three coupled equations which are linear and homogeneous in the coordinates of $\underline{E}^{(1)}$. These equations imply a dispersion relation for a wave of frequency ω and wavevector $\underline{k}$ propagating in a plasma described by the steady state distribution functions II-2 and II-4 and the orbits determined by equation III-3.

This dispersion relation may be conveniently represented in terms of a mobility matrix, $M_{i,j}$, for species α defined as

$$J_i^{(1)} = \sum_\alpha \int d^3v\, q_\alpha v_i f_\alpha^{(1)} = \sum_\alpha \frac{q_\alpha}{\Omega_\alpha m_\alpha} M_{ij}^\alpha E_j^{(1)} \qquad \text{(III-13)}$$

When this expression is used in equation III-12, the result with appropriate normalization is the vector equation

$$\sum_j R_{ij} E_j^{(1)} = 0 \qquad \text{(III-14)}$$

where the 3x3 matrix, R_{ij}, is defined by

$$R_{ij} = \frac{K_i K_j}{K^2} + \delta_{ij}\left\{\left(\frac{\omega}{CK}\right)^2 - 1\right\} + i\left(\frac{\omega}{CK}\right)^2 \sum_\alpha \frac{\omega_{p\alpha}^2}{\Omega_\alpha} M_{ij}^\alpha \qquad \text{(III-15)}$$

where subscripts i and j stand for one of the three Cartesian coordinates x,y,and z and $\omega_{p\alpha}^2 = 4\pi n_o e^3/m_\alpha$. The vanishing of the determinate of R_{ij} is the necessary condition for nontrivial solutions of equation III-14 and formally constitutes the dispersion relation to be solved.

When the unperturbed orbits for charged particles used in the solution of $f^1(\underline{k},\underline{v},\omega)$ and determined by equations III-3 are specified, all information needed to explicitly calculate the above dispersion relation will be known. These orbits have been chosen to be consistent with the constants of motion used to construct the electron and ion distribution functions of Chapter II, equations II-2 and II-4. Therefore the ion orbits are the straight line orbits of a particle which makes no response to the steady state fields, while the electron orbits undergo both cyclotron motion due to the steady state magnetic field $B_0\,\hat{e}_z$ and ∇B and $\underline{E}x\underline{B}$ drift motion.

Magnetic effects on a plasma component are known in this theory not only through a possible distortion of the steady state distribution functions but also through the form of the individual particle orbits. In section II it has been argued that ion magnetic effects in the shock configuration are negligible because of the relatively short time an ion stays in the shock. This argument does not apply to a stationary sheath. Consequently not only must the effect of a non-Maxwellian ion distribution be considered but also the effect of ion cyclotron orbits and drift velocities through the orbit integration of equation III-11.

Generally ion magnetic contributions to the ion orbit equations are considered to have negligible effects on the dispersion properties of waves of frequencies much greater than the ion cyclotron frequency and wavelengths much shorter than the ion Larmor radius. More specific criteria for neglecting ion cyclotron effects have been based on an analysis of the electrostatic dispersion relation for waves in a homogeneous plasma (Gary,1970; Detyna and Wooding,1975). These authors have shown that ion gyro effects are (1) confined to a cone in wave

vector space around the direction of the crossfield drifts defined by an angle

$$\cos\theta < \left(\frac{m_e}{m_i}\right)^{1/2}$$

and (2) are significant only for weakly unstable waves with growth rates such that

$$\gamma \lesssim \Omega_i$$

Since the latter condition is not satisfied by the crossfield drift instabilities considered in this dissertation ion gyro effects will not be important. Consequently when the boundary conditions of equation III-4 are used the ion orbit equations are

$$\begin{aligned} X'(\tau) &= X + V_x\tau \\ y'(\tau) &= y + V_y\tau \\ z'(\tau) &= z + V_z\tau \\ V_x, V_y, V_z &= \text{constants} \end{aligned} \qquad \text{(III-16)}$$

The electrons respond to the steady state fields of equation II-1. However when the normalized $\underline{E}\times\underline{B}$ and ∇B drift velocities, respectively, v_o/v_e and $\langle v_B\rangle/v_e$, are treated as small quantities as they were in

Chapter II, an orbit equation which retains only the first order effect of these small quantities may be constructed. This is accomplished by solving zero order equations of motion in which electron drifts are ignored, then substituting the result into the complete equation of motion and solving again (Krall and Trivelpiece, Sec. 8.15,1973). When this is done the resulting electron orbit equations are

$$V_x'(T) = V_\perp \cos(\phi+\Omega_e' T) + \frac{\epsilon_B V_\perp^2}{2\Omega_e}\{\sin 2(\phi+\Omega_e T) - \sin(2\phi+\Omega_e T) - \sin\Omega_e T\} \qquad \text{(III-17)}$$

$$V_y'(T) = V_\perp \sin(\phi+\Omega_e' T) + \frac{\epsilon_B V_\perp^2}{2\Omega_e}\{\cos(2\phi+\Omega_e T) + \cos\Omega_e T - \cos 2(\phi+\Omega_e T) - 1\} + V_0$$

$$V_z' = V_z$$

$$X'(T) = X - \frac{V_\perp}{\Omega_e'}\{\sin\phi - \sin(\phi+\Omega_e' T\} + \frac{\epsilon_B V_\perp^2}{4\Omega_e}\{2\cos(2\phi+\Omega_e T) - \cos 2(\phi+\Omega_e T) - \cos 2\phi + 2\cos\Omega_e T - 2\}$$

$$Y'(T) = Y - \frac{V_\perp}{\Omega_e}\{\cos(\phi+\Omega_e' T) - \cos\phi\} + \Omega_e T\left\{\frac{V_0}{\Omega_e} - \frac{\epsilon_B V_\perp^2}{2\Omega_e}\right\} + \frac{\epsilon_B V_\perp^2}{4\Omega_e}\{2\sin(2\phi+\Omega_e T) - \sin 2(\phi+\Omega_e T) - \sin 2\phi + 2\sin\Omega_e T\}$$

$$Z'(T) = Z + V_z T$$

where

$$V_y - V_o = V_\perp \sin\phi$$

$$V_x = V_\perp \cos\phi$$

and

$$\Omega_e' = \Omega_e\left(1 + \epsilon_B X - \frac{\epsilon_B V_\perp}{\Omega_e}\sin\phi\right)$$

When all terms in the equations for $\underline{v}'(\tau)$ which are products of trigonometric functions and terms porportional to ϵ_B are dropped, equations III-17 become

$$V_x'(\tau) = V_\perp \cos(\phi + \Omega_e\tau)$$

$$V_y'(\tau) = V_\perp \sin(\phi + \Omega_e\tau) + V_o - \frac{\epsilon_B V_\perp^2}{2\Omega_e}$$

$$V_z'(\tau) = V_z$$

and

$$X'(\tau) = X - \frac{V_\perp}{\Omega_e}\left\{\sin\phi - \sin(\phi+\Omega_e\tau)\right\} \qquad \text{(III-18)}$$

$$y'(\tau) = y - \frac{V_\perp}{\Omega_e}\left\{\cos\phi - \cos(\phi+\Omega_e\tau)\right\} + \tau\left(V_o - \frac{\epsilon_B V_\perp^2}{2\Omega_e}\right)$$

$$z'(\tau) = z + V_z\tau$$

The contribution of the omitted terms to the dispersion relation is discussed in Appendix B.

If equations III-16 and III-18 are employed for the electron and ion orbit equations $f_{e,i}(\underline{k},\underline{v},t)$, M_{ij}, and R_{ij} may be expressed in terms of standard functions and expansions(see Stix,1962; Krall and Trivelpiece,1973). Then the time integration of equation III-6 results in

$$f_i^{(1)}(\underline{K},\underline{V},\omega) = \frac{e}{T_i}\,\frac{\underline{E}^{(1)}\cdot\underline{V}}{i(\omega - K_y V_o)}\,f_i^{(o)} \qquad \text{(III-19)}$$

$$f_e^{(1)}(\underline{K},\underline{V},\omega) = \frac{-ie}{\omega T_e}\,f_e^{(o)}\left[\omega - K_y V_o + \epsilon_n\left(\frac{K_y V_e^2}{\Omega_e} - \frac{\omega V_\perp \sin\phi}{\Omega_e}\right)\right]\times$$

$$\sum_{m,n=-\infty}^{\infty}\frac{J_m\, e^{i(\phi+\pi/2)(m-n)}}{\left\{\omega - K_z V_z + n\Omega_e - K_y\left(V_o - \frac{\epsilon_B V_e^2}{2\Omega_e}\right)\right\}}\times \qquad \text{(III-20)}$$

$$\left[E_z V_z J_n + E_y\left(V_o - \frac{\epsilon_B V_\perp^2}{2\Omega_e} - \frac{n\Omega_e}{K_y}\right)J_n + i V_\perp E_x J_n'\right]$$

where J_n and J_m are spherical Bessel functions of the first kind, with arguments $k_y v_\perp / \Omega_e$, integer order, and defined by their generating function as

$$e^{i\lambda \sin\theta} = \sum_{n=-\infty}^{\infty} J_n(\lambda) e^{in\theta}$$

Integrations of $f_e^{(1)}$ and $f_i^{(1)}$ over all of velocity space are now required in calculating elements of the matrix R_{ij}. These integrations are done with the cylindrical velocity space coordinates ϕ, $v_\perp$, and v_z defined above. Integrations over the ϕ coordinate and $v_\perp$ coordinate in the ion integral are performed analytically while integrations over v_z lead to the Fried-Conte function $Z(\zeta)$ (Fried and Conte,1961)

$$Z(\zeta) = \frac{1}{2\pi} \int_{-\infty}^{\infty} dz \; \frac{e^{-z^2}}{z-\zeta}$$

where the above is a contour integration with the integration contour defined so as to go beneath the pole at $z = \zeta$ in the complex z plane. The $v_\perp$ integrations in the electron integrals are done numerically.

Upon performing these integrations and using the definitions of equations III-13 and III-15 the following expressions are derived

$$R_{xx} = \left(\frac{\omega}{ck}\right)^2 - 1 + \left(\frac{\omega_{pi}}{ck}\right)^2 \zeta_i Z(\zeta_i) \qquad \text{(III-21)}$$

$$+ \left(\frac{\omega_{pe}}{ck}\right)^2 \frac{\Lambda}{\sqrt{2}\, k_z v_e^5} \int\!\!\int \sum_{n=-\infty}^{\infty} v_\perp^2 J_n'^2 Z(\zeta_n^e)$$

$$R_{yy} = \left(\frac{\omega}{ck}\right)^2 - \left(\frac{k_z}{k}\right)^2 + \zeta_i\left[\left(\frac{k_z}{k}\right)^2 Z(\zeta_i) - \zeta_i\left(\frac{k_y}{k}\right)^2 Z'(\zeta_i)\right]\left(\frac{\omega_{pi}}{ck}\right)^2$$
$$+\left(\frac{\omega_{pe}}{ck}\right)^2 \frac{\omega}{\Omega_e}\frac{(\epsilon_B - \epsilon_n)}{k_y} + \left(\frac{\omega_{pe}}{ck}\right)^2 \left(\frac{v_0 - \epsilon_B v_e^2/\Omega_e}{v_e}\right)\left(\frac{v_0 - \epsilon_B v_e^2/\Omega_e}{v_e}\right)$$
$$+\left(\frac{\omega_{pe}}{ck}\right)^2 \frac{\Lambda}{\sqrt{2}\,k_z v_e^5} \coprod \sum_{n=-\infty}^{\infty} J_n^2 Z(\zeta_n^e)\left(v_0 - \frac{\epsilon_B v_\perp^2}{2\Omega_e} - \frac{n\Omega_e}{k_y}\right)^2$$

$$R_{zz} = \left(\frac{\omega}{ck}\right)^2 - \left(\frac{k_y}{k}\right)^2 + \left(\frac{\omega_{pi}}{ck}\right)^2 \zeta_i\left[\left(\frac{k_y}{k}\right)^2 Z(\zeta_i) - \zeta_i\left(\frac{k_z}{k}\right)^2 Z'(\zeta_i)\right]$$
$$-\left(\frac{\omega_{pe}}{ck}\right)^2 \frac{\Lambda}{\sqrt{2}\,k_z v_e^3} \coprod \sum_{n=-\infty}^{\infty} J_n^2\, \zeta_n^e\, Z'(\zeta_n^e)$$

$$R_{xy} = -R_{yx} = -i\left(\frac{\omega_{pe}}{ck}\right)^2 \frac{\Lambda}{\sqrt{2}\,k_z v_e^5} \coprod \sum_{n=-\infty}^{\infty} v_\perp J_n J_n' \times$$
$$\left(v_0 - \frac{\epsilon_B v_\perp^2}{2\Omega_e} - \frac{n\Omega_e}{k_y}\right) Z(\zeta_n^e)$$

$$R_{xz} = -R_{zx} = i\left(\frac{\omega_{pe}}{ck}\right)^2 \frac{\Lambda}{\sqrt{2}\,k_z v_e^4} \coprod \sum_{n=-\infty}^{\infty} v_\perp J_n J_n' Z'(\zeta_n^e)$$

$$R_{yz} = R_{zy} = \frac{k_y k_z}{k^2} + \left(\frac{\omega_{pi}}{ck}\right)^2 \frac{k_y k_z}{2k^2}\, \zeta_i\, Z''(\zeta_i)$$
$$-\left(\frac{\omega_{pe}}{ck}\right)^2 \frac{\Lambda}{2k_z v_e^4} \coprod \sum_{n=-\infty}^{\infty} J_n^2 Z'(\zeta_n^e)\left(v_0 - \frac{\epsilon_B v_\perp^2}{2\Omega_e} - \frac{n\Omega_e}{k_y}\right)^2$$

where

$$\Lambda = \omega - k_y V_0 + \frac{\epsilon_n k_y V_e^2}{\Omega_e}$$

$$\zeta_n^e = \frac{\omega + n\Omega_e - k_y\left(V_0 - \frac{\epsilon_0 V_\perp^2}{2\Omega_e}\right)}{\sqrt{2}\, k_z V_e}$$

$$\zeta^i = \frac{\omega}{\sqrt{2}\, k V_i}$$

and $\mathbb{I}$ represents the operator defined by

$$\mathbb{I}\, A(V_\perp) = \int_0^\infty dV_\perp\, V_\perp\, e^{-\frac{m_e V_\perp^2}{2T_e}}\, A(V_\perp)$$

The corresponding dispersion relation is

$$R_{xx}\left(R_{yy}R_{zz} - R_{yz}^2\right) + R_{xy}\left(R_{xy}R_{zz} - R_{xy}R_{yz}\right) + R_{xz}\left(R_{yx}R_{yz} - R_{xz}R_{yy}\right) = 0 \qquad \text{(III-22)}$$

Within the context of local linear dispersion relations for waves in a weakly inhomogeneous plasma of magnetized electrons and unmagnetized ions this dispersion relation is quite general. It includes wave propogation with arbitrary wave vectors, k_z and k_y,

arbitrary polarizations of the transverse fields, and effects due to density and magnetic field gradients. Therefore the dispersion relation is complicated. It does however reduce to dispersion relations which have been derived and solved in less general limits.

The electrostatic dispersion relation may be recovered from the above dispersion relation by letting the parameter $(\omega_{pe}/ck)^2$ or equivalently $\beta_e/(ka_e)^2$ vanish. Callen and Guest (1973) have shown that this is most easily done by transforming the electric field and matrix $R_{i,j}$ of equation III-15 to a Cartesian coordinate system with one coordinate parallel to the direction of wave propagation and two coordinates perpendicular to it. When this is done it is found that the diagonal element of $R_{i,j}$ which multiplies the longitudinal electric field, $\underline{k}\cdot\underline{E}^{(1)}/\underline{k}$, is

$$R_{yy}K_y^2 + R_{zz}K_z^2 + 2R_{yz}K_yK_z \qquad \text{(III-23)}$$

The vanishing of this factor results in an electrostatic dispersion relation which when $\varepsilon_n = 0$ is identical to the electrostatic dispersion relation of Gary and Sanderson (1970). This transformation allows the general dispersion relation to be expressed as the sum of the above factor from the electrostatic dispersion relation and terms which represent the effect of transverse fields. The coupling between the two is proportional to $\beta_e/(ka_e)^2$.

Recently a dispersion relation which includes partial electromagnetic effects and propogation perpendicular to $\underline{B}^{(o)}$ ($k_z = 0$) has been used to study crossfield drift instabilities (Davidson et.

al.,1976). That dispersion relation is included in equation III-22 and may be derived from it when the following approximations are made: (1) Only contributions of transverse fields with extraordinary mode polarization are allowed. That is $E^{(1)}_z = 0$ in equation III-13. (2) The ion contribution to R_{xx}, R_{xy}, R_{yx}, R_{xz}, and R_{zx} are dropped. (3) All terms containing Bessel functions of non zero order are dropped. (4) The leading term in R_{xx}, $(\omega/ck)^2$, is dropped.

Finally a dispersion relation for waves with full electromagnetic effects in a homogeneous plasma is recovered from equation III-22 in the limit of no gradients, ϵ_n and $\epsilon_B = 0$. In this limit the integrations over the $v_\perp$ variable may be done and transform the Bessel functions into modified Bessel functions, I_n, with arguments of $(k_y a_e)^2$. The result is

$$R_{xx} = \left(\frac{\omega}{ck}\right)^2 - 1 + \left(\frac{\omega_{pi}}{ck}\right)^2 \zeta_i Z(\zeta_i) \qquad \text{(III-24)}$$
$$+ \left(\frac{\omega_{pe}}{ck}\right)^2 \zeta_0^e e^{-\lambda} \sum_{n=-\infty}^{\infty} Z(\zeta_n^i)\left[\frac{n^2}{\lambda} I_n + 2\lambda(I_n - I_n')\right]$$

$$R_{yy} = \left(\frac{\omega}{ck}\right)^2 - \left(\frac{k_z}{k}\right)^2 + \left(\frac{\omega_{pi}}{ck}\right)^2 \zeta_i \left[\left(\frac{k_z}{k}\right)^2 Z(\zeta_i) + \zeta_i \left(\frac{k_y}{k}\right)^2 Z'(\zeta_i)\right]$$
$$+ \frac{\omega_{pe}^2}{(ck)^2} e^{-\lambda} \sum_{n=-\infty}^{\infty} \frac{I_n(n\Omega_e - k_y v_0)}{k_y^2 v_e^2} \times$$
$$\left[(n\Omega_e - k_y v_0)\zeta_0^e Z(\zeta_n^e) - v_0 k_y\right]$$

$$R_{zz} = \left(\frac{\omega}{ck}\right)^2 - \left(\frac{k_y}{k}\right)^2 + \left(\frac{\omega_{pi}}{ck}\right)^2 \varrho_i \left[\left|\frac{k_y}{k}\right|^2 Z(\varrho_i) - \varrho_i \left(\frac{k_z}{k}\right)^2 Z'(\varrho_i)\right]$$

$$- \left(\frac{\omega_{pe}}{ck}\right)^2 \varrho_0^e e^{-\lambda} \sum_{n=-\infty}^{\infty} \varrho_n^e Z(\varrho_n^e)\, I_n$$

$$R_{xy} = -R_{yx} = -i \left(\frac{\omega_{pe}}{ck}\right)^2 \varrho_0^e e^{-\lambda} \sum_{n=-\infty}^{\infty} \frac{(n\Omega_e - V_0 k_y)}{\Omega_e} Z(\varrho_n^e)(I_n - I_n')$$

$$R_{xz} = -R_{zx} = -i \left(\frac{\omega_{pe}}{ck}\right)^2 \frac{\varrho_0^e k_y V_e}{\sqrt{2}\,\Omega_e} e^{-\lambda} \sum_{n=-\infty}^{\infty} Z'(\varrho_n^e)(I_n - I_n')$$

$$R_{yz} = R_{zy} = \frac{k_y k_z}{k^2} + \left(\frac{\omega_{pi}}{ck}\right)^2 \frac{k_y k_z}{2k^2} \varrho_i Z''(\varrho_i)$$

$$+ \left(\frac{\omega_{pe}}{ck}\right)^2 \varrho_0^e e^{-\lambda} \sum_{n=-\infty}^{\infty} \frac{(n\Omega_e - k_y V_0)}{\sqrt{2}\, k_y V_e} Z'(\varrho_n^e) I_n$$

where $\lambda = (k_y a_e)^2$ and the modified Bessel functions are defined by $I_n(\lambda) = i^{-n} J_n(i\lambda)$. The resulting dispersion relation may be used to study full electromagnetic effects in cross field drift instabilities in the limit of a homogeneous plasma (Lemons and Gary, 1977).

IV. REVIEW OF LINEAR INSTABILITIES

There are five linear plasma instabilities driven by currents flowing perpendicular to a magnetic field which have been suggested as sources of turbulence: the ion acoustic, Buneman, electron cyclotron drift, modified two stream, and lower hybrid drift instabilities.

The ion acoustic instability requires $T_e > T_i$ and drift velocities on the order of the ion sound speed. It propagates in a broad cone in $\underline{k}$ space around the direction of $\underline{v_d}$, the relative electron-ion drift velocity, with relatively short wavelengths, $\lambda k_D \gtrsim 1$, and high frequencies, $\omega \sim \omega_{pi}$, where λ_D is the electron Debye length and ω_{pi} is the ion plasma frequency. Also it is an electrostatic instability which is independent of the magnetic field for a sufficiently large component of wave vector parallel to the magnetic field (Gary,1970).

The linear theory of the ion acoustic instability gives agreement with turbulence measurements in laboratory experiments in which $T_e > T_i$ (Daughney et al.,1970; Muraoka et.al.,1973; Craig et. al.,1974). Recent evidence also indicates this instability is often present in the earth's bow shock (Rodriguez and Gurnett,1975,1976). These authors have observed a high frequency component of fluctuations ($> 10^2$ H_z) in the bow shock which is predominantly electrostatic in nature, and shows a positive correlation with upstream T_e/T_i and a negative correlation with upstream T_i. These characteristics indicate the ion acoustic instability is the most likely source of this turbulence.

However as is sometimes the case in the solar wind (Feldman et. al., 1976), in the earth's bow shock (Feldman et. al.,1973), and in some laboratory shocks (Keilhacker and Steuer,1971) T_e/T_i is not large enough to allow the ion acoustic instability to grow. In this case other instabilities become important.

The Buneman instability evolves from the ion acoustic instability as the temperature ratio is decreased to $T_e/T_i = 1$ and the drift velocity is increased to the electron thermal velocity, $v_d = v_e$. In contrast to the ion acoustic mode the Buneman is a fluid instability with frequencies and growth rates on the order of $(\omega_{pi}\omega_{pe}^2)^{1/2}$. However, there are other instabilities which do not require $T_e > T_i$ and have threshold drift velocities lower than those of the Buneman.

One of these is the electron cyclotron drift instability (Wong,1970; Gary and Sanderson ,1970; Forslund et. al. 1970). It propagates in small fan-like regions in $\underline{k}$ space in the plane perpendicular to $\underline{B}^{(o)}$ and centered on $\underline{v}_d$, with Doppler shifted frequencies near negative harmonics of the electron cyclotron frequency and wave numbers over a wide range, $1/a_e \lesssim k \lesssim 1/\ _D$. Furthermore it can exist in a plasma with both $T_e = T_i$ and $v_d = v_i$. Therefore it has been suggested as a source of the electrostatic turbulence observed in the bow shock (Wu and Fredericks,1972) and in certain experiments (Keilhacker and Steuer,1971) when these condition prevail.

More detailed studies have shown this is not likely. The electron cyclotron drift instability was found to be crucially dependent upon the condition $\underline{k}\ \underline{B}$ (Gary,1971) and significantly reduced by non-zero beta (Gary,1972). Furthermore it was found to non-linearly saturate at relatively low levels of turbulence (Lampe et. al.,1972). These

reasons have led Biskamp (1973) to conclude the electron cyclotron drift instability is not important in shocks. For the same reasons Gladd (1976) has concluded the same for sheaths.

Other instabilities with low threshold drift velocities $v_d < v_e$ in a finite beta, $T_e = T_i$ plasma are the modified two stream instability and its generalization in an inhomogeneous plasma, the lower hybrid drift instability (Krall and Liewer,1971). In a high density plasma, $\omega_{pe}/\Omega_e > 1$ they have frequencies near the lower hybrid frequency, $\Omega_{LH} = \sqrt{\Omega_e \Omega_i}$, relatively long wavelengths, respectively, $ka_e \sim 1/2$ and $ka_e \sim 1$, and propagate within an angle of several degrees from $\underline{v_d}$. Since they have drift velocity thresholds below those of the Buneman and ion acoustic instabilities and do not share the special properties of the electron cyclotron drift instabilities which inhibit its growth and influence, they have been proposed as sources of turbulence in interplanetary and laboratory shocks and post implosion sheaths (Davidson and Gladd,1975; Lemons and Gary,1977A).

The modified two stream instability has maximum growth rates at oblique angles in the plane of $\underline{B}$ and $\underline{v_d}$ (McBride et. al.,1973). With the addition of magnetic field and density gradients the modified two stream can evolve into the lower hybrid drift instability which has maximum growth rates with $\underline{k} \perp \underline{B_0}$ (Gladd,1976). For this reason the lower hybrid has received greater attention recently. Anomalous collision frequencies and resistivities due to the lower hybrid drift instability in its electrostatic limit have been computed (Davidson and Gladd,1975) and comparisons with values from simulations have been published (Liewer and Davidson,1977).

Unlike the ion acoustic, Buneman and electron cyclotron drift instabilities which, because of their relatively short wave lengths, can be studied correctly in the electrostatic limit, both the modified two stream and lower hybrid drift instabilities require the inclusion of electromagnetic terms in their dispersion relations in order to accurately determine their dispersion properties in a finite beta plasma. Unfortunately the fully electromagnetic dispersion relation for crossfield current instabilities is much more complicated than its electrostatic counterpart. This accounts for the fact that many calculations of linear growth rates of these instabilities have been based on electrostatic dispersion relations (Davidson and Gladd, 1975; Huba and Wu,1976). Some research on the electromagnetic contributions to these instabilities has been done in the fluid limit (McBride and Ott,1972; McBride et. al.,1972; Detyna and Wooding,1972,1975; Lakhina and Sen,1973)

More recent work has included kinetic effects, but only part of the electromagnetic fields in the dispersion relation. Gladd (1975) has dropped the fluctuating electric field pointing in the direction of the gradients, $E^{(1)}_x$, while the dispersion relation used by Davidson et. al. (1977) is for propagation only in the direction parallel to $\underline{v}_d$ and ignores the ordinary mode electric field, $E^{(1)}_z$.

As derived in Chapter III, the dispersion relation used in this dissertation is very general and has none of these limitations. All of the instabilities mentioned in this chapter are contained in this dispersion relation. However the emphasis in this dissertation will be primarily on studying the dispersion properties of the modified two stream and lower hybrid drift instabilities since these instabilities

are most likely to affected by electromagnetic fields and alone are present in a plasma in the important regime defined by finite beta, $T_e \sim T_i$, and $v_d < v_e$.

V. NUMERICAL METHODS

The dispersion relation derived in Chapter III has been numerically solved in its most general form for electromagnetic waves in an inhomogeneous plasma, equations III-21 and III-22, in the limit of purely electrostatic waves, equation III-23, and in the limit of a homogeneous plasma, equation III-21 and III-24, for various numerical values of the steady state paramenters. Numerical solutions are presented in Chapter VI. In this chapter the numerical methods used in computing these solutions are reported.

The first step in writing a program to solve these dispersion relations is to recast the matrix elements, $R_{i,j}$, of equations III-22 and III-24 into a form in which all quantities are expressed as dimensionless parameters. Among these parameters those with physical significance can be divided into two groups according to their role within the program, input parameters and output parameters.

The input parameters have been discussed before. Some of them represent the steady state configuration: m_e/m_i, T_e/T_i, ω_{pe}/Ω_e, β_e, v_o/v_i, v_n/v_i, and $\langle v_B \rangle/v_i$, while the others specify the wave vector magnitude and orientation: ka_e and θ.

Output from the program is in the form of parameters which describe the wave solution to the dispersion relation. These are the normalized frequency and growth rate, respectively, ω/Ω_{LH} and γ/Ω_{LH} and parameters describing the polarization of the electric fields in the wave. These latter parameters are ratios of the squares of the

magnitudes of the longitudinal electric field to the total electric field, $|E^{(1)}_L/E^{(1)}_{tot}|^2$, the electric field component in the x direction to the total transverse electric field, $|E^{(1)}_x/E^{(1)}_{tr}|^2$, the energy in the transverse field to the total electric and magnetic field energy $\mathcal{E}_{tr}/\mathcal{E}_{tot}$, and the ratio of the energy of the fluctuating electric fields to the energy in the fluctuating magnetic fields, $|E^{(1)}/B^{(1)}|^2$. The three homogeneous equations for the field components $E_x^{(1)}$, $E_y^{(1)}$, and $E_z^{(1)}$ are used to define these parameters in terms of components of $R_{i,j}$. A straight forward calculation reveals:

$$\left|\frac{E_L^{(1)}}{E_{tot}^{(1)}}\right|^2 = \frac{K_z^2|P_1|^2 + K_y|P_2|^2 - 2K_yK_z\,\mathrm{Real}\{P_2^*P_1\}}{K^2\left(|P_1|^2 + |P_2|^2 + |P_3|^2\right)} \qquad \text{(V-1)}$$

$$\left|\frac{E_x^{(1)}}{E_{tr}^{(1)}}\right|^2 = \frac{K^2|P_3|^2}{K_y^2|P_1|^2 + K_z|P_2|^2 + 2K_yK_z\,\mathrm{Real}\{P_2^*P_1\}} \qquad \text{(V-2)}$$

$$\frac{\mathcal{E}_{tr}}{\mathcal{E}_{tot}} = \frac{\left\{1+\left(\frac{\omega}{CK}\right)^2\right\}\left\{1-\left|\frac{E_L^{(1)}}{E_{tot}^{(1)}}\right|^2\right\}}{\left\{1+\left(\frac{\omega}{CK}\right)^2\right\}\left\{1-\left|\frac{E_L^{(1)}}{E_{tot}^{(1)}}\right|^2\right\} + \left|\frac{E_L^{(1)}}{E_{tot}^{(1)}}\right|^2\left(\frac{\omega}{CK}\right)^2} \qquad \text{(V-3)}$$

$$\left|\frac{E^{(1)}}{B^{(1)}}\right|^2 = \frac{\left(\omega/CK\right)^2}{\left(1-\left|\frac{E_L^{(1)}}{E_{tot}^{(1)}}\right|^2\right)} \qquad \text{(V-4)}$$

where $P_1 = R_{xx}R_{yy}+R_{xy}^2$, $P_2 = R_{xy}R_{xz}+R_{yz}R_{xx}$, and $P_3 = R_{xx}R_{yz}-R_{yy}R_{xz}$.

It is interesting to note a specification of the steady state dimensionless parameters listed above does not uniquely determine values of the associated dimensional quantities. For example, consider a homogeneous electron-ion plasma with no drifts. In this case there are three dimensionless parameters to be specified: T_e/T_i, ω_{pe}/Ω_e, and β_e. However, contained in these are four independent dimensional parameters: T_e, T_i, n_o, B_o. Therefore care must be taken in interpreting the dimensional parameters in terms of dimensionless ones since more than one interpretation is possible.

In preparation for programing, all infinite sums contained in expressions III-21 and III-24 were changed to sums with only positive integers. The elements of the matrix, $R_{i,j}$, and its determinate $D(\omega,\underline{k})$, were then programmed with Fortran code. The complete Fortran program used in the solution of equations III-21, III-22, and III-24 is given in Appendix C, along with sample input and output.

The computation of the dispersion relation proceeded in the following order. First the special functions $Z(\zeta)$, I_n, and J_n were computed with well tested subroutines accurate to four or five places. Basically these subroutines use a combination of series and asymptotic expansions. Then the infinite sums were approximated with a sum of a number of the first terms in the infinite sum necessary for convergence. In practice the number used was determined by comparing solutions of the dispersion relation with solutions obtained with an increased number of terms in the sum. When the two solutions agreed to four significant figures convergence was assumed. The number required increased with the value of ka_e used. Most calculations were for

$ka_e \lesssim 1$, in which case four or five terms in each sum were adequate. Next, the $v_\perp$ integrals were done with a subroutine using Simpson's formula. Convergence of these integrals was assured by the presence of an exponential factor $\exp(-v_\perp^2/2v_e^2)$ in the integrand, and their accuracy was periodically checked by halving the integration step used and extending the upper limit of the integrals.

The determinant, $D(\omega,\underline{k})$, was then calculated. The zeros of its real and imaginary parts, which determine the frequency, ω/Ω_{LH}, and growth rate, γ/Ω_{LH}, were found with an iterative root finding procedure employing the secant method. Usually only four or five iterations were necesary for convergence of ω/Ω_{LH} and γ/Ω_{LH} to three place accuracy. When a root was found the field quantities $|E_L/E_{tot}|^2$, $|E_x/E_{tr}|^2$, and $\mathcal{E}_{tr}/\mathcal{E}_{tot}$ were calculated and printed along with values of frequency and growth rate.

The programs which implemented this procedure were usually employed in the interactive mode of the computers used. Therefore the input parameters could be entered into the program, the program executed, and the output parameters received relatively quickly via a remote terminal. Using the most general dispersion relation, equations III-21 and III-22, actual computer time required by a PDP-10 computer to process one set of input parameters is about 20 seconds. It is estimated a total of approximately twenty hours of computer time was used in the course of this dissertation work on both the Los Alamos Scientific Laboratory's PDP-10 and the College of William and Mary's IBM 370.

VI. SOLUTIONS

This chapter presents numerical solutions to the dispersion relations derived in Chapter III. It is divided into three subsections which treat the cases of (A) a homogeneous plasma, (B) a plasma with magnetic field gradients, and (C) a plasma with both magnetic field and density gradients according to either the shock or sheath conditions.

Of the linear instabilities reviewed in Chapter IV, numerical studies of three are presented. Emphasis is initially placed on the modified two stream instability because it is found in a homogeneous plasma. With the addition of gradients the modified two stream evolves into the lower hybrid drift instability under certain conditions. In addition the relationship of these two instabilities to the ion acoustic instability is explored.

The numerical values of the steady state parameters are chosen and varied both in order to approximate conditions in physical plasmas and to facilate comparison of results with previous numerical solutions of linear dispersion relations. In all that follows the ratio of electron and ion masses used is that of a hydrogen plasma, $m_e/m_i = 1836$. Other parameters are usually varied only one at a time. For instance in much of the present work the values $\omega_{pe}/\Omega_e = 68$ and $T_e/T_i = 1.0$ are used although variations of growth rates of the lower hybrid drift instability with both these parameters are included. This value of ω_{pe}/Ω_e corresponds to conditions in a particular Z pinch shock experiment (Paul,1969) and to previous numerical work (e.g. Gary and

Sanderson,1970; Lashmore-Davies and Martin,1973). As long as $\omega_{pe}/\Omega_e > 10$, which is often the case in both space and experimental plasmas(Table 1-1,Boyd and Sanderson, 1969), its exact value has little influence on the modified two stream instability(Lashmore-Davies and Martin,1973). Present results indicate the same is true for the lower hybrid drift instability. Likewise the condition of equal electron and ion temperatures is commonly found in both the bow shock and in laboratory plasmas, although in the former instance T_e/T_i is also sometimes greater than one while in the later it is sometimes less than one, particularly in the post-implosion phase of linear theta pinches.

The other dimensionless parameters are β_e and v_d/v_i. β_e can vary between 0 and order unity in both the quasi-perpendicular bow shock and in thermonuclear plasmas. Accordingly the numerical variations will span this range. In the homogeneous plasma dispersion relation, equations III-22 and III-24, β_e serves to introduce electromagnetic effects according to the size of the factor $\beta_e/(ka_e)^2$, while in the inhomogeneous plasma dispersion relation, equations III-21 and III-22, it also introduces gradient B effects according to Ampere's Law, equation II-8. The size of v_d in actual shocks and sheaths can be estimated from the size of the resulting magnetic field gradients. In a well diagnosed theta pinch shock experiment (Keilhacker and Steuer,1971) this drift was estimated to be on the order of a few ion thermal speed throughout the shock. Drifts of this size were often used in the numerical calculations. On the other hand v_d within post implosion sheaths may be much smaller. For example, symmetry considerations require the crossfield current in linear theta pinches to approach zero near the axis, implying that there is a region in

which the electron drift falls below the ion thermal speed. In this case the crossfield current instabilities considered here have wave lengths and frequencies on the order of, respectively, the ion Larmor radius and the ion cyclotron frequency. Ion gyro effects are important in this regime. Since the derivation of the dispersion relations in Chapter III assumed straight line orbits for the ions, the low drift regime must be avoided. Therefore $v_d/v_i \gtrsim 1$ in the following numerical work.

A. Homogeneous Plasma

Results in this section are numerical solutions of equations III-22 and III-24. The parameter values $\omega_{pe}/\Omega_e = 68$ and $T_e/T_i = 1.0$ are used while v_d/v_i and β_e are varied in order to study the electromagnetic contributions to the modified two stream instability.

Figure 2 shows that electromagnetic modifications to the dispersion properties of cross field drift instabilities are significant only at wave numbers such that $\beta_e/(ka_e)^2 > 1.0$, and the general property that electromagnetic effects reduce growth rates. In this figure ω/Ω_{LH} and γ/Ω_{LH} are plotted versus ka_e for $v_d/v_i = 5.0$ at the angle $\theta = 87^o$. The $\beta_e = 0.01$ curves are equivalent to those from the electrostatic dispersion relation, equation III-22, while the $\beta_e = 1.0$ curves show the changes due to electromagnetic effects. For $ka_e > 1.0$ there is little difference between the two cases. For $ka_e < 1.0$ the maximum growth rate of the modified two stream instability is reduced, a result which is in qualitive agreement with the theory and numerical results of Lakhina and Sen(1973), who studied

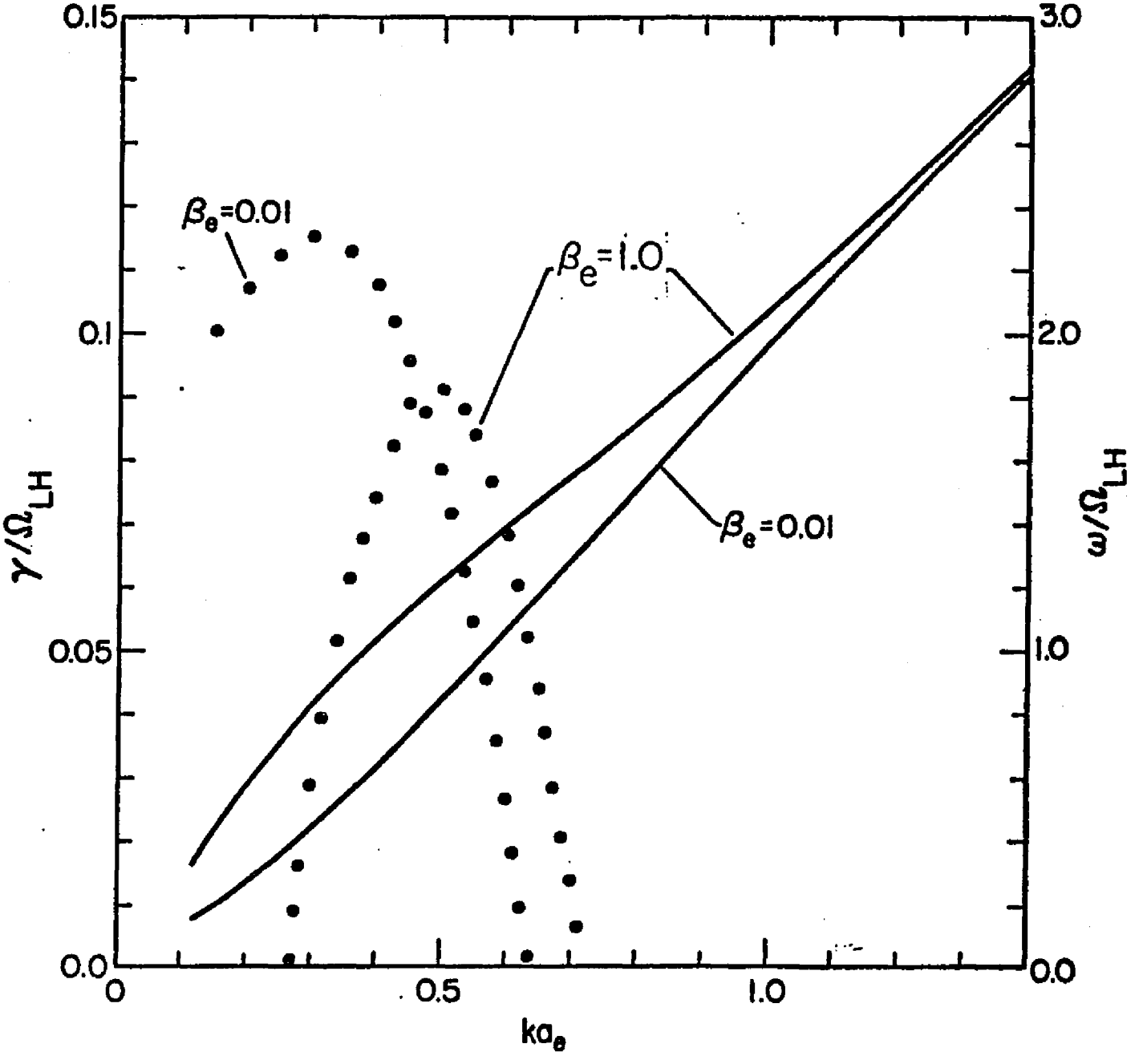

Fig. 2. Frequency, ω/Ω_{LH}, and growth rate γ/Ω_{LH}, of the modified two stream instability versus wavenumber, ka_e, for $\theta = 87^o$. There are no gradients, $v_n = \langle v_B \rangle = 0$. Other parameters are $v_d/v_i = 5.0$ and $T_e/T_i = 1.0$. Here and in all subsequent figures $m_e/m_i = 1836$; also $\omega_{pe}/\Omega_e = 68.0$ except in Fig. 16.

the modified two stream in its fluid and low density($\omega_{pe}/\Omega_e < 1.0$) limits. Furthermore the instability is moved to higher wave numbers while the real part of the frequency is shifted slightly.

Figure 3a shows another important electromagnetic effect. Here growth rates, maximized over variations in ka_e, are plotted against θ for $v_o/v_i = 5.0$ with $\beta_e = 1.0$ and 0.01. Figure 3b shows frequencies (solid lines) and wave numbers (dashed lines) which accompany the growth rates of Figure 3a. For propagation perpendicular to the magnetic field ($\theta = 90^o$) the modified two stream is stable for both $\beta_e = 0.01$ and $\beta_e = 1.0$ as the figure suggests. The maximum growth rate in the $\beta_e = 1.0$ curve is reduced from that in the $\beta_e = 0.01$ curve and is shifted away from the perpendicular. Furthermore the electromagnetic ($\beta_e = 1.0$) modified two stream mode is unstable for propagation over a wider range of angles than the electrostatic ($\beta_e = 0.01$) mode. For these parameters the $\beta_e = 1.0$ instability curve actually extends to an angle of about 60^o. However the wavelength of the instability at this angle is on the order of an ion Larmor radius , and consequently ion gyro effects should reduce the growth rate or completely stabilize the instability in this region(Freidberg and Gerwin,1977). Nonetheless, even though electromagnetic effects reduce maximum growth rates of the modified two stream instability, the contribution of this instability to anamolous transport coefficients may become more important since the volume in $\underline{k}$ space in which the mode is unstable becomes larger with increasing β_e.

The mechanism by which,the modified two stream instability is extended in θ space away from the direction of the crossfield current

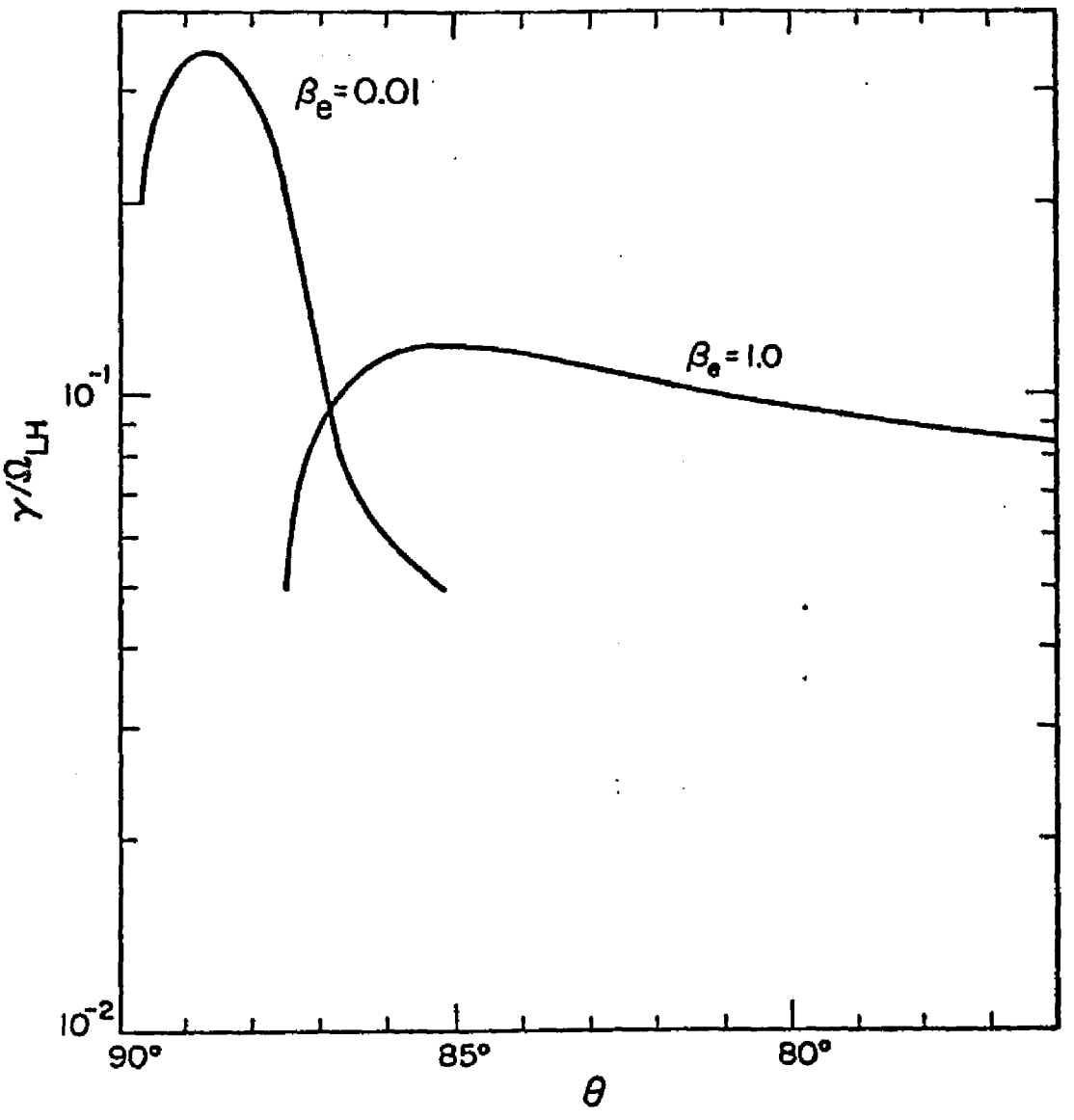

Fig. 3a. γ/Ω_{LH}, maximized with respect to ka_e, versus θ for the modified two-stream instability. Electromagnetic effects (high β_e) reduce growth rates, shift them away from $\theta = 90^{\circ}$, and spread them in space. Other parameters are the same as in Fig. 2.

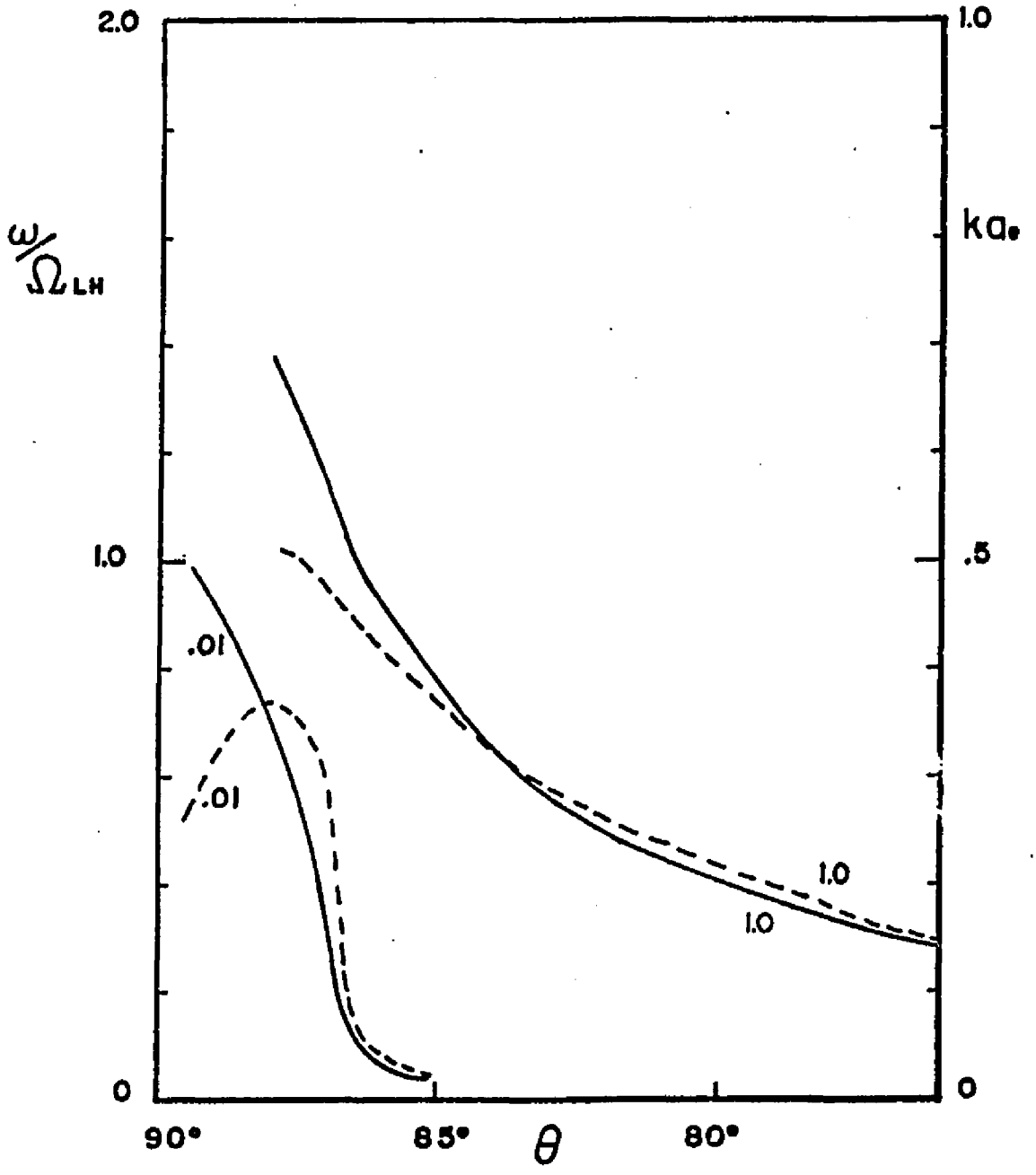

Fig. 3b. γ/Ω_{LH} (solid lines) and ka_e (dashed line) corresponding to growth rates in Fig. 3a. Numbers labelling curves refer to β_e.

($\theta = 90^{o}$) by electromagnetic effects is the coupling of two distinct solutions to the dispersion relation. This is illustrated in Figure 4 which plots the dispersion properties of these two solutions for $\beta_e = 1.0$ and $v_d/v_i = 5.0$, and two different angles of propagation, $\theta = 82^{o}$ and $\theta = 81^{o}$. The growth rates in the $\theta = 82^{o}$ graph are represented with the dotted line and are associated with the frequencies denoted with the solid line. This is the mode which is also found in the electrostatic dispersion relation and upon which the ion acoustic, Buneman, and electron cyclotron instabilities appear. In this graph it is unstable but close in frequency to a heavily damped mode whose frequency is represented with the cross-dashed line and growth rates with crosses. In the other graph the same symbolism and parameters apply except that now wave propagation is at 81^{o}. The frequency of the damped mode at $\theta = 82^{o}$ can be topologically identified with the mode at 81^{o} which is unstable. At lower values of θ the instability is also carried by this mode, characterized by low frequencies.

This new mode is due to electromagnetic terms in the dispersion relation since it can not be found in the electrostatic approximation to the dispersion relation. Furthermore it evolves into a damped zero frequency mode when the source of instability, v_d, is slowly removed and can be identified with the zero frequency mode which carries the electron mirror instability.

This identification was made by generalizing the homogeneous plasma dispersion relation and the computer code to include the possibility of different electron temperatures in the plane

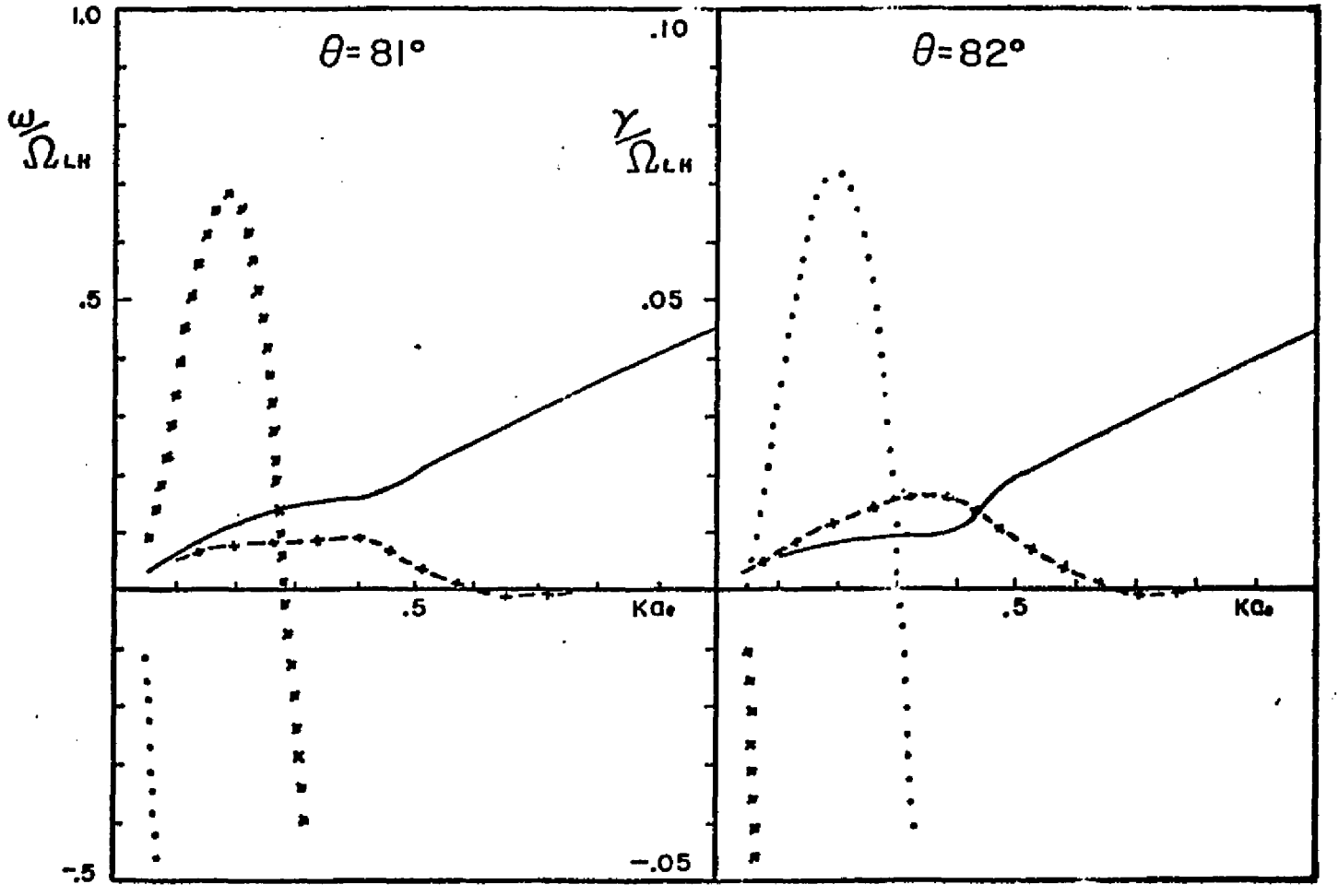

Fig. 4. ω/Ω_{LH} and γ/Ω_{LH} for two different modes at two angles of propagation, $\theta = 81^{\circ}$ and $\theta = 82^{\circ}$. $v_d/v_i = 4.0$, $\rho_e = 1.0$, and $v_n = v_B = 0$. Also $T_e/T_e = 1.0$. In both graphs the growth rates represented by crosses are associated with the frequencies represented with the line of alternate dashes and crosses. Likewise growth rates of the other mode shown by dots go with frequencies represented with the solid line. Notice that when the value of θ is changed from 82° to 81°, all other numbers remaining constant, the instability is shifted from one mode to the other.

perpendicular to the magnetic field, $T_{\perp e}$, and along the direction of the magnetic field, $T_{\parallel e}$. When the temperature anisotropy parameter $T_{\perp e}/T_{\parallel e}$ was increased above one, with $v_d/v_i = 0$, this zero freqency mode became unstable at oblique angles. This is the electron mirror instability, a zero frequency electromagnetic mode driven unstable when $T_{\perp e}/T_{\parallel e} > 1/\beta_{\perp e}+1$ (Sec. 9.8,Stix,1962). It is interesting to note that when $T_{\perp e}/T_{\parallel e} = 2.0$ the electron mirror mode is unstable within the range of angles $60^o < \theta < 85^o$, the same range over which this low frequency mode extends the modified two sream instability when $v_d/v_i = 4.0$.

The exchange of instability from one solution to the other is made quickly as θ is decreased and for no value of θ have both modes been found unstable. This type of phenomena has been studied by Cayton (1977) and apparently occurs at the crossing in ω,γ space of the two solutions to the dispersion relation. In any case Figures 2 and 3 show that the growth rates and frequencies of the modified two stream instability are a continuous function of θ.

Figure 5 is addressed to the question of the polarization of the modified two stream instability. Here the ratio of energy in the fluctuating electric fields to the energy in the fluctuating magnetic fields is shown versus ka_e at an angle of propagation of $\theta = 89.6^o$ for $T_e/T_i = 10.0$, and a drift of $v_d/v_i = 20.0$. The high temperature ratio represents extreme conditions in the earth's bow shock and extends the range of instability to short wavelengths. The dotted lines indicate growth rates. Notice again that high beta reduces growth rates only for $\beta_e/(ka_e)^2 > 1$. Solid lines represent the ratio $|E^{(1)}/B^{(1)}|^2$. The

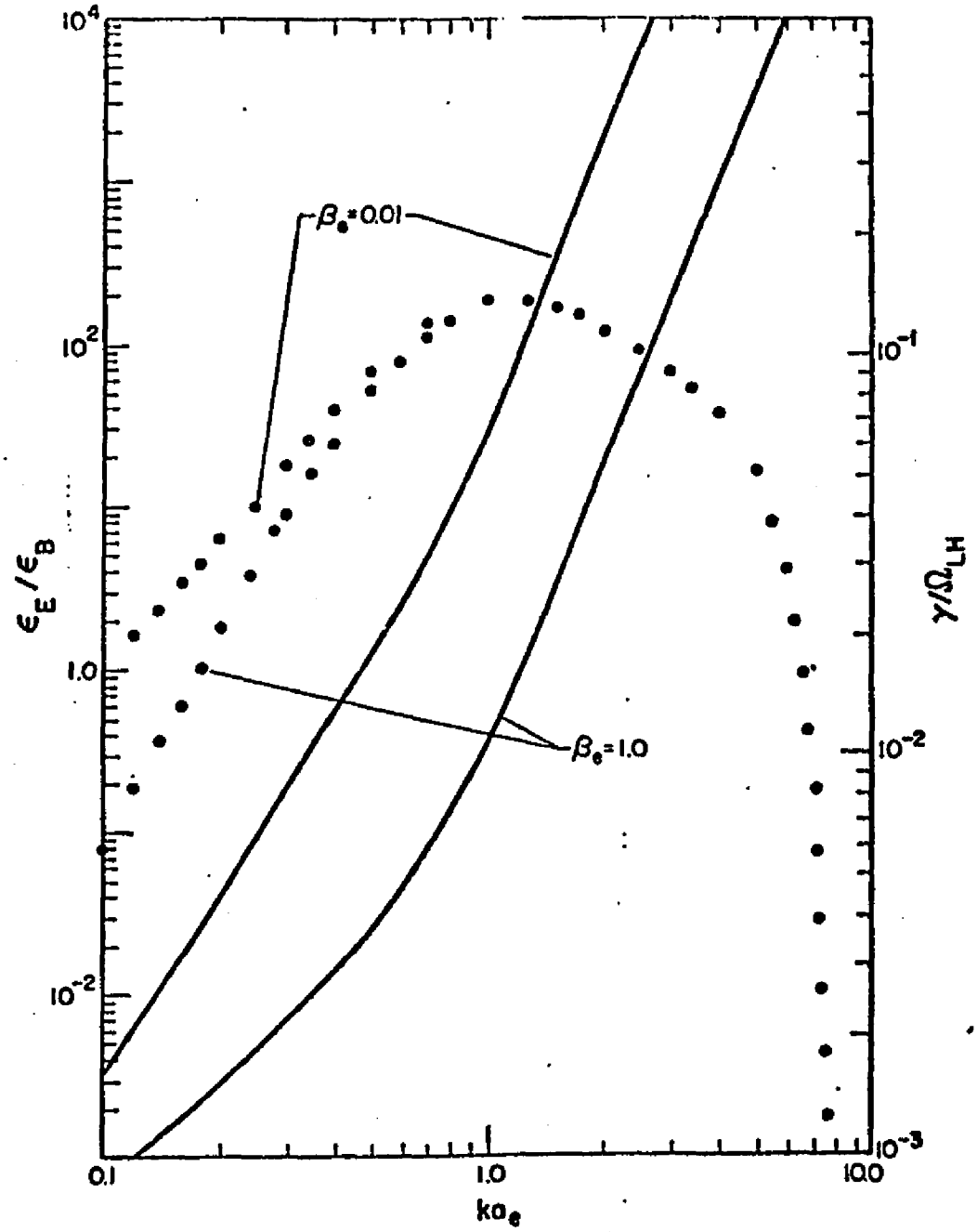

Fig. 5. Plots of $|E^{(1)}/B^{(1)}/B^{(1)}|^2$ (solid line; left hand ordinate axis) and γ/Ω_{LH} (dots) for the modified two stream instability. $\theta = 89.6^{o}$, $v_d/v_i = 20.0$, $T_e/T_i = 10.0$, and $v_n = \langle v_B \rangle = 0$.

size of this ratio is an indication of the electromagnetic nature of the cross field drift instabilities which are predominately electrostatic at short wavelengths and exhibit progressively greater electromagnetic properties as ka_e decreases.

Over the whole range of instability for these parameters the magnitude of $|E^{(1)}/B^{(1)}|^2$ varies over seven orders. This wide range of values is in agreement with measurements of this ratio in the earth's bow shock(Figure 9,Rodriguez and Gurnett,1975). However, they conclude that purely electromagnetic waves are necessary for the low values of $|E^{(1)}/B^{(1)}|^2$. In contrast, Figure 5 indicates low values of this ratio at long wavelengths can be a result of electromagnetic contributions to crossfield drift instabilities which are predominently electrostatic at shorter wavelengths. This fact is emphasized by an examination of the ratio of transverse fluctuating electric field, $|E_{tr}^{(1)}|$, to longitudinal fluctuating electric fields, $|E_L^{(1)}|$. The ratio $|E_{tr}^{(1)} / E_L^{(1)}|$ has for all parameters and instabilities investigated found to be no greater than 1%. Specifically, for the relatively long wavelength crossfield current instabilities $|E_{tr}^{(1)} / E_L^{(1)}| = 0.01$ at most, while for the ion acoustic instability $|E_{tr}^{(1)} / E_L^{(1)}| << 0.01$. The long wavelength crossfield current instabilities contain most of their energy within the fluctuating magnetic field because of their low phase velocity which is suggested by equation V-4.

The reduction of growth rates by electromagnetic effects over a range of drift veleocities is shown in Figure 6 where growth rates maximized with respect to both ka_e and θ, are plotted versus v_d/v_i. Numbers labelling the curves in this and in all subsequent figures in

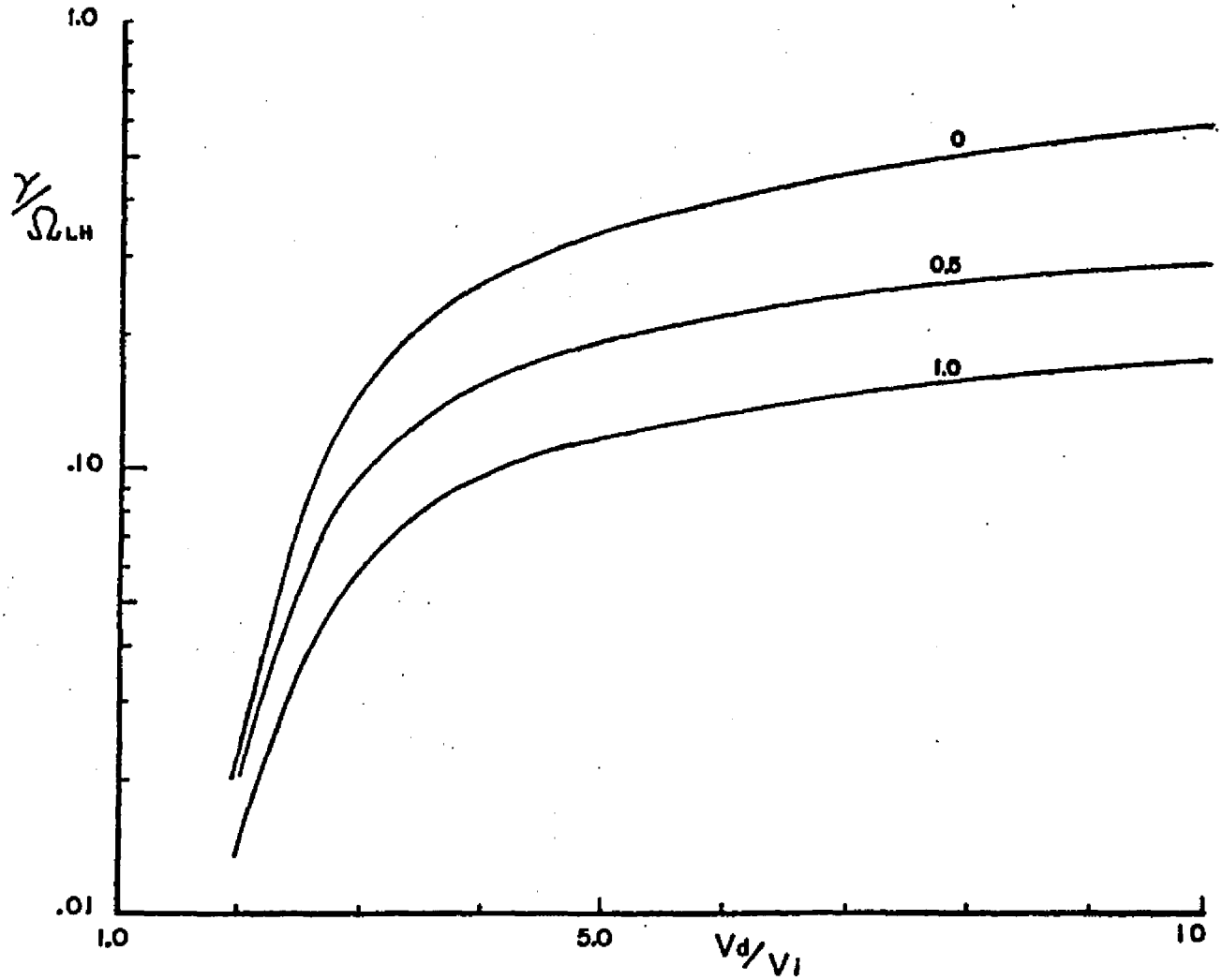

Fig. 6. γ/Ω_{LH}, maximized with respect to ka_e and θ, versus v_d/f_i for various values of β_e. $T_e/T_i = 1.0$. Here and in all subsequent figures numbers labelling curves refer to values of β_e.

this chapter refer to values of β_e. Growth rates for the electrostatic ($\beta_e = 0.01$) modified two stream instability agree with previously published growth rates in Figure 3 of Gary (1973) and Figure 21 of Lashmore-Davies and Martin (1973). The effect of increasing β_e is to reduce the growth rates, especially at larger drift velocities. The drift velocity at marginal stability is, in this case, about $v_d/v_i = 2.0$ and is unaffected by β_e. Notice also that maximum growth rates seem to approach an asymptotic value with increasing drift speed. This condition is also characteristic of the lower hybrid drift instability.

In summary, electromagnetic effects are influential only when $\beta_e/(ka_e)^2 > 1.0$. Their effect upon the modified two stream instability is to reduce growth rates, move the instability away from the perpendicular and spread the region of instability in θ space. Threshold drift speeds are not substantially changed by electromagnetic effects. Furthermore, much of the energy of the instability is associated with the fluctuating magnetic field.

B. Magnetic Field Gradient

According to Ampere's Law, equation II-8, the presence of finite β_e and v_d/v_i require a non zero magnetic field gradient drift, $\langle v_B \rangle$, although not necessarily a density gradient drift. Since the dispersion relation used in section A neglected magnetic field gradient effects, it is not based upon a consistent steady state. However it has been convenient for isolating electromagnetic effects on a

crossfield drift instability since they alone are introduced with finite β_e.

In the present section magnetic field gradient effects are included in the dispersion relation through the electron orbit integrals, III-18, although maintaining use of the Maxwellian and drifting Maxwellian ion and electron distribution functions of the previous section. This is done by using the dispersion relation of equations III-21 and III-22 with $v_n = 0$. The parameter values $\omega_{pe}/\Omega_e = 68$ and $T_e/T_i = 1.0$ are also used throughout this section.

The effect of gradient B on the modified two stream mode is seen in Figure 7a. There both growth rates(solid lines) maximized with respect to wave number and the corresponding wave number at maximum growth rate(dashed line) are plotted versus θ. Drift velocities of $v_o = 0.1v_e = 4.28v_i$ are used. Growth rates with $\beta_e = 0.01$ are again essentially the same as those of the purely electrostatic modified two stream which has maximum growth rates at angles away from the perpendicular.

Increasing β_e to 0.25 and 1.0 not only spreads the instability in space as it does for the modified two stream (Figure 3a) but also moves the maximum instability to the perpendicular direction. This latter effect has been studied by Gladd(Figure 4,1976) and establishes the main difference between the modified two stream instability with maximum growth rates at $\theta \neq 90^o$ and the lower hybrid drift instability with maximum growth rates at $\theta = 90^o$.

Polarization of the transverse fields for the lower hybrid drift instability is shown in Figure 7b where the ratio of the square of the

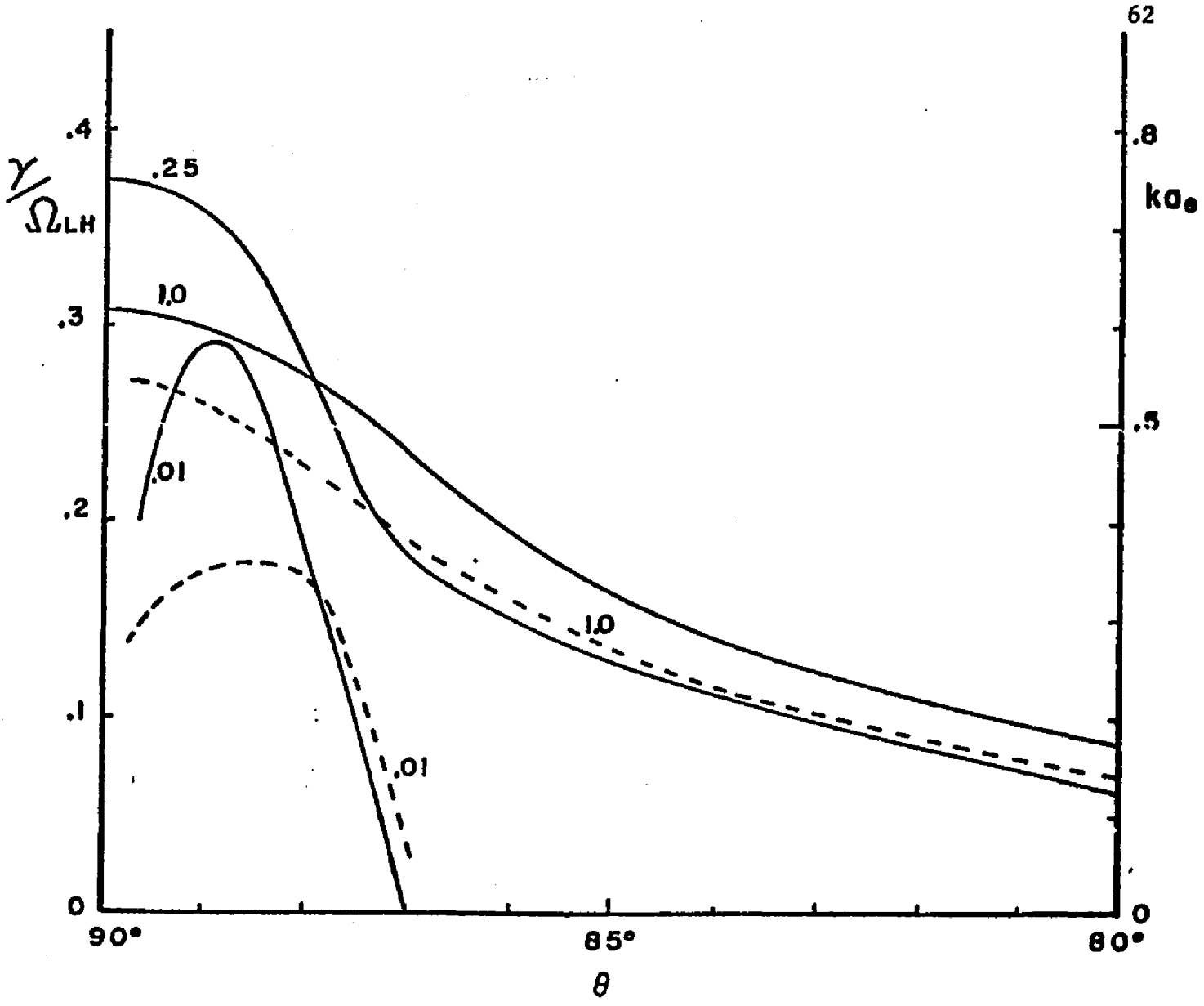

Fig. 7a. γ/Ω_{LH} (solid line), maximized with respect to ka_e and ka_e at maximum growth rate (dashed line) versus θ for $\beta_e = 0.01$ and 1.0. Both electromagnetic and gradient B effects are introduced with finite β_e. $v_d/v_i = 4.28$, $T_e/T_i = 1.0$, and $v_n = 0$. $\langle v_B \rangle$ is finite and is determined by Ampere's Law, equation II-8.

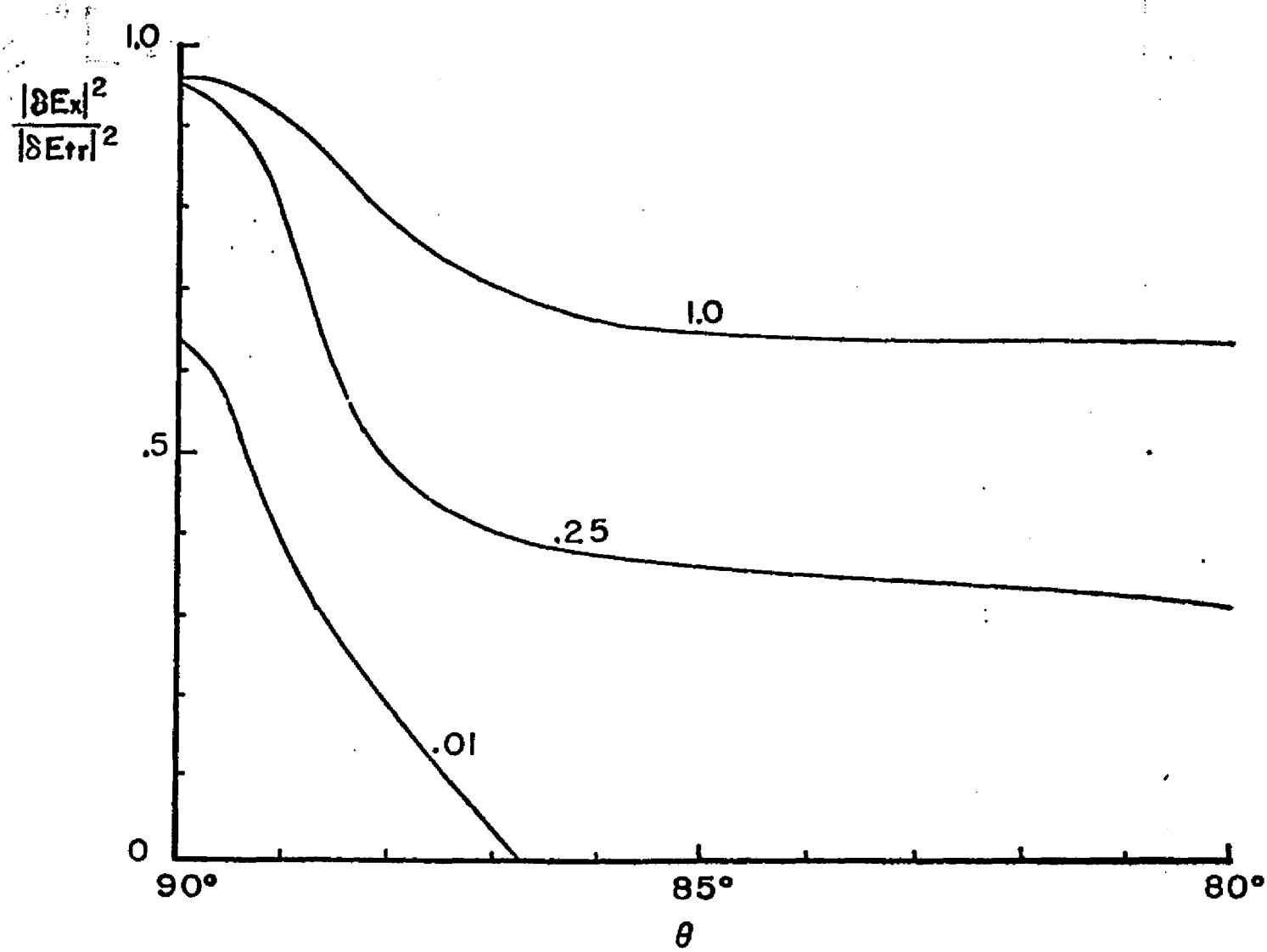

Fig. 7b. $|E_x^{(1)}/E_{tr}^{(1)}|^2$ (ordinate axis) versus θ associated with the graph in Fig. 7a.

fluctuating electric field in the x direction to the square of the magnitude of the total transverse electric field, $|E_x^{(1)}/E_{tr}^{(1)}|^2$ is plotted. Parameter values are the same as in Figure 7a. Since wave propagation is in the y-z plane E_x is a pure transverse field and when $\theta = 90^o$ the ratio $|E_x^{(1)\,2}/E_{tr}^{(1)}|^2$ becomes $|E_x^{(1)}|^2/(|E_x^{(1)}|^2+|E_z^{(1)}|^2)$. Notice in this instance the transverse electric fields are almost completely in the x direction. This fact has been exploited by Davidson et. al.(1977) who have derived an electromagnetic dispersion relation for propagation of the lower hybrid drift instability in the $\theta = 90^o$ direction by neglecting the fluctuating E_z field. On the other hand, Gladd(1976) dropped $E_x^{(1)}$ and kept $E_z^{(1)}$ in deriving his dispersion relation and so neglected the most important electromagnetic contributions to the dispersion relation.

The total effect of finite β_e on the maximum growth rates is not monotonic, as is further illustrated in Figure 8. Here $v_d/v_i = 3.0$ and the maximum growth rates throughout ka_e and θ space are shown as a function of β_e. Electromagnetic effects and gradient B effects are shown independently and together. Electromagnetic effects on the modified two stream instability are therefore illustrated by the curve labelled e-m, $\nabla B \neq 0$. On the log plot γ/Ω_{LH} decreases linearly with β_e. In contrast effects of gradient B alone on the lower hybrid drift instability, denoted by the curve labelled e-s, $\nabla B = 0$, are more complicated due to the fact that gradient B terms enter into the dispersion relation, equations III-21 and III-22, via resonant denominators. The instability is enhanced by low values of β_e and

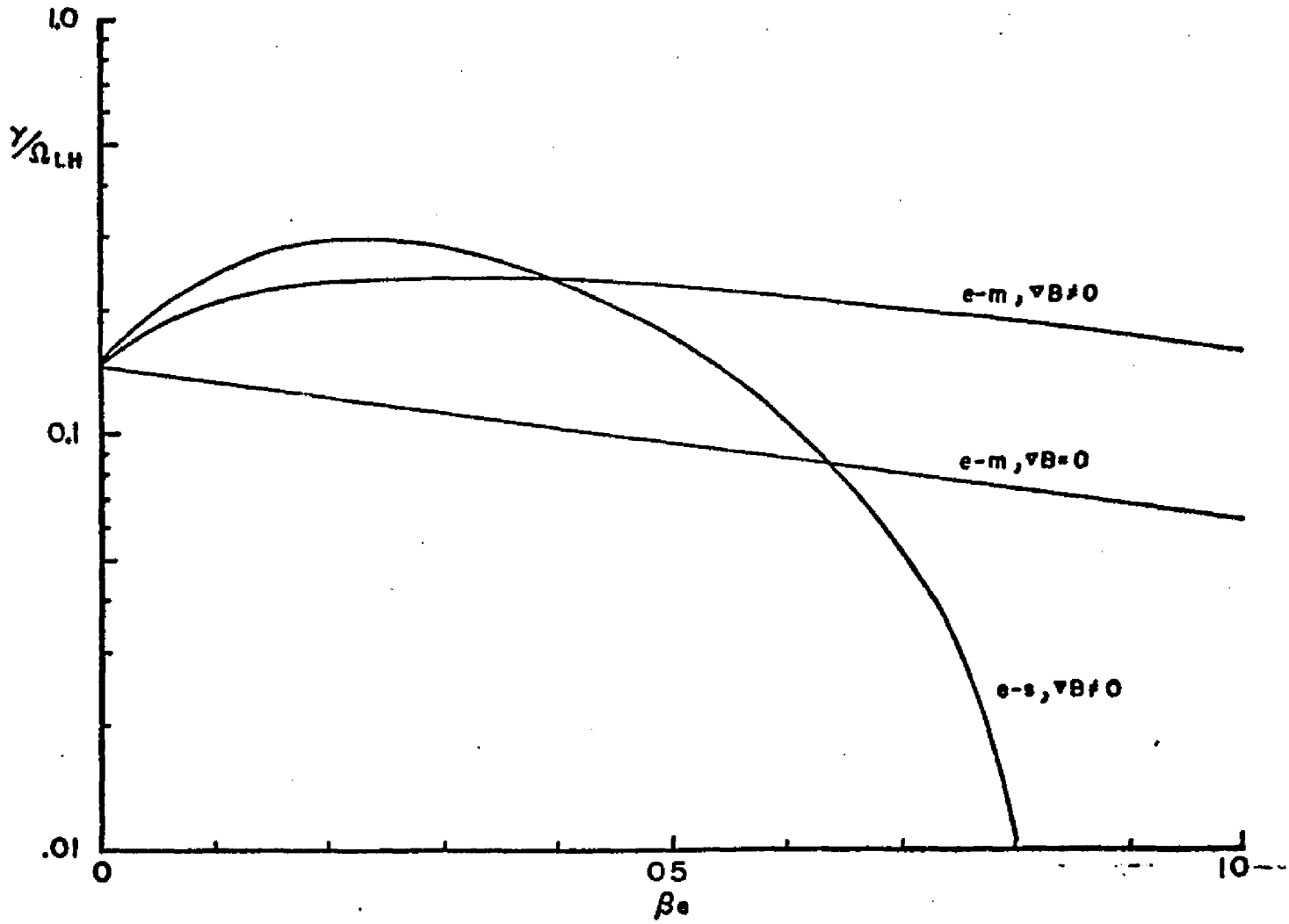

Fig. 8. γ/Ω_{LH} maximized with respect to ka_e and θ versus β_e. $v_d/v_i = 3.0$ and other parameters are the same as in Fig. 7a. Curves are labelled according to whether finite β_e introduces only gradient B effects, (e-s, $\nabla B \neq 0$), only electromagnetic effects (e-m, $\nabla B = 0$), or both electromagnetic and gradient B effects (e-m, $\nabla B \neq 0$).

stabilized by higher values. This result has been studied by Huba and Wu(1976) who showed that the damping of the electrostatic lower hybrid drift is an example of electron resonance damping. Neither of these finite β_e effects have proven to be amenable to representation with simple analytic expressions.

Figure 9 is analagous to Figure 6 and shows growth rates of the lower hybrid drift instability driven by an $\underline{E}x\underline{B}$ electron drift and magnetic field gradient for various drift speeds. In contrast to the modified two stream instability finite β_e has greater effect on the lower hybrid drift instability at low drift veleocities than at high drift velocities, and actually increases growth rates and lowers thresholds from values in the $\beta_e = 0$ case.

In summary, gradient B effects transform the modified two stream instability into the lower hybrid drift instability with maximum growth rates in the perpendicular direction, enhanced growth rates and reduced threshold drift speeds. Electromagnetic effects are almost completely carried by the fluctuating E_x field.

C. Density Gradient

In this section solutions to the dispersion relation in its most general form, equations III-21 and III-22, are presented. The magnitude of the density gradient drift, v_n, is now determined in two different ways: the sheath condition, $v_n = -(T_e/T_i)v_0$, and the shock condition, $v_n = \langle v_B \rangle$. Figures 10a and 10b show a comparison of the consequences of the two conditions. Figure 10a shows growth rates

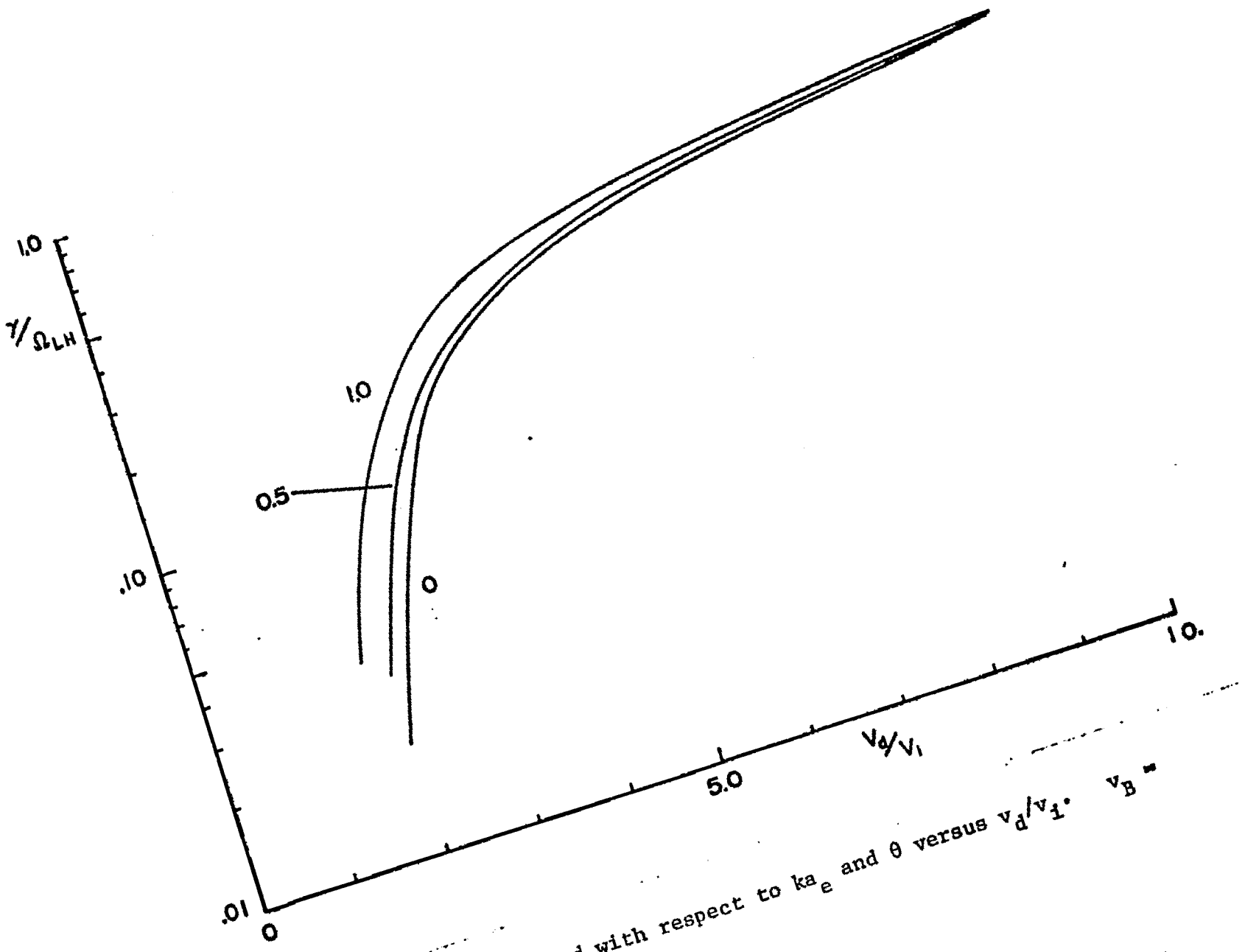

Fig. 9. γ/Ω_{LH} maximized with respect to ka_e and θ versus v_d/v_i. v_B = $\beta_e v_d/2$, and T_e/T_i = 1.0.

maximized with respect to ka_e as a function of θ for $v_d/v_i = 4.0$ and $\beta_e = 0.25$. The corresponding frequencies and wavenumbers are shown in Figure 10b. Here and in the rest of this section $\omega_{pe}/\Omega_e = 68$ and $T_e/T_i = 1.0$ unless otherwise indicated.

The dotted line in Figure 10a is the modified two stream instability ($\langle v_B \rangle = v_n = 0$). Characteristically its maximum growth rate is in an oblique direction. Maximum growth rates are shifted to the perpendicular direction when non zero ∇B is allowed as shown by the cross-dashed curve. Finally, the solid lines represent the addition of the density gradient drift, which is added in such a way as to keep the total crossfield drift, v_d, at the constant value of $v_d/v_i = 4.0$. This requires drifts of $\langle v_B \rangle = v_n = (\beta_e/2)v_d = v_i/2$ and $v_o = (1+\beta_e/2)v_d = 5v_i$ for the shock condition and $\langle v_B \rangle = (\beta_e/2)v_d$, $v_n = -(T_e/T_i)v_d/(1+T_e/T_i) = -2.0v_i$, and $v_o = v_d/(1+T_e/T_i) = 2.0v_i$ for the sheath condition. What happens depends upon whether the density gradient is in the same direction as the magnetic field gradient (shock condition) or in opposite directons (sheath condition). In the former case the maximum growth rate is reduced and moved back to oblique angles, essentially restoring the modified two stream instability. In the latter case the maximum growth rate is slightly enhanced and maintained in the perpendicular direction.

Two points should be made in connection with this graph. First, the maximum growth rates of the instability when the shock condition obtains are for oblique propagation for all values of β_e and v_d/v_i considered in this study. Apparently, magnetic field and density

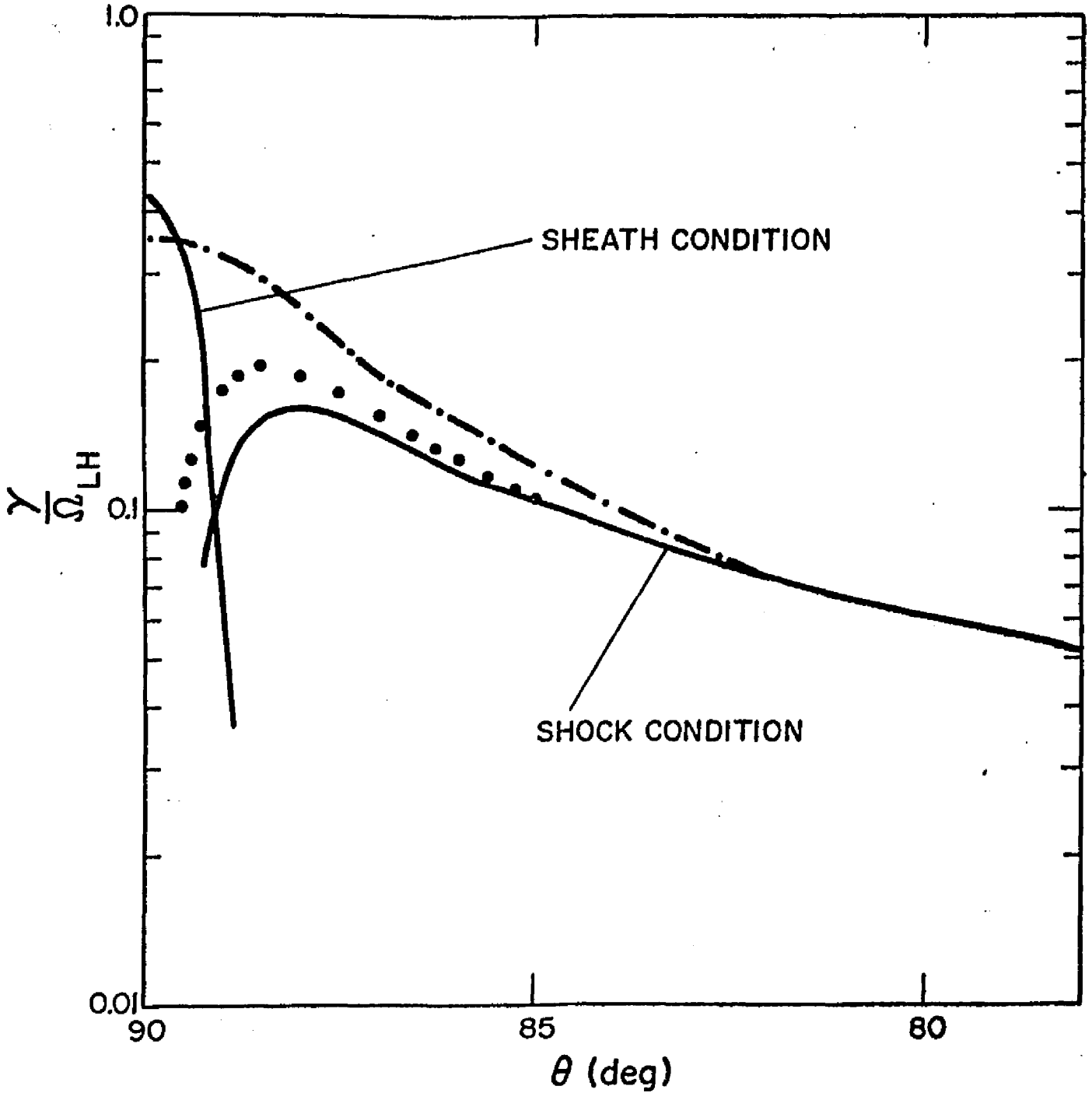

Fig. 10a. γ/Ω_{LH} maximized with respect to ka_e versus θ. $v_d/v_i = 4.0$, $\beta_e = 0.25$, $T_e/T_i = 1.0$. Different curves show growth rates when $v_n = \langle v_B \rangle = 0$ (dotted line) and $v_n = 0$, $\langle v_B \rangle = \beta_e v_d/2$ (dot-dashed line). The solid line with the larger maximum growth rate corresponds to v_n given by the sheath condition while the solid line with the smaller maximum growth rate corresponds to $v_n = \langle v_B \rangle$, the shock condition.

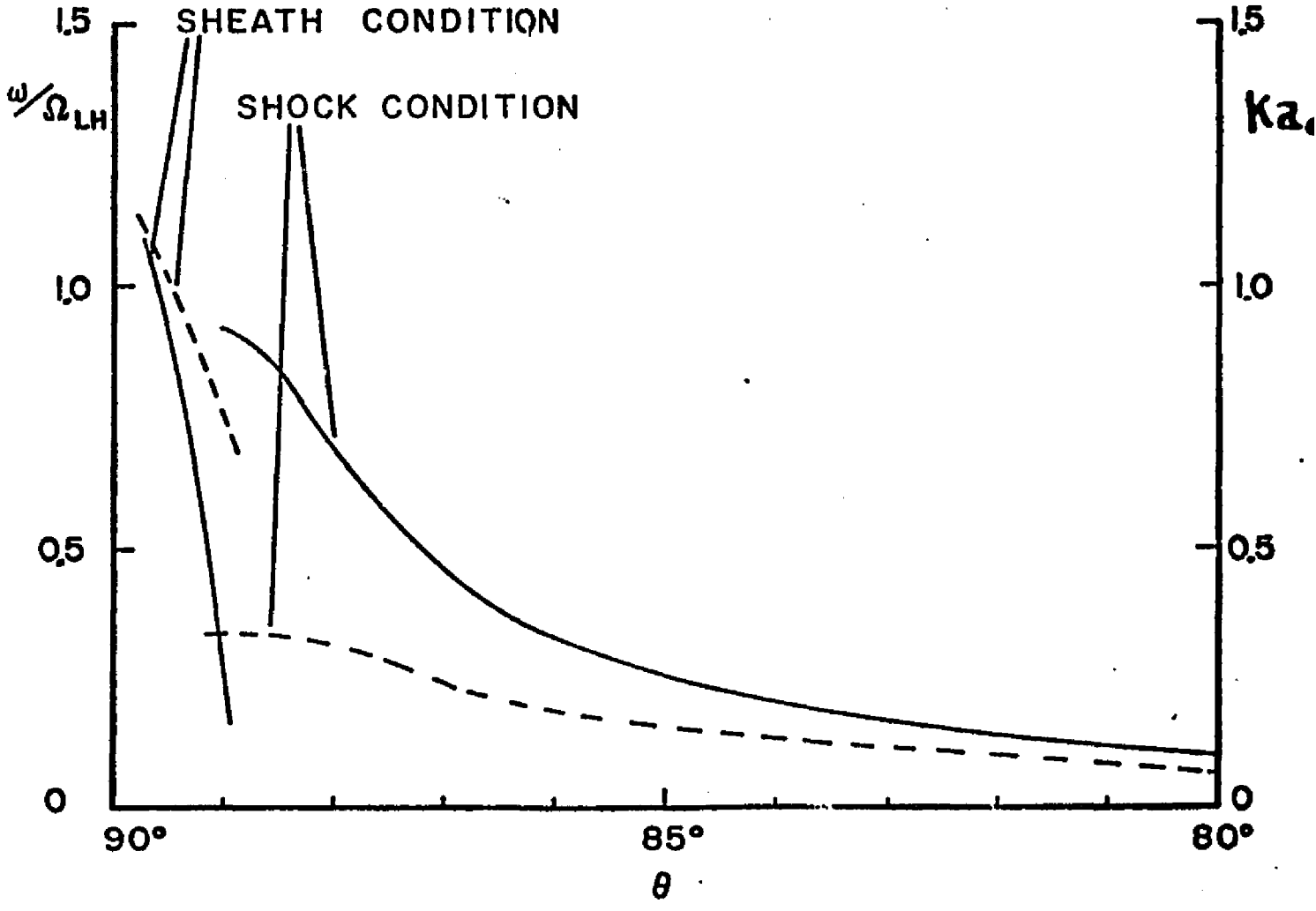

Fig. 10b. ω/Ω_{LH} (solid lines) and wavenumbers at maximum growth rate (dashed lines) for sheath and shock condition cases in Fig. 10a plotted versus θ.

gradients of equal magnitude pointing in opposite direction restore the modified two stream instability.

Secondly, under the sheath condition, the instability present is usually the lower hybrid drift instability which is no longer extended in θ space away from $\theta = 90^{o}$ as it is under the shock condition and is confined to a narrow angle of about 1^{o} from the perpendicular. Analysis of the electrostatic dispersion relation has shown that the modified two stream instability has maximum growth rates at angles corresponding to $\cos\theta = k_z/k = (m_e/m_i)^{1/2}$ $(\theta = 88.7^{o})$(McBride et. al.,1972), while in section A of this chapter it was shown that electromagnetic effects move the angle of maximum growht rate to smaller θ and spread the instability in θ space(Figure 3a). However, as illustrated in Figure 10a, the density gradient according to the sheath condition reverses these results by confining the instability to an even smaller range of angles about the perpendicular direction than the electrostatic modified two stream.

The role of the density gradient drift in determining the extent of oblique propagation is indicated in Figure 11. Here the angle, $\theta_{1/2}$, at which the growth rate falls to one half of its maximum value as decreases is plotted versus v_n/v_i. Parameters values are the same as those in Figure 10a except that now the density gradient is added in arbitrary amounts in such a way as to keep $v_d/v_i = 4.0$. The extreme left hand point in the curve corresponds to the sheath condition while the extreme right hand point corresponds to the shock condition. The v_n/v_i at which the instability changes from the lower hybrid drift to the modified two stream instability is indicated by a solid vertical

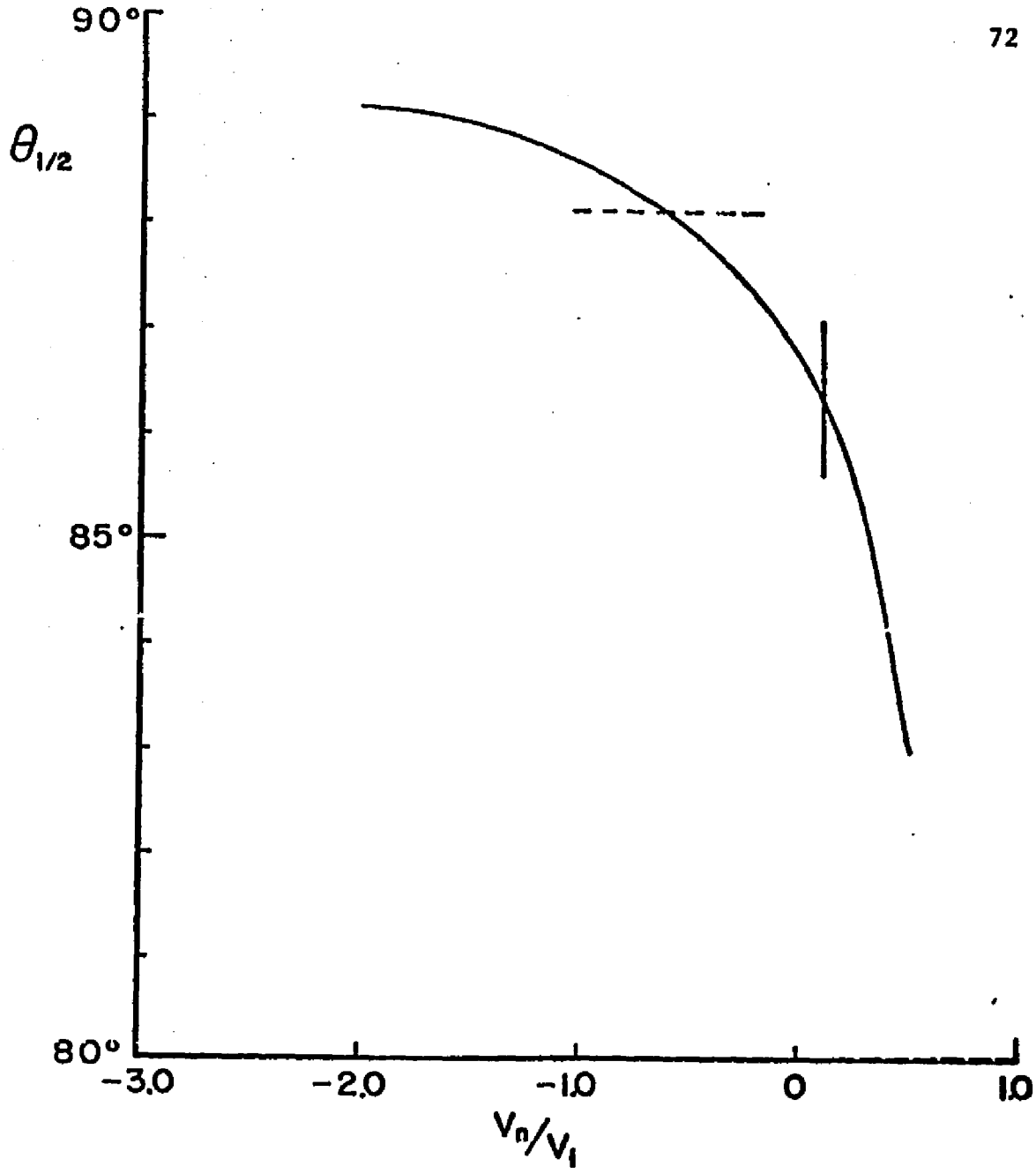

Fig. 11. Angle at which γ/Ω_{LH} falls to one half of its maximum value as θ is decreased, $\theta_{1/2}$, versus v_n/v_i. Other parameters are held constant at $v_d/v_i = 4.0$, $\beta_e = 0.25$, and $T_e/T_i = 1.0$. Leftmost point on the curve corresponds to a value of v_n/v_i which satisfies the sheath condition while rightmost point on the curve corresponds to the shock condition. The solid vertical line represents the minimum value of v_n/v_i at which the maximum growth rate is at $\theta = 90^o$. The horizontal dashed line indicates the $\theta_{1/2}$ of the modified two stream instability in its electrostatic approximation with no gradients and other parameters remaining the same.

bar. The curve shows how density gradients in the direction opposite to the magnetic field tend to confine the instability in the perpendicular direction while the opposite trend is evident when the density and magnetic field gradients are in the same direction. These results are in qualitative agreement with similiar plots by Gladd(Figure 3,1975).

For comparative purposes the $\theta_{1/2}$ associated with the modified two stream in its electrostatic limit with no gradients and a drift of $v_d/v_i = 4.0$ is provided by the horizontal dashed line. Notice that this value ascribes more oblique propagation to the instability than is present when the sheath condition is applied.

The degree of wave propagation in the oblique direction is crucial in determing how much a cross field current instability contributes to anamolous transport along field lines. For example, Caponi and Krall (1975) have determined that the ratio of the anomalous heat production frequency produced by turbulence driven by cross field drift instabilities along field lines $\nu_{\|}$ and across field lines $\nu_{\perp}$, $\nu_{\|}/\nu_{\perp}$, is proportional to the ratio $k_z^2/k_\perp^2$ where k_z and $k_\perp$ are values of wave number components averaged over the region in $\underline{k}$ space containing the instaiblity. Therefore Figure 11 provides a measure of the size of $\nu_{\|}/\nu_{\perp}$ and shows that its magnitude depends upon the magnitude and sign of the density gradient drift.

With respect to the shock case it is important to consider the relationship and relative importance of the modified two stream and ion acoustic instabilities since both of these may be active in a shock when $T_e > T_i$, a condition which is not unusual in the plasma of the

earth's bow shock(Montgomery et.al.,1970). In Figure 12 $T_e/T_i = 10$, $v_d/v_i = 20$, and $\beta_e = 0.25$ are used with the shock condition. In this illustration, θ is fixed at 85^o and the wavenumber is varied so that at $ka_e < 1$ the modified two stream instability is present, but as ka_e increases, the ion acoustic instability appears.

The three curves shown in the figure represent the electrostatic approximation (line of open circles), fully electromagnetic results without gradients (dotted line), and fully electromagnetic results with gradients determined by the shock condition (solid curve). The modified two stream instability at $ka_e < 1$ is influenced by both electromagnetic effects and by gradients. The ion acoustic instability at $ka_e > 1$, however, is not changed by either electromagnetic effects because of its short wave length or by gradients. The latter fact has previously been noticed by Gary(1970) and is also due to the relatively short wavelength nature of this mode.

These results are extended to other drift velocities in Figure 13 where growth rates as a function of the electron drift speed are plotted at $T_e/T_i = 4.0$ for both the ion acoustic instability (dotted lines) and the modified two stream mode (solid lines). Like the modified two stream instability with no gradient effects in Figure 6, growth rates of this instability in the present case are reduced by finite β_e effects more at higher than at lower drift speeds. More significantly β_e does not substantially affect the ion acoustic instability. This coupled with the fact that estimates of the anomalous resistivity due to turbulence produced by the ion acoustic instability are much greater than estimates due to turbulence produced

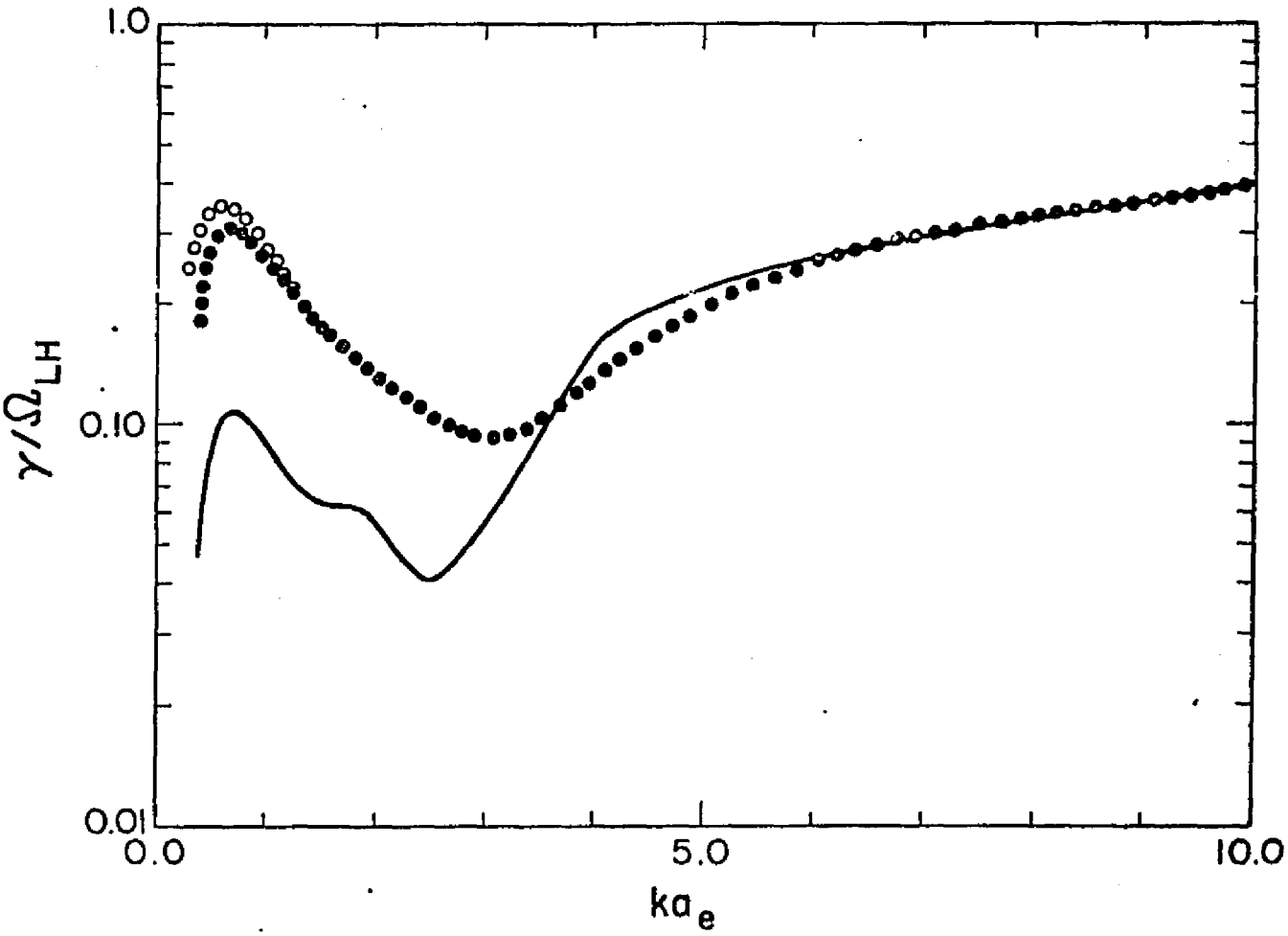

Fig. 12. γ/Ω_{LH} versus ka_e for $\theta = 85^{\circ}$, $v_d/v_i = 20$, $\beta_e = 0.25$, and $T_e/T_i = 10$. The line of open circles is the electrostatic approximation with $v_n = \langle v_B \rangle = 0$; the dashed curve is the electromagnetic dispersion relation also with no gradients; and the solid curve includes electromagnetic effects and $v_n = \langle v_B \rangle = \beta_e v_d/2$. Both the modified two stream and ion acoustic instabilities are present.

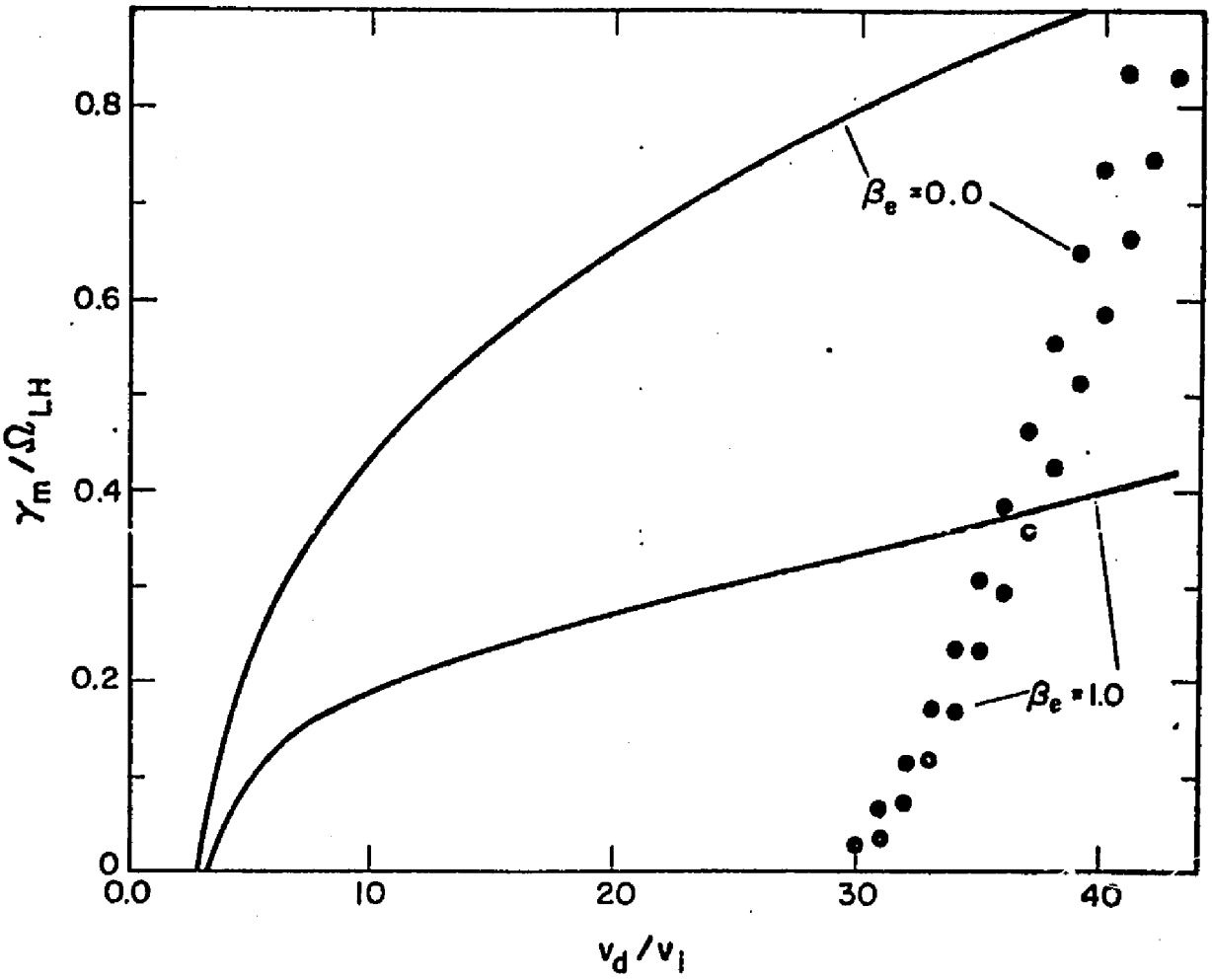

Fig. 13. Maximum growth rate, γ/Ω_{LH}, when the shock condition is satisfied, as a function of electron drift speed v_d/v_i for $\beta_e = 0$ and 1.0. $T_e/T_i = 4.0$. The solid lines represent the modified two stream instability; the dotted curves, the ion acoustic.

by the modified two stream instability (Lemons and Gary,1977AA) suggests that in high T_e/T_i shocks the ion acoustic is the dominant instability.

In theta pinch sheaths and future thermonuclear reactors $T_e/T_i \lesssim 1$ is the more likely condition. Therefore in these applications the ion acoustic instability need not be considered and the lower hybrid drift is probably the most important instability. Maximum growth rates of the lower hybrid drift instability are shown in Figure 14 as a function of v_d/v_i for various β_e when the sheath condition is satisfied. All these growth rates occur for $\theta = 90^o$ and substantially agree with those of Davidson et. al. (Figure 4,1977). Increasing β_e decreases growth rates monotonically for all v_d/v_i although the effect is larger at relatively small values of the drift speed. This lead Davidson et. al. (1977) to suggest that finite β_e effects may be able to stabilize the lower hybrid drift instability in the low drift velocity regime, $v_d/v_i < 1$, characteristic of post implosion theta pinches. However, an accurate determination of the β_e necessary for stabilization requires consideration of ion magnetic effects for reasons already discussed.

Figure 15 also concerns the lower hybrid drift instability under the sheath condition. Like Figure 5 for the modified two stream instability, it plots growth rates(dotted lines) and $|E^{(1)}/B^{(1)}|^2$ (solid line) versus ka_e. Parameter values are $\beta_e = 1.0$ and $v_d/v_i = 8.0$. As in Figure 5 the parameter which determines the extent to which the energy of the instability is contained in the magnetic field is the wavenumber. However in contrast to the modified two stream instability, the lower hybrid drift is predominately

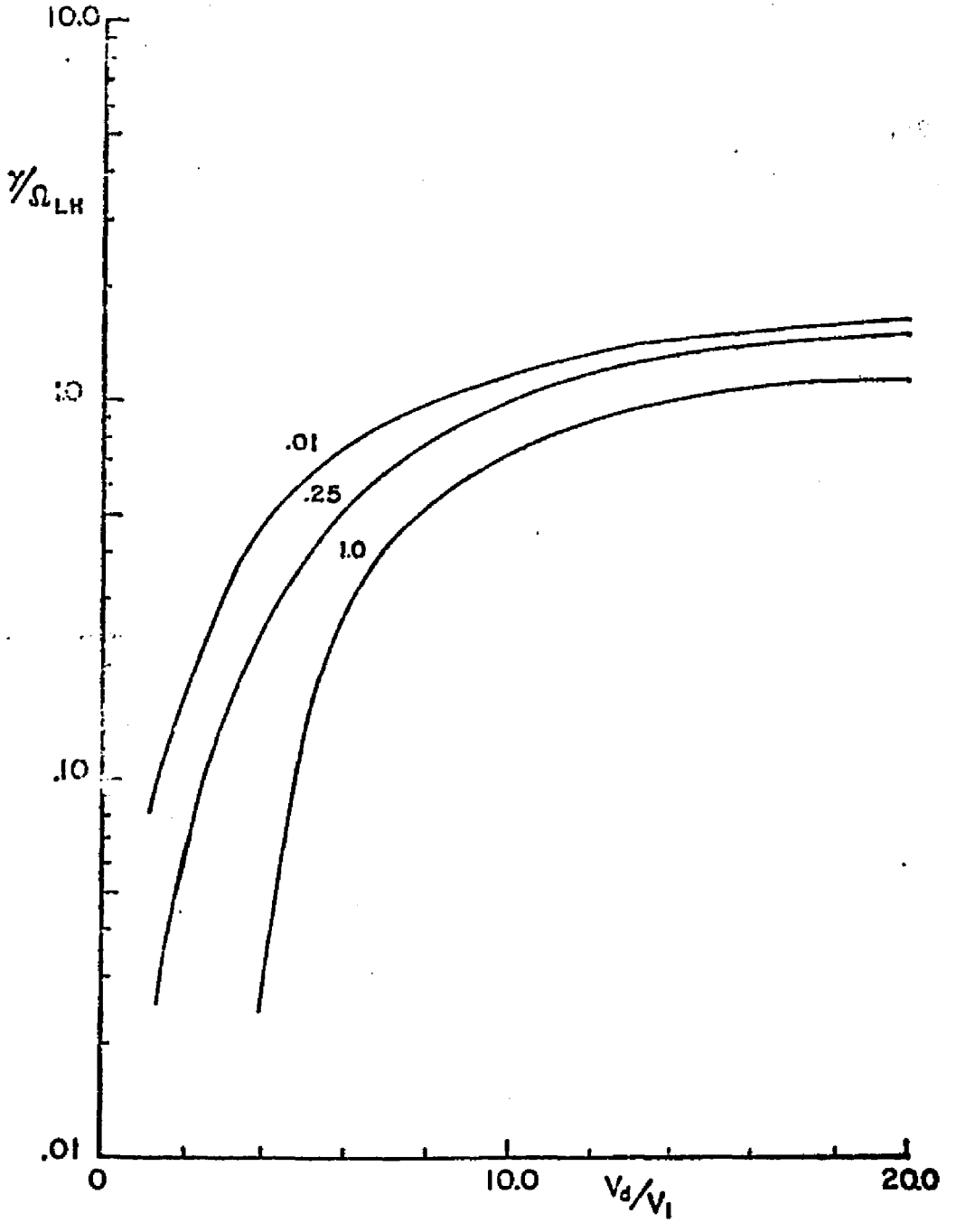

Fig. 14. Maximum growth rate of the lower hybrid drift instability as a function of v_d/v_i for β_e = 0.01, 0.25, and 1.0. The sheath condition holds, $v_n = -(T_e/T_i)v_o$. T_e/T_i = 1.0.

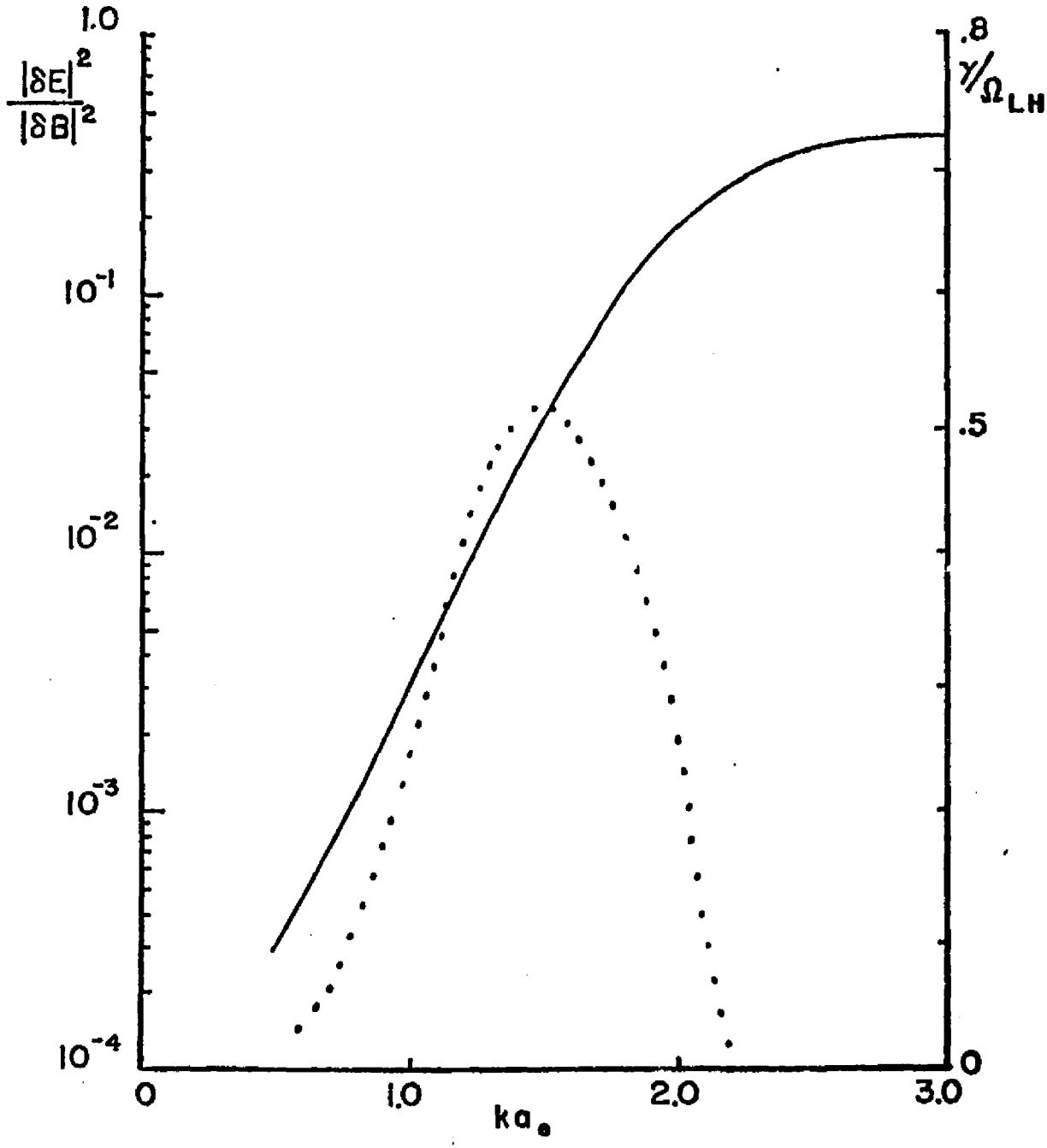

Fig. 15. Plot of $|E^{(1)}/B^{(1)}|^2$ (solid line; left hand ordinate axis) and γ/Ω_{LH} (dotted line) versus ka_e at $\theta = 89.5^\circ$ for the lower hybrid drift instability when the sheath condition is satisfied. $v_d/v_i = 8.0$, $\beta_e = 1.0$, and $T_e/T_i = 1.0$.

electromagnetic at $ka_e = 1.0$. This suggests that nonlinear theories of the lower hybrid drift instability based on the electrostatic approximation (Davidson and Gladd, 1976) need reexamination.

This section concludes with two figures illustrating the general effects of different values of ω_{pe}/Ω_e and T_e/T_i on the lower hybrid drift instability when the sheath condition holds. Throughout these variations the angle of maximum growth rate is always 90°. In both figures $v_o/v_i = 4.0$, the growth rates are represented by solid lines, and wave numbers by dashed lines.

ω_{pe}/Ω_e is varied over three orders of magnitude in Figure 16. For many space and thermonuclear plasmas of interest $\omega_{pe}/\Omega_e \gtrsim 10$ (Table 1-1, Boyd and Sanderson, 1969). In this parameter regime growth rates change by less than one percent from $\omega_{pe}/\Omega_e = 10$ to $\omega_{pe}/\Omega_e = 100$. This result holds for the electromagnetic ($\beta_e = 1.0$) as well as the electrostatic ($\beta_e = 0.01$) instability.

In Figure 17, ω_{pe}/Ω_e is set equal to 68 and T_e/T_i is changed. Growth rates increase with T_e/T_i although the effect is not strong.

The dispersion properties reported in this section can be summarized by dividing them into those associated with the shock condition which implies the presence of the modified two stream instability and those associated with the sheath condition and the lower hybrid drift instability. The modified two stream instability has substantial oblique propagation. Its growth rates are reduced by finite β_e and therefore have growth rates much less than the ion acoustic instability in a shock with $T_e > T_i$ when both modes are unstable. The lower hybrid drift instability is confined to a

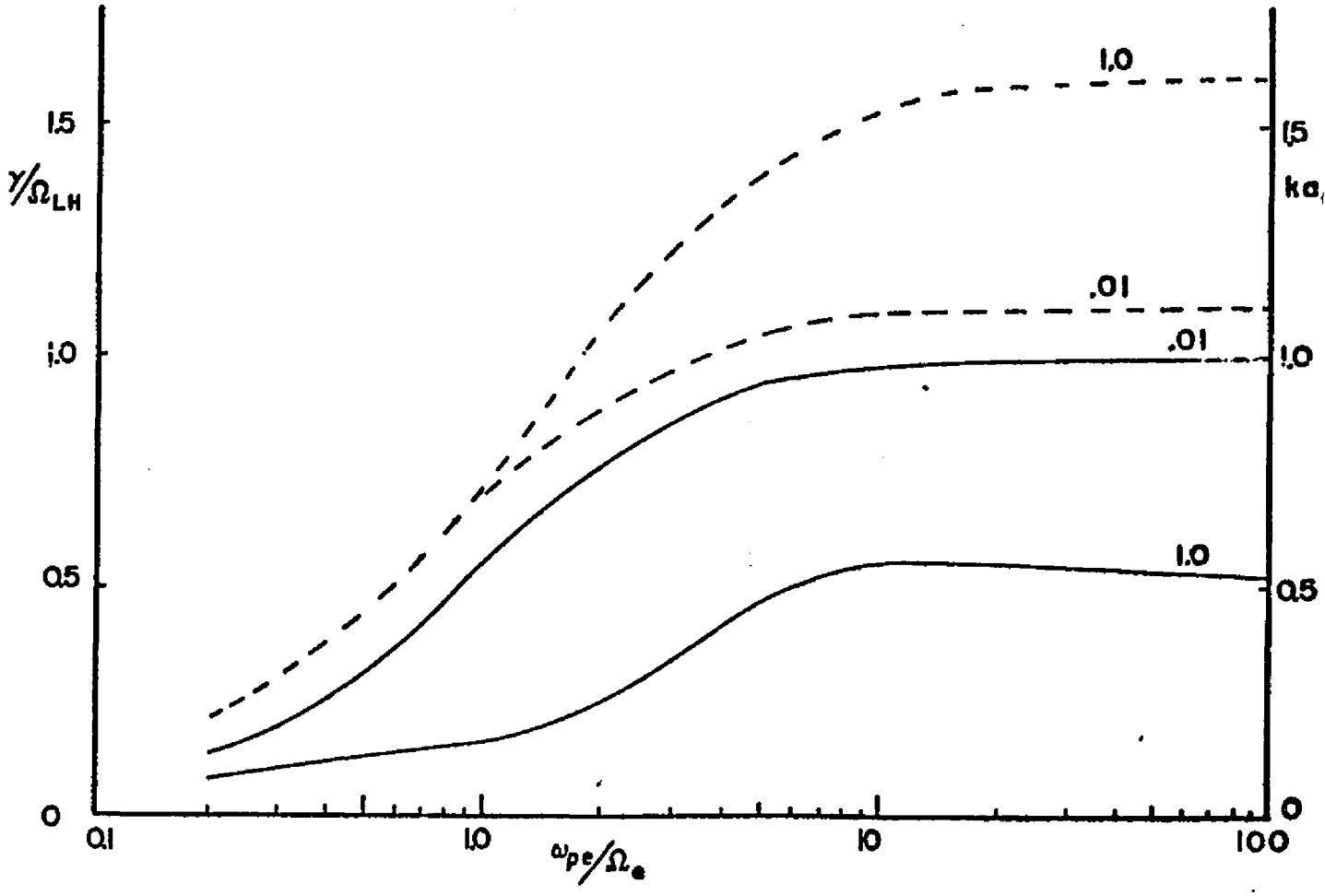

Fig. 16. Variation of lower hybrid drift instability maximum growth rates γ/Ω_{LH} with ω_{pe}/Ω_e for β_e = 0.01 and 1.0. Sheath condition is satisfied, v_d/v_i = 8.0 and T_e/T_i = 1.0.

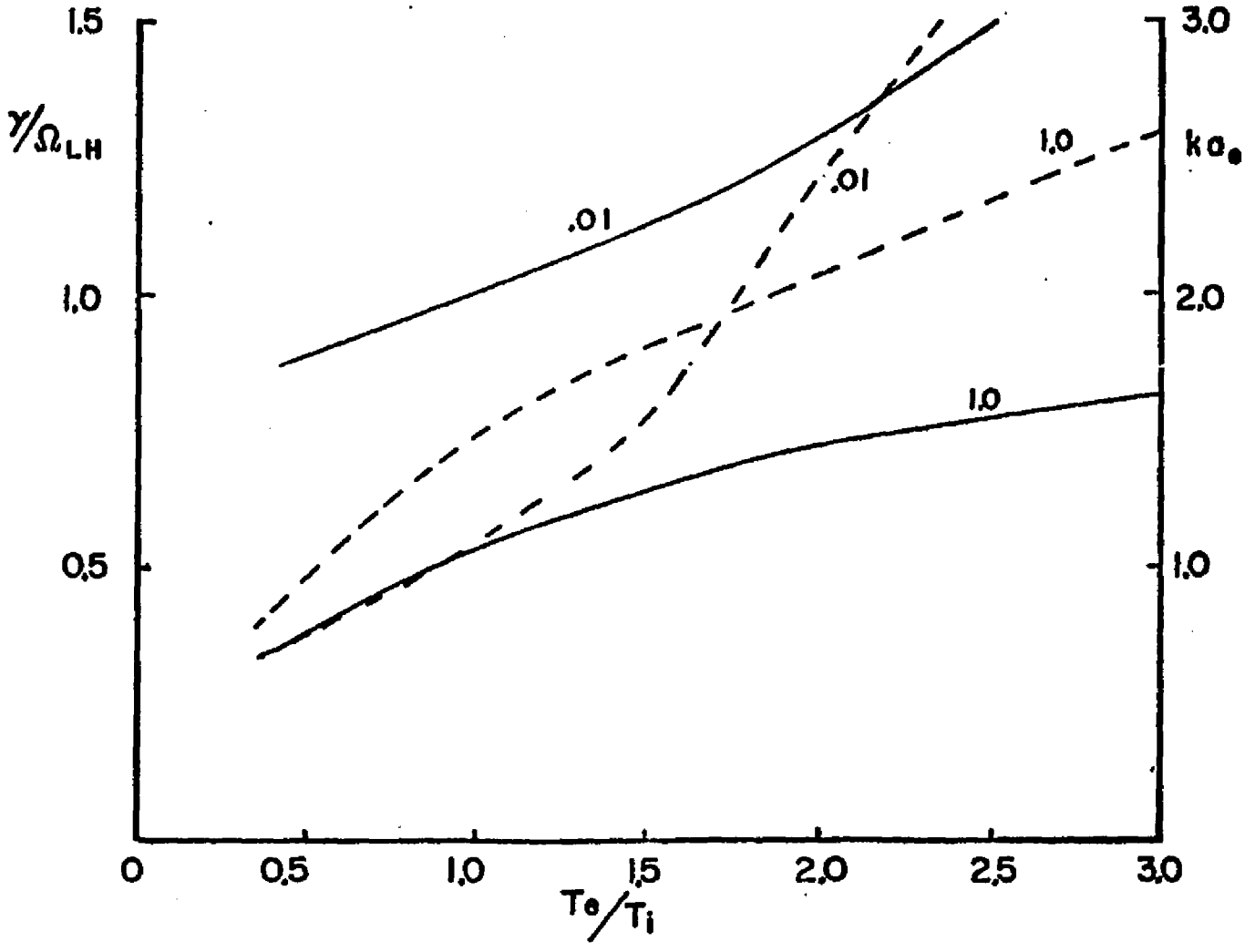

Fig. 17. Variation of lower hybrid drift instability maximum growth rates with T_e/T_i for β_e = 0.01 and 1.0. Sheath condition is satisfied and v_d/v_i = 8.0.

relatively small cone of propagation around the perpendicular to the magnetic field. Its growth rates are also reduced by finite β_e especially at low drift speeds. The major portion of its energy is contained in fluctuating magnetic fields and variations in parameters ω_{pe}/Ω_e and T_e/T_i make little difference in its dispersion properties.

Since the steady state electron distribution function used in this dissertation does not include an electron temperature gradient, results from other work on this gradient will now be summarized. In general an electron temperature gradient causes a macroscopic drift, $\underline{v}_T$, given by

$$\underline{V}_T = \frac{c\,\underline{B} \times \nabla T}{e B^2}$$

When the geometry of equations III-1 is used $\underline{v}_T$ may either add to or subtract from the $\underline{E}\times\underline{B}$ drift depending upon whether or not the temperature gradient respectively opposes or is in the same direction as the magnetic field gradient.

In a perpendicular shock if the plasma adiabatically heats as it passes through the magnetic gradient, the temperature gradient, as well as the magnetic field and density gradients will point in the same direction. Priest and Sanderson (1972) and Allen and Sanderson (1974) have demonstrated that in this case the temperature gradient enhances the growth rate of the ion acoustic instability. Huba and Wu (1975) and Davidson et. al. (1977) have demonstrated the same result for the lower hybrid drift instability.

In plasma sheaths characteristic of various magnetic confinement devices the temperature gradient could conceivably point in either

direction depending upon whether the major heat loss is across or along field lines. When the temperature gradient is in the direction opposite to the magnetic field, as might be the case in a toroidal Z pinch where the only heat loss is across the magnetic field, growth rates of the lower hybrid drift instability are reduced (Davidson et. al.,1977). More detailed statements concerning the role of temperature gradients in cross field drift instabilities must wait further research.

VII. SUMMARY AND CONCLUSIONS

The results of this work include both dispersion properties of cross field current instabilities and conculsions concerning the consequences of these properties for shocks and sheaths. In this chapter these results are summarized and discussed.

Several statements may be made summarizing dispersion properties of crossfield current instabilities found in the course of this study. First, electromagnetic effects are important only when $\beta_e/(ka_e)^2 > 1$. This has been demonstrated by the analytical work of others (e.g. Callen and Guest,1973) and confirmed by the present numerical results (Figures 2,3,and 13). In general, electromagnetic effects reduce growth rates (Figures 6,8,13,and 14) and spread the direction of propagation of the instability away from the perpendicular (Figures 3a, and 7a) although the latter effect applies more to the modified two stream instability than to the lower hybrid drift instability (Figure 10a). In the absence of temperature gradients the orientation of the density gradient with respect to the magnetic field determines the direction of propagation of the instability (Figures 10a and 11). When these two gradients are in opposite directions maximum growth rate occurs for propagation in the oblique direction implying the modified two stream instability. When the gradients are in the same direction the instability has a maximum growth rate in the perpendicular direction implying the presence of the lower hybrid drift instability.

Both of these instabilities have a substantial part of their field energy in the fluctuating magnetic field.

Finite beta effects are different for the modified two stream and lower hybrid drift instabilities. On the former they reduce growth rates produced by high drift speeds, $v_d > v_i$, more than they reduce growth rates near marginal stability, $v_d \sim v_i$ (Figures 6 and 13). In contrast, lower hybrid drift instability growth rates are reduced more at low drift speeds than at high ones (Figure 14).

Unlike the lower hybrid drift and modified two stream instabilities the ion acoustic instability is influenced neither by electromagnetic or magnetic field and density gradient effects (Figure 12). In a $T_e > T_i$ shock it competes with the modified two stream instability. In this situation the ion acoustic has higher threshold drift speeds but also larger growth rates than the modified two stream (Figures 12 and 13).

These dispersion properties suggest several conclusions regarding wave and wave processes in the earth's bow shock. The conclusions, however, are made tentatively and are meant to provide direction for further research.

(1) The modified two stream instability can cause appreciable growth in the bow shock. An instability driven by crossfield currents within the bow shock must grow for a period of several e-folding times while it is in the shock in order to have any influence upon the transport process within it. Therefore the number of e-folding times of an instability in the bow shock, n, is related to the instability

growth rate γ, the bow shock width, ΔL, and the solar wind speed parallel to the shock normal, v_{sw}, by $n = \Delta L\gamma / v_{sw}$.

In order to arrive at an estimate of the size of n, values for ΔL and v_{sw} are taken from four observations of the quasi perpendicular laminar bow shock reported by Greenstadt et. al. (1975). In these cases $\Delta L/v_{sw}$ was a measured quantity with values spanning .26 to 1.4 seconds, while the average magnetic field in the bow shock took on values of 7.5 to 13.5 gammas. The average magnetic field is necessary to determine Ω_{LH}, the frequency which characterizes the size of γ. Consulting Figure 13, $\gamma = \Omega_{LH}/2$ is chosen as a representative growth rate of the modified two stream instability in a finite beta shock. When the above numbers are used the result is $7 < n < 47$. Since $n = 7$ corresponds to a 1000 fold increase in field amplitude, the modified two stream instability may undergo appreciable growth in the bow shock.

(2) When $T_e > T_i$ the ion acoustic mode is the most important in the bow shock. At large temperature ratios, the ion acoustic threshold drift speed is well beow the electron thermal speed. In this regime, β_e has little effect on this instability and the electron cyclotron drift instability is probably wiped out by its very narrow range of propagation about the perpendicular. We disagree with the conclusion of Wu and Fredricks (1972) that $\beta = 1$ "practically excludes" the cross field ion acoustic instability. Their conclusion was based on the assumption that $ka_e \sim 1$ was necessary to obtain this mode; Figure 12 illustrates that this is not the case.

Comparison of the ion acoustic with the modified two stream instability involves more detailed arguments. Figure 13 shows that the

growth rate for the former mode increases much more rapidly after threshold than that of the latter instabilities. Figure 3 of Rodriquez and Gurnett (1975) shows that the increase in electric fluctuations for the ion acoustic frequencies through the shock is several orders of magnitude greater than that for the lower frequencies.

In certain cases a shock width may be determined by the drift velocity threshold of a cross field current instability according to a criterion due to Manheimer and Boris (1972) which states, in effect, that the nonlinear action of turbulence due to a current-driven instability is to maintain v_d above, but close to, an instability threshold. This drift may then be related to the magnetic field increase across the shock ΔB and shock width ΔL via Ampere's Law. Morse and Greenstadt (1972) have used this criterion and the above mentioned data to determine that at least in these cases the bow shock width is consistent with threshold drift speeds of the ion acoustic instability. This justifies our use of a growth rate of $\gamma = \Omega_{LH}/2$ for the modified two stream instability calculation (e.g. Figure 13) but raises the question of why the threshold v_d of the modified two stream instability, which is lower than that of the ion acoustic instability, does not determine the bow shock width.

The answer to this question may have to do with the different ways in which these instabilities scatter particles. If the wave-particle interactions due to an instability of low threshold (the modified two stream) are not strong enough to significantly slow the electron drift speed, the macroscopic forces in the shock will continue to increase v_d until it reaches the higher threshold of a stronger instability (in

this case, the ion acoustic). This conjecture is supported by a comparison of the anomalous resistivity due to these instabilities (Lemons and Gary,1977B).

(3) Rodriguez and Gurnett (1975) have suggested that the low values of the ratio $|E^{(1)}/B^{(1)}|^2$ observed in the bow shock are due to electromagnetic whistler modes. This could be the case. However observations are also consistent with the possibility that these fluctuations are due to crossfield drift instabilities at long wave lengths (Figure 5).

With regard to plasma sheaths these results have several implications which in turn point the way to future studies.

(1) The lower hybrid drift instability appears to be the most important instability in the sheath configuration (Figure 10a), as previously indicated by Gladd (1976). Indeed, Figure 10a shows that the modified two stream instability is not present when density and magnetic field gradients point in the same direction. The effects of electron temperature gradients may be important in this context and need to be studied before a more conclusive statement can be made.

(2) Finite beta effects reduce growth rates (Figures 8 and 14) of the this instability and also raise threshold drift velocities. This conculsion was earlier suggested by Davidson et. al. (1977). However, an investigation of this possibility requires working in the low drift velocity regime, $v_d < v_i$, in which $\omega \sim \Omega_i$ and $ka_i \sim 1$ where ion magnetic effects must be considered.

(3) Electromagnetic fields and their effects are an important part of the lower hybrid drift instability. Fluctuating magnetic fields

contain most of its energy and therefore need to be included in both particle simulations and theories of anomalous transport. Among the latter, in particular, are those theories which the use the Fowler bound method by assuming a limited amount of free energy in the plasma and relating this energy to the energy of the fluctuating fields (Fowler,T.K.,1968). Amplitudes of the fluctuating fields driven by the lower hybrid drift instability in a finite beta plasma calculated by this method will be in error by orders of magnitude unless the energy of the fluctuating magnetic field is taken into account.

VIII. APPENDIX

A. Steady State Fluid Equations

The choice of fields and distribution functions in Chapter II, Steady State, and their relationship to shock and sheath configurations may be motivated from an examination of the steady state fluid equations for a single species of an inhomogeneous plasma. In the following geometry, field and fluid quantities are allowed to be functions of only one Cartesian coordinate, x, magnetic field lines are straight lines with unit vectors pointing in the z direction, and electric fields and flow velocities $\underline{V}$ lie in the x-y plane:

$$\frac{\partial}{\partial \underline{x}} = \left(\frac{\partial}{\partial x}, 0, 0\right)$$

$$\underline{B} = (0, 0, B)$$

$$E = (E_x, E_y, 0)$$

$$\underline{U} = (U_x, U_y, 0)$$

Using this geometry the first two velocity moments of the steady state Vlasov equation yield;

$$\frac{\partial}{\partial x} n U_x = 0 \qquad \text{(A-1)}$$

$$\frac{\partial}{\partial x}\left(nT_{\perp} + mnU_x\right) = qn\left(E_x + \frac{U_y B}{c}\right) \tag{A-2}$$

$$\frac{\partial}{\partial x}\left(mnU_x U_y\right) = qn\left(E_y - \frac{U_x B}{c}\right) \tag{A-3}$$

Equation A-1 is the time independent continuity equation while equation A-2 and A-3 represent momentum balance. In addition the steady state Maxwell equations require, in a two fluid electron-ion plasma,

$$\frac{\partial}{\partial x} E_y = 0 \tag{A-4}$$

$$\frac{\partial}{\partial x} B = \frac{4\pi e}{c}\left(n_e U_{ye} - n_i U_{yi}\right) \tag{A-5}$$

$$0 = \left(n_e U_{xe} - n_i U_{xi}\right) \tag{A-6}$$

$$\frac{\partial E_x}{\partial x} = 4\pi e\left(n_i - n_e\right) \tag{A-7}$$

Here equation A-4 is implied by Faraday's Law, equations A-5 and A-6 by Ampere's Law and equation A-7 by Poisson's equation. Subscripts "i" and "e" refer respectively to ion and electron.

The steady state sheath is characterized by the absence of any plasma flow through the magnetic inhomogeneity. In the present notation this flow is represented by V_x. According to equation A-3 the vanishing of V_x also requires a zero E_y. Therefore the sheath limit is

attained by taking $V_x = 0$ and $E_y = 0$. In this case equations A-1,A-3, and A-6 are identically satisfied. Equation A-2 may then be solved for the drift velocity V_y

$$V_y = -\frac{cE_x}{B} + \frac{1}{\Omega}\frac{T_\perp}{m}\frac{\partial}{\partial x}\ln n T_\perp \qquad \text{(A-8)}$$

When expressions for the steady state fields, equation II-1, are used and temperature gradients are ignored, the resulting expression for the electron drift from the fluid equation A-8 is identical to that implied by the electron distribution function constructed from constants of motion in Chapter II, equation II-3. Equation A-8 also applies to the ions within a sheath if they have had time to respond sufficiently to the fields.

When the pressure gradient acting on the ions is balanced by the electric field in the x direction the ions are "electrostatically confined". In this limit , $V_y = 0$, and in the absence of temperature gradients equation A-8 for the ions reduces to

$$\frac{cE_x}{B} = \frac{T_{\perp i}}{\Omega_i m_i}\frac{\partial}{\partial x}\ln n$$

or

$$V_o = -\frac{T_{\perp i}}{T_{\perp e}} V_n \qquad \text{(A-9)}$$

which is identical to equation II-7 in Chapter II.

A consistent shock steady state with sufficient simplicity for use as a basis for a linear dispersion relation has not yet been constructed. The shock configuration ($V_x \neq 0$) is in general much more complicated than that of the sheath and consequently can be represented by the steady state in Chapter II only under several approximations. Here we identify these approximations.

In the limit of massless electrons, the electron fluid equations A-1 through A-4 can be reduced to the following equations

$$n U_x = \text{const.} \tag{A-10}$$

$$B U_x = \text{const.} \tag{A-11}$$

$$U_y = -\frac{cE_x}{B} + \frac{1}{\Omega}\frac{T_i}{m}\frac{\partial}{\partial x}\ln nT_i \tag{A-12}$$

$$U_x = \frac{cE_y}{B} \tag{A-13}$$

Equations A-10 and A-11 imply equal electron density and field gradients, a result identified as the "shock condition" in Chapter II, while equation A-12 is identical to A-8 and equation II-3.

When the ion thermal velocity is small compared to the flow velocity, V_x, and other drift velocities, a condition which is not always met in this dissertation, the cold ion limit ($T_i = 0$) becomes valid. Then when charge nuetrality, $n_e = n_i$, is required the ion fluid equations reduce to

$$U_y = 0 \tag{A-14}$$

$$m U_x \frac{dU_x}{dx} = q E_x \tag{A-15}$$

$$U_x = c E_y / B \tag{A-16}$$

Equation A-16 is identical to A-13 and emphasizes the fact that the ions and electrons flow through the shock at the same speed. Equation A-15 indicates that the E_x field serves only to slow down the ions as they pass through the shock while A-14 says that no macroscopic ion drifts are driven by gradients.

B. Neglect of Small Terms in Orbit Equation

The neglect of terms in the orbit equations, III-17, proportional to trigonometric functions and $\epsilon_B v_1/\Omega_e$ is reasonable because of the way in which these terms enter into the dispersion relation. The dispersion relation formed with equations III-6 and III-13 contains integrals of the form

$$\int_0^{2\pi} d\phi \int_0^{\infty} d\tau \; e^{i\underline{k}\cdot(\underline{x}'-\underline{x})} \; q(\phi,\tau)$$

where $g(\phi,\tau)$ is a function of the time parameter τ and velocity variable θ which is determined by the zero order distribution function, while the vector $\underline{x}'-\underline{x}$ is determined by the orbit equations. From the complete orbit equations through first order in $\epsilon_B v_\perp/\Omega_e$, III-17, the above exponential function would contain terms to first order in $\epsilon_B v_\perp/\Omega_e$ which are both oscillatory

$$e^{\frac{iK_y V_\perp}{\Omega_e}\sin\left(\frac{\epsilon_B V_\perp}{\Omega_e}\sin\phi\right)}$$

$$e^{\frac{i\epsilon_B K_y V_\perp^2}{\Omega_e^2}\sin\Omega_e\tau}$$

and secular in $\Omega_e\tau$

$$e^{\frac{i\epsilon_B K_y V_\perp^2}{2\Omega_e^2}\Omega_e\tau}$$

For weak gradients, $\epsilon_B v_\perp/\Omega_e \ll 1$, as is considered in this dissertation the exponentials may be expanded so that

$$e^{\frac{iK_y V_\perp}{\Omega_e}\sin\left(\frac{\epsilon_B V_\perp}{\Omega_e}\sin\phi\right)} \approx 1 + \frac{i\epsilon_B K_y V_\perp^2}{\Omega_e^2}\sin\phi$$

$$e^{\frac{iK_y\epsilon_B V_\perp^2}{2\Omega_e^2}\sin\Omega_e\tau} \approx 1 + \frac{i\epsilon_B K_y V_\perp^2}{2\Omega_e^2}\sin\Omega_e\tau$$

Therefore when integrations over ϕ and τ are performed the $\sin\phi$ and $\sin\theta\tau$ terms are small compared to the secular term.

These expansions and integrations have been done explicitly in the case of the electrostatic dispersion relation. Numerical evaluation of the resulting dispersion relation has revealed that the contribution of the oscillating terms to first order in $\epsilon_B v_\perp/\Omega_e$ treated in this approximation are indeed negligible. Although contributions of these terms to an electromagnetic dispersion relation have not been calculated it is felt that results will be no different from those based on an electrostatic dispersion relation since the integrations involved are formally similar.

C. Computer Programs and Sample Output

Below are listings of the computer programs and output discussed in Chapter V. First is a program solving the dispersion relation, equation III-22, with the matrix elements $R_{i,j}$ associated with gradient drifts, equation III-21. This is followed by a similiar program for the homogeneous case, equation III-24. A typical page of computer output for the latter program completes this appendix.

PLEASE NOTE:

Pages 98-108 are a computer print-out. Print is very broken and indistinct. Best avialable copy. Filmed as received.

UNIVERSITY MICROFILMS

```
T1,40
  1 C   IONS:  HOT,UNMAGNETIZED
  2 C   ELECTRONS:  HOT,MAGNETIZED
  3 C         E CROSS B, GRAD B, AND GRAD N DRIFTS
  4 C         PERPENDICULAR TO B
  5 C   WAVES:  OBLIQUE PROPAGATION
  6 C   REQUIRES SUBROUTINES:  PDF,FCFCN,OBJ,CQSF,ZEARCH,OUTPUT
  7 C
  8         COMMON C,S,ZERO,NBMAX,NTRIAL,INDC,NELS
  9         COMMON/PARAM/ BETAE,TEOTI,MEOMI,VEOVI,VD,VN,VB,WRATIO,THETA
 10         COMMON/FIELDS/ PHASQ,EXOESQ,TNOTOT,EOBSQ
 11         DIMENSION FACTP(500),FACTM(500)
 12         DIMENSION BSJ(100),DBSJ(100),BSJSQ(100),BLOW(100)
 13         REAL MEOMI
 14         COMPLEX S,SSQ,SNEW,ZERO,ZEROLD,IMAG,LAMBDA
 15         COMPLEX ZARGI,ZI,DZI,DDZI
 16         COMPLEX ZARGEP(100),ZEP(100),DZEP(100),DDZEP(100)
 17         COMPLEX ZARGEM(100),ZEM(100),DZEM(100),DDZEM(100)
 18         COMPLEX RXX,RYY,RZZ,RXY,RYZ,RXZ
 19         COMPLEX XX,YY,ZZ,XY,XZ,YZ
 20         COMPLEX XXG(500),YYG(500),ZZG(500),XYG(500),XZG(500),YZG(500)
 21         COMPLEX XXI(500),YYI(500),ZZI(500),XYI(500),XZI(500),YZI(500)
 22         COMPLEX P1,P2,P1C,P2C
 23         COMPLEX CHECK
 24         DATA STOP/1.0 E-3/
 25         IMAG=CMPLX(0.0,1.0)
 26         NBMAX=4
 27 C
 28 C
 29 C   PLASMA PARAMETERS
 30         NELS=2
 31         MEOMI=1.0/3674
 32         TEOTI=1.0
 33         VEOVI=SQRT(TEOTI/MEOMI)
 34         BETAE=0.25
 35         VN=0.0
 36         VD=4.0
 37         WRATIO=68
 38         WRSQ=WRATIO*WRATIO
 39       5 TYPE 810
 40     810 FORMAT(/5X,10HENTER DATA/)
```

```
T41,90
      READ(5,815)NELS
  815 FORMAT(I1)
      READ(5,820) VD,BETAE,THETA,NBMAX
  820 FORMAT(3F10.0,I2)
      BETWO=BETAE/2.0
      VB=BETWO*VD
      VN=-TEOTI*VD/(1+TEOTI)
      VD=VD+VN
      VD=VD/VEOVI
      VN=VN/VEOVI
      VB=VB/VEOVI
      COSINE=COSD(THETA)
      COSQ=COSINE*COSINE
      SINE=SIND(THETA)
      SINSQ=SINE*SINE
      TAN=SINE/COSINE
      TANSQ=TAN*TAN
C
C  FIRST GUESS FOR WAVE NUMBER C AND FREQUENCY S
   20 READ(5,830) CSTART,S,DC,NPRINT
  830 FORMAT(4F10,I2)
C
C  INCREMENT WAVE NUMBER BY DC WITH DO LOOP
      DO 600 INDC=1,NPRINT
      C=CSTART+(INDC-1)*DC
      CSQ=C*C
      NTRIAL=-1
C
C  CALCULATE ELEMENTS OF DISPERSION RELATION
   50 SSQ=S*S
      ZARGI=S*VEOVI/(1.414213*C)
      CALL PDF(ZARGI,ZI,DZI)
      DDZI=-2.0*(ZI+ZARGI*DZI)
      RXX=SSQ*BETWO/WRSQ-CSQ+MEOMI*BETWO*ZARGI*ZI
      RYY=SSQ*BETWO/WRSQ-CSQ*COSQ+MEOMI*BETWO*ZARGI*(COSQ*ZI-SINSQ*
     $      *ZARGI)+S*BETWO*(VB-VN)/(C*SINE)+BETWO*(VD-VN)*(VD-VB)
      RZZ=SSQ*BETWO/WRSQ-CSQ*SINSQ+MEOMI*BETWO*ZARGI
     $      *(SINSQ*ZI-COSQ*DZI*ZARGI)
      RYZ=COSINE*SINE*(CSQ+MEOMI*BETWO*ZARGI*DDZI/2.0)
      LAMBDA=(S-SINE*C*(VD-VN))/(1.414213*C*COSINE)
C
C
C  INTEGRATION OF V-PERP INTEGRALS
C  STEP SIZE:  H
C  UPPER LIMIT OF INTEGRATION:  VMAX
C  INTEGRATION VARIABLE:  V
      H=0.05
      IF(THETA.GE.89.51)H=0.05
      VMAX=6.0
      INMAX=VMAX/H+1.0
```

```
T91,140
 91 C  DO LOOP TO PREPARE VECTOR WITH VALUES OF INTEGRANDS
 92       DO 90 IN=1,INMAX
 93       V=H*(IN-1)
 94       VSQ=V*V
 95       BARG=SINE*C*V
 96 C
 97 C  CALCULATION OF ALL FRIED-CONTE AND BESSEL FUNCTIONS WITH DO LOOP
 98       NBMAP=NBMAX
 99       IF(NBMAX.EQ.1)NBMAP=NBMAX+1
100       DO 65 NN=1,NBMAP
101       N=NN-1
102       CALL BESJ(BARG,N,BSJ(NN),1.E-3,1000)
103       BSJSQ(NN)=BSJ(NN)*BSJ(NN)
104       VFACT=(VO-VB*VSQ*.5)
105       FACTM(NN)=VFACT-N/(C*SINE)
106       FACTP(NN)=VFACT+N/(C*SINE)
107       ZARGEP(NN)=(S+N-C*SINE*VFACT)/(1.414213*C*COSINE)
108       ZARGEM(NN)=(S-N-C*SINE*VFACT)/(1.414213*C*COSINE)
109       CALL PDF(ZARGEP(NN),ZEP(NN),DZEP(NN))
110       CALL PDF(ZARGEM(NN),ZEM(NN),DZEM(NN))
111       IF(NN-1)65,65,60
112    60 DBSJ(1)=-BSJ(2)
113       IF(BARG.EQ.0.0)BARG=1.0 E-6
114       DBSJ(NN)=BSJ(NN-1)-N*BSJ(NN)/BARG
115    65 CONTINUE
116 C
117 C  CALCULATION OF INTEGRANDS
118 C  ZERO ORDER (NN=1) BESSEL FUNCTION PART
119       XX=DBSJ(1)*DBSJ(1)*ZEP(1)
120       YY=BSJSQ(1)*ZEP(1)*VFACT*VFACT
121       ZZ=BSJSQ(1)*ZARGEP(1)*DZEP(1)
122       XY=BSJ(1)*DBSJ(1)*ZEP(1)*VFACT
123       XZ=BSJ(1)*DBSJ(1)*DZEP(1)
124       YZ=BSJSQ(1)*DZEP(1)*VFACT
125 C  INFINITE SUM PART
126       IF(NBMAX.EQ.1)GO TO 85
127       DO 75 J=2,NBMAX
128       XX=XX+DBSJ(J)*DBSJ(J)*(ZEP(J)+ZEM(J))
129       YY=YY+BSJSQ(J)*(ZEP(J)*FACTM(J)*FACTM(J)+
130      $       ZEM(J)*FACTP(J)*FACTP(J))
131       ZZ=ZZ+BSJSQ(J)*(ZARGEP(J)*DZEP(J)+ZARGEM(J)*DZEM(J))
132       XY=XY+BSJ(J)*DBSJ(J)*(ZEP(J)*FACTM(J)+
133      $       ZEM(J)*FACTP(J))
134       XZ=XZ+BSJ(J)*DBSJ(J)*(DZEP(J)+DZEM(J))
135       YZ=YZ+BSJSQ(J)*(DZEP(J)*FACTM(J)+
136      $       DZEM(J)*FACTP(J))
137    75 CONTINUE
138 C  INTEGRAND VECTORS DENOTED WITH A "G"
139    85 EXARG=V*EXP(-VSQ/2.0)
140       XXG(IN)=EXARG*VSQ*XX
*
```

```
T141,190
141         YYG(IN)=EXARG*YY
142         ZZG(IN)=EXARG*ZZ
143         XYG(IN)=EXARG*V*XY
144         XZG(IN)=EXARG*V*XZ
145         YZG(IN)=EXARG*YZ
146      90 CONTINUE
147 C
148 C   CALL INTEGRATION SUBROUTINE AND PREPARE ELEMENTS OF DISPERSION RELATI
149 C   INTEGRAL VECTORS DENOTED WITH A "I"
150         CALL COSF(H,XXG,XXI,INMAX)
151         CALL COSF(H,YYG,YYI,INMAX)
152         CALL COSF(H,ZZG,ZZI,INMAX)
153         CALL COSF(H,XYG,XYI,INMAX)
154         CALL COSF(H,XZG,XZI,INMAX)
155         CALL COSF(H,YZG,YZI,INMAX)
156         RXX=RXX+BETWO*LAMBDA*XXI(INMAX)
157         RYY=RYY+BETWO*LAMBDA*YYI(INMAX)
158         RZZ=RZZ-BETWO*LAMBDA*ZZI(INMAX)
159         RXY=-IMAG*BETWO*LAMBDA*XYI(INMAX)
160         RXZ=IMAG*BETWO*LAMBDA*XZI(INMAX)/1.414213
161         RYZ=RYZ-BETWO*LAMBDA*YZI(INMAX)/(1.414213)
162 C
163 C
164 C   DISPERSION RELATION
165         ZERO=RXX*(RYY*RZZ-RYZ*RYZ)+RXY*(RXY*RZZ-2*RXZ*RYZ)+RXZ*RXZ*RYY
166         IF(NELS.EQ.1)ZERO=RYY*SINSQ+RZZ*COSQ+2.0*SINE*COSINE*RYZ
167    400 FORMAT(2X,2E10.3,5X,2E10.3,5X,2E10.3)
168 C
169 C
170 C   SEARCH FOR ZEROS OF DISPERSION RELATION VIA SUBROUTINE "ZEARCH"
171         CALL ZEARCH(S,ZERO,SNEW,NTRIAL)
172 C
173 C   IF RELATIVE CHANGE IN S IS SMALL PUT RESULTS IN OUTPUT
174 C   OR IF AIMAG S IS OF ORDER OF REAL S STOP SEARCHING
175         RTEST=(REAL(SNEW)-REAL(S))/REAL(S)
176         AITEST=(AIMAG(SNEW)-AIMAG(S))/AIMAG(S)
177         S=SNEW
178         IF(ABS(RTEST).LT.STOP.AND.ABS(AITEST).LT.STOP)GO TO 500
179         IF(NTRIAL-10)50,500,500
180 C
181 C
182 C   BEFORE OUTPUTING RESULTS CALCULATE WAVE PHASE INFORMATION
183 C   PHASQ=SQUARE OF AMPLITUDE OF LONGITUDINAL E FIELD OVER TOTAL E FIELD
184 C   EXOESQ=SQUARE OF AMPLIUDE OF X E FIELD OVER TRANSVERSE E FIELD
185 C   TNOTOT=RATIO OF ENERGY IN TRANSVERSE FIELDS TO ENERGY IN TOTAL FIELD
186 C   EOBSQ=RATIO OF MAGNETIC FIELD ENERGY TO ELECTRIC FIELD ENERGY
187    500 P1=RXX*RYY+RXY*RXY
188         P1C=CONJG(P1)
189         P1SQ=REAL(P1*P1C)
190         P2=RXY*RXZ+RYZ*RXX
*
```

```
T191,240
191         P2C=CONJG(P2)
192         P2SQ=REAL(P2*P2C)
193         P3SQ=REAL((RXY*RYZ-RYY*RXZ)*CONJG(RXY*RYZ-RYY*RXZ))
194         PSQ=P1SQ+P2SQ+P3SQ
195         S2=REAL(S*CONJG(S))
196         DUM1=SINSQ*P2SQ+COSQ*P1SQ-2.0*COSINE*SINE*REAL(P2C*P1)
197         DUM2=COSQ*P2SQ+SINSQ*P1SQ+P3SQ+2.0*COSINE*SINE*REAL(P2C*P1)
198         DUM=S2*BETAE/(2.0*CSQ*WRSQ)
199         DUM3=1.0+DUM
200         PHASQ=DUM1/PSQ
201         EXDESQ=P3SQ/DUM2
202         EDBSQ=DUM*PSQ/DUM2
203         TNOTOT=(DUM3*DUM2)/(DUM3*DUM2+DUM1*S2*BETAE/(2.0*CSQ*WRSQ))
204 C
205         CALL OUTPUT
206    600  CONTINUE
207    700  GO TO 5
208 C
209 C
210 C
211 C
212    900  STOP
213         END
214         SUBROUTINE OUTPUT
215         COMMON C,S,ZERO,NBMAX,NTRIAL,INDC,NELS
216         COMMON/PARAM/ BETAE,TEQTI,NEQMI,VEQVI,VQ,VN,VB,WRATIO,THETA
217         COMMON/FIELDS/ PHASQ,EXDESQ,TNOTOT,EDBSQ
218         COMPLEX S,ZERO
219         REAL NEQMI
220 C
221 C   FIRST TIME THROUGH "OUTPUT" PRINT HEADINGS
222         IF(INDC.NE.1)GO TO 200
223         VQQVI=VEQVI*VQ
224         VNQVI=VEQVI*VN
225         VBQVI=VEQVI*VB
226 C
227         TYPE 900
228         IF(NELS.EQ.1)TYPE 905
229         IF(NELS.NE.1)TYPE 906
230         TYPE 910,TEQTI,WRATIO,BETAE,THETA
231         TYPE 930,VQ,VN,VB
232         TYPE 940,VQQVI,VNQVI,VBQVI
233         TYPE 950
234 C   EACH TIME THROUGH "OUTPUT" PRINT DATA
235    200  GAMOLH=AIMAG(S/SQRT(NEQMI))
236         ABZERO=CABS(ZERO)
237         TYPE 960,C,S,GAMOLH,PHASQ,EXDESQ,EDBSQ,ABZERO,NBMAX,NTRIAL
238    800  RETURN
239 C
240    900  FORMAT(///,1X,20HINHOMOGENEOUS PLASMA)
*
```

```
T241,290
241    905 FORMAT(1X,33HELECTROSTATIC DISPERSION RELATION)
242    906 FORMAT(1X,35HELECTROMAGNETIC DISPERSION RELATION)
243    910 FORMAT(//,2X,6HTE/TI=,F4.1,6X,8HWPE/WCE=,F6.3,2X,6HBETAE=,F6.3,
244       $      4X,6HTHETA=,F5.2)
245    930 FORMAT(2X,6HVO/VE=,F6.3,4X,6HVN/VE=,F6.3,4X,6HVB/VE=,F6.3)
246    940 FORMAT(2X,6HVO/VI=,F6.3,4X,6HVN/VI=,F6.3,4X,6HVB/VI=,F6.3)
247    950 FORMAT(//,4X,1HK,6X,5HOMEGA,3X,5HGAMMA,12X,6HEL2/E2,1X,7HEX2/ET2
248       $      1X,6HE2/B2,3X,4HZERO,4X,2HNB,2X,6HTRIALS,/)
249    960 FORMAT(1X,F7.3,F8.4,2X,1PE9.2,2X,E9.2,2X,
250       $      0PF4.2,1X,F4.2,1X,E7.2,1X,E8.1,2X,I3,2X,I3)
251        END
◆
```

```
T1,50
  1 C   IONS:  HOT, UNMAGNETIZED
  2 C   ELECTRONS:  HOT, MAGNETIZED
  3 C            DRIFTS PARALLEL AND PERPENDICULAR TO B FIELD
  4 C            TEMPERATURE ANISOTROPY
  5 C   WAVES:  OBLIQUE PROPAGATION
  6 C   REQUIRES SUBROUTINES:  PDF,FCFCN,EXBI,SEARCH,OUTPUT
  7 C
  8         COMMON INDC,C,ZERO,NTRIAL,NB,S,NELS
  9         COMMON/PARAM/ AE,BETAE,TEOTI,MEOMI,VPERP,VPAR,WRATIO,THETA
 10         COMMON/FIELDS/ PHASO,EXOESO,TNOTOT
 11         REAL MEOMI
 12         COMPLEX S,SSO,SNEW,ZERO,ZEROLD,TEST,IMAG
 13         COMPLEX ZARGI,ZI,DZI
 14         COMPLEX ZARGEP,ZEP,DZEP,ZARGEM,ZEM,DZEM
 15         COMPLEX ZARGED,ZED,DZED,DELTA,DELTAO,GAMMA
 16         COMPLEX RXX,RYY,RZZ,RXY,RYZ,RXZ
 17         COMPLEX FACT,FACTSO
 18         COMPLEX P1,P2,P1C,P2C
 19         DATA END/1.E-5/
 20         DATA STOP/1.E-5/,NBSTOP/50/
 21         IMAG=CMPLX(0.0,1.0)
 22 C
 23 C   PLASMA PARAMETERS
 24         NELS=0.0
 25         MEOMI=1.0/1836.0
 26         TEOTI=1.0
 27         BETAE=1.0
 28         WRATIO=68.0
 29         WRSO=WRATIO*WRATIO
 30         VEOVI=SQRT(TEOTI/MEOMI)
 31         AE=0.0
 32         VPAR=0.0
 33       5 TYPE 810
 34     810 FORMAT(/5X,10HENTER DATA/)
 35         READ(5,815)NELS
 36     815 FORMAT(I1)
 37         READ(5,820) VPERP,BETAE,THETA
 38     820 FORMAT(3F10.0)
 39         VPERP=VPERP/VEOVI
 40         COSIN=COSD(THETA)
 41         COSO=COSIN*COSIN
 42         SINE=SIND(THETA)
 43         SINSO=SINE*SINE
 44         TAN=SINE/COSIN
 45         TANSO=TAN*TAN
 46 C
 47 C   VARIABLE INITIALIZATION
 48        20 READ(5,830) CSTART,S,DC,NPRINT
 49     830 FORMAT(4F10.0,I2)
 50 C
```

```
T50,100
 50 C
 51 C  INCREMENT WAVE NUMBER BY DC WITH DO LOOP
 52       DO 600 INDC=1,NPRINT
 53       C=CSTART
 54       C=C+(INDC-1)*DC
 55       CSQ=C*C
 56 C
 57 C  INITIALIZE NUMBER OF ATTEMPTS TO SEARCH FOR ZERO
 58       NTRIAL=-1
 59 C
 60 C  CALCULATE ELEMENTS OF DISPERSION RELATION
 61    50 SSQ=S*S
 62       FACT=S-C*SINE*VPERP
 63       FACTSQ=FACT*FACT
 64       ZARGI=S*VEDVI/(1.414213*C)
 65       CALL PDF(ZARGI,ZI,DZI)
 66       RXX=-2*CSQ/BETAE+SSQ/WRSQ+MEOMI*ZARGI*ZI
 67       RYY=-2*CSQ*COSQ/BETAE+SSQ/WRSQ+2*ZARGI*ZARGI*SINSQ*MEOMI
 68      $     +MEOMI*ZARGI*ZI*COSQ*(1+2*ZARGI*ZARGI*TANSQ)
 69       RZZ=-2*CSQ*SINSQ/BETAE+SSQ/WRSQ+2*MEOMI*ZARGI*ZARGI*COSQ
 70      $     +MEOMI*ZARGI*ZI*SINSQ*(1+2*ZARGI*ZARGI/TANSQ)
 71       RYZ=2*CSQ*SINE*COSIN/BETAE+(2*MEOMI*ZARGI*ZARGI*SINE*COSIN)
 72      $      *(1+ZARGI*ZI*(1-1/(2*ZARGI*ZARGI)))
 73       NB=0
 74       BARG=CSQ*SINSQ*(1-AE)
 75       CALL EXBI(BARG,NB,EXB,IER)
 76       CALL EXBI(BARG,NB+1,EXBPL,IER)
 77       ZARGEO=(S-C*SINE*VPERP-C*COSIN*VPAR)/(1.414213*C*COSIN)
 78       CALL PDF(ZARGEO,ZEO,DZEO)
 79       DELTAO=-AE*DZEO-2*ZARGEO*ZEO
 80       RXX=RXX-BARG*DELTAO*(EXB-EXBPL)
 81       RYY=RYY+VPERP*VPERP*CSQ*SINSQ*(1-EXB*DELTAO/2)/BARG
 82       RZZ=RZZ+TANSQ*FACTSQ*(1-EXB*DELTAO/2)/BARG
 83       RXY=-IMAG*VPERP*C*SINE*(EXB-EXBPL)*DELTAO/2
 84       RXZ=-IMAG*TAN*FACT*(EXB-EXBPL)*DELTAO/2
 85       RYZ=RYZ+TAN*C*SINE*VPERP*FACT*(1-EXB*DELTAO/2)/BARG
 86       ZERO=RXX*(RYY*RZZ-RYZ*RYZ)+RXY*(RXY*PZZ-2*RXZ*RYZ)+RXZ*RXZ*RYY
 87       IF(NELS.EQ.1)ZERO=RYY*SINSQ+RZZ*COSQ+2.0*SINE*COSIN*RYZ
 88 C
 89 C  SUM OF TERMS WITH MODIFIED BESSEL FUNCTIONS
 90    60 ZEROLD=ZERO
 91       NB=NB+1
 92       NBSQ=NB*NB
 93       EXB=EXBPL
 94       CALL EXBI(BARG,NB+1,EXBPL,IER)
 95       ZARGEP=(S+NB-C*SINE*VPERP-C*COSIN*VPAR)/(1.414213*C*COSIN)
 96       ZARGEM=(S-NB-C*SINE*VPERP-C*COSIN*VPAR)/(1.414213*C*COSIN)
 97       CALL PDF(ZARGEP,ZEP,DZEP)
 98       CALL PDF(ZARGEM,ZEM,DZEM)
 99       GAMMA=-AE*(DZEP-DZEM)/2-ZARGEO*(ZEP-ZEM)
100       DELTA=-AE*(DZEP+DZEM)/2-ZARGEO*(ZEP+ZEM)
*
```

```
T101,150
101         RXX=RXX-DELTA*(EXB*(NBSQ/BARG+2*BARG-2*NB)-2*BARG*EXBPL)
102         RYY=RYY-(EXB*(CSQ*SINSQ*VPERP*VPERP+NBSQ)*DELTA
103        $-2*EXB*VPERP*NB*GAMMA*C*SINE)/BARG
104         RZZ=RZZ-TANSQ*EXB*(DELTA*(FACTSQ+NBSQ)+2*GAMMA*NB*FACT)/BARG
105         RXY=RXY+IMAG*(EXB*(1-NB/BARG)-EXBPL)*(NB*GAMMA-VPERP*
106        $C*SINE*DELTA)
107         RXZ=RXZ-IMAG*TAN*(EXB*(1-NB/BARG)-EXBPL)*(NB*GAMMA+FACT*DELTA)
108         RYZ=RYZ+TAN*EXB*(DELTA*(NBSQ+CSQ*SINSQ*VPERP*VPERP-C*SINE*S*VPERP)
109        $      +NB*GAMMA*(S-2*C*SINE*VPERP))/BARG
110         ZERO=RXX*(RYY*RZZ-RYZ*RYZ)+RXY*(RXY*RZZ-2*RXZ*RYZ)+RXZ*RXZ*RYY
111         IF(NELS.EQ.1)ZERO=RYY*SINSQ+RZZ*COSQ+2.0*SINE*COSIN*RYZ
112 C
113 C   IF ADDITION OF NEW BESSEL FUNCTION TERM TO "ZERO" RESULTS IN
114 C   ONLY A SMALL CHANGE OR IF NUMBER OF BESSEL FUNCTIONS USED EXCEEDS
115 C   NBSTOP STOP CALCULATION OF "ZERO"
116         IF(CABS(ZERO-ZEROLD).LE.CABS(ZERO)*END.AND.NB.GT.3)GO TO 100
117         IF(NB-NBSTOP) 60,100,100
118 C
119 C   SEARCH FOR ZEROS OF DISPERSION RELATION VIA "SEARCH"
120    100 CALL ZEARCH(S,ZERO,SNEW,NTRIAL)
121    400 FORMAT(/,2E9.3,5X,2E9.3,5X,2E9.3)
122 C
123 C   IF RELATIVE CHANGE IN S IS SMALL OUTPUT RESULTS
124 C   OR IF AIMAG S IS OF ORDER OF REAL S STOP SEARCHING
125         TEST=(SNEW-S)/S
126         S=SNEW
127         RTEST=REAL(TEST)
128         AITEST=AIMAG(TEST)
129         IF(ABS(RTEST).LT.STOP.AND.ABS(AITEST).LT.STOP) GO TO 500
130         IF(NTRIAL-15)50,500,500
131 C
132 C
133 C   BEFORE OUTPUTING RESULTS CALCULATE WAVE PHASE INFORMATION
134 C   PHASQ=SQUARE OF AMPLITUDE OF LONGITUDINAL E FIELD OVER TOTAL E FIELD
135 C   EXDESQ=SQUARE OF AMPLITUDE OF X E FIELD OVER TOTAL E FIELD
136 C   TNOTOT=RATIO OF ENERGY IN TRANSVERSE FIELDS TO ENERGY IN TOTAL FIELDS
137    500 P1=RXX*RYY+RXY*RXY
138         P1C=CONJG(P1)
139         P1SQ=REAL(P1*P1C)
140         P2=RXY*RXZ+RYZ*RXX
141         P2C=CONJG(P2)
142         P2SQ=REAL(P2*P2C)
143         P3SQ=REAL((RXY*RYZ-RYY*RXZ)*CONJG(RXY*RYZ-RYY*RXZ))
144         PSQ=P1SQ+P2SQ+P3SQ
145         S2=REAL(S*CONJG(S))
146         DUM1=SINSQ*P2SQ+COSQ*P1SQ-2.0*COSIN*SINE*REAL(P2C*P1)
147         DUM2=COSQ*P2SQ+SINSQ*P1SQ+P3SQ+2.0*COSIN*SINE*REAL(P2C*P1)
148         DUM3=1.0+S2*BETAE/(2.0*CSQ*WPSQ)
149         PHASQ=DUM1/PSQ
150         EXDESQ=P3SQ/DUM2
*
```

```
*151,201
151         TNOTOT=(DUM3+DUM2)/(DUM3+DUM2+DUM1+S2+BETAE/(2.0+CSQ+WRSQ))
152         CALL OUTPUT
153       600 CONTINUE
154       700 GO TO 5
155 C
156 C
157 C
158       900 STOP
159         END
160         SUBROUTINE OUTPUT
161         COMPLEX S,ZERO
162         REAL MEOMI
163         COMMON INDC,C,ZERO,NTRIAL,NR,S,NELS
164         COMMON/PARAM/ AE,BETAE,TEOTI,MEOMI,VPERP,VPAR,WRATIO,THETA
165         COMMON/FIELDS/ PHASO,EXDESO,TNOTOT
166 C
167 C
168 C FIRST TIME THROUGH "OUTPUT" PRINT HEADINGS
169         IF(INDC.NE.1) GO TO 200
170         VAOCSQ=MEOMI/(WRATIO+WRATIO)
171         VAOC=SQRT(VAOCSQ)
172         VEOVI=SQRT(TEOTI/MEOMI)
173         VOOVI=VPERP+VEOVI
174         TRATIO=1.0-AE
175 C
176         TYPE 900
177         IF(NELS.EQ.1)TYPE 905
178         IF(NELS.NE.1)TYPE 906
179         TYPE 910, TEOTI,VEOVI,VAOC,WRATIO
180         TYPE 916, BETAE,AE,TRATIO,THETA
181         TYPE 912, VPERP,VOOVI,VPAR
182         TYPE 920
183 C EACH TIME THROUGH "OUTPUT" TYPE DATA
184       200 GAMOLH=AIMAG(S/SQRT(MEOMI))
185         ABZERO=CABS(ZERO)
186         TYPE 922,C,S,GAMOLH,PHASO,EXDESO,TNOTOT,ABZERO,NR,NTRIAL
187       800 RETURN
188 C
189       900 FORMAT(///,1X,18HHOMOGENEOUS PLASMA)
190       905 FORMAT(1X,33HELECTROSTATIC DISPERSION RELATION)
191       906 FORMAT(1X,35HELECTROMAGNETIC DISPERSION RELATION)
192       910 FORMAT(/,3X,6HTE/TI=,F4.1,9X,6HVE/VI=,E9.2,4X,5HVA/C=,E9.2,7X,
193          +8HWPE/WCE=,F6.2)
194       912 FORMAT(3X,9HVPERP/VE=,F6.3,4X,9HVPERP/VI=,F6.3,4X,9HVPAR/VE=,F6.
195       916 FORMAT(3X,7HE BETA=,F5.2,7X,3HAE=,F4.1,12X,10HTPEP/TPAR=,F5.2,
196          + 6X,6HTHETA=,F5.2)
197       920 FORMAT(//,4X,1HW,6X,5HOMEGA,3X,5HGAMMA,12X,6HEL2/E2,1X,7HEX2/ET2
198          $     1X,6HTN/TOT,3X,4HZERO,4X,2HNB,2X,6HTRIALS,/)
199       922 FORMAT(1X,F7.3,F8.4,2X,1PE9.2,2X,E9.2,2X,
200          $     0PF4.2,1X,F4.2,1X,F4.2,3X,E8.1,3X,I3,3X,I3)
201         END
*
```

%FRSAPR FLOATING UNDERFLOW PC= 7345

%FRSAPR FLOATING UNDERFLOW PC= 7345

HOMOGENEOUS PLASMA
ELECTROMAGNETIC DISPERSION RELATION

TE/TI= 1.0 VE/VI= 0.43E+02 VA/C= 0.34E-03 WPE/WCE= 68.00
E BETA= 0.25 AE= 0.0 TPER/TPAR= 1.00 THETA=87.00
VPERP/VE= 0.093 VPERP/VI= 4.000 VPAR/VE= 0.000

K	OMEGA	GAMMA		EL2/E2	EX2/ET2	TN/TOT	ZERO	NB	TRIALS
0.300	0.0121	3.34E-03	1.43E-01	1.00	.30	1.00	0.3E-09	7	4
0.280	0.0116	3.49E-03	1.50E-01	1.00	.30	1.00	0.1E-08	6	4
0.260	0.0111	3.59E-03	1.54E-01	1.00	.31	1.00	0.8E-09	6	4
0.240	0.0106	3.62E-03	1.55E-01	1.00	.32	1.00	0.6E-09	6	4
0.220	0.0101	3.58E-03	1.53E-01	1.00	.33	1.00	0.5E-09	6	4
0.200	0.0096	3.48E-03	1.49E-01	1.00	.34	1.00	0.3E-09	6	4
0.180	0.0090	3.30E-03	1.41E-01	1.00	.35	1.00	0.3E-09	6	4
0.160	0.0085	3.05E-03	1.31E-01	1.00	.37	1.00	0.3E-09	6	4
0.140	0.0078	2.73E-03	1.17E-01	.99	.39	1.00	0.2E-09	5	4
0.120	0.0071	2.35E-03	1.01E-01	.99	.41	1.00	0.1E-09	5	4

ENTER DATA

1
4.0 0.25 8870
0.3 0.012 0.003 -0.02 10

HOMOGENEOUS PLASMA
ELECTROSTATIC DISPERSION RELATION

TE/TI= 1.0 VE/VI= 0.43E+02 VA/C= 0.34E-03 WPE/WCE= 68.00
E BETA= 0.25 AE= 0.0 TPER/TPAR= 1.00 THETA=87.00
VPERP/VE= 0.093 VPERP/VI= 4.000 VPAR/VE= 0.000

K	OMEGA	GAMMA		EL2/E2	EX2/ET2	TN/TOT	ZERO	NB	TRIALS
0.300	0.0101	-1.23E-03	-5.25E-02	1.00	.40	1.00	0.1E-08	6	15
0.280	0.0094	-1.10E-03	-4.73E-02	1.00	.43	1.00	0.1E-08	6	5
0.260	0.0086	-9.91E-04	-4.25E-02	1.00	.46	1.00	0.2E-08	5	5
0.240	0.0079	-8.85E-04	-3.79E-02	1.00	.49	1.00	0.3E-08	4	5
0.220	0.0072	-7.87E-04	-3.37E-02	1.00	.53	1.00	0.5E-08	6	5
0.200	0.0065	-6.96E-04	-2.98E-02	1.00	.57	1.00	0.8E-08	5	5
0.180	0.0058	-6.10E-04	-2.62E-02	1.00	.62	1.00	0.1E-07	4	5
0.160	0.0051	-5.30E-04	-2.27E-02	1.00	.67	1.00	0.1E-09	4	6
0.140	0.0045	-4.54E-04	-1.95E-02	1.00	.72	1.00	0.5E-10	5	6
0.120	0.0038	-3.82E-04	-1.64E-02	1.00	.78	1.00	0.7E-09	4	6

ENTER DATA

VIII. REFERENCES

Allan, W., and J.J. Sanderson, Temperature gradient driven ion acoustic instability, Plasma Phys., 16, 753-767 (1974).

Biskamp, D., Collisionless shock waves in plasmas, Nucl. Fusion, 13, 719-740 (1973).

Boyd, T.J.M., and J.J. Sanderson, Plasma Dynamics, Barnes and Noble, New York, 1969; Chapter 6.

Callen, J.D. and G.E. Guest, Electromagnetic effects on electrostatic modes in a magnetized plasma, Nucl. Fusion 13, 87-110 (1973).

Caponi, M.Z., and N.A. Krall, Anomalous heat conduction along field lines for turbulently heated plasmas, Phys. Fluids, 18, 699-709 (1975).

Cayton, T., private communication (1977).

Commisso, R.J., and H.R. Griem, Experimental study of the post-implosion phase of a theta pinch, Phys. Fluids, 20, 44-50 (1977).

Craig, A.D., S. Nakai, D.D.R. Summers, and J.W.M. Paul, Measurement of long-wavelength turbulence within a collisionless schook by scattering of radiation from a CO_2 laser, Phys. Rev. Lett., 32, 975-978 (1974).

Daughney, C.C., L.S. Holmes, and J.W.M. Paul, Measurement of spectrum of turbulence within a collsionless shock by collective scattering of light, Phys. Rev. Lett., 25, 497-499 (1970).

Davidson, R.C., and N.T. Gladd, Anomalous transport properties associated with the lower hybrid-drift instability, Phys. Fluids, 18, 1327-1335 (1975).

Davidson, R.C., N.T. Gladd, C.S. Wu, and J.D. Huba, Effects of finite plasma beta on the lower-hybrid-drift instability, Phys. Fluids, 20, 301-310 (1977).

Davidson, R.C., Vlasov equilibrium and nonlocal stability properties of an inhomogeneous plasma column, Phys. Fluids, 19, 1189-1202 (1976).

Detyna, E., and E.R. Wooding, Ultra-High frequency drift waves, Plasma Physics, 14, 97-101 (1972).

Detyna, E., and E.R. Wooding, High frequency electromagnetic drift waves, Plasma Phys., 17, 539-546 (1975).

Feldman, W.C., Solar wind heat transport in the vicinity of the earth's bow shock, J. Geophys. Res., 78, 3697-3713, (1973).

Feldman, W.C., J.R. Asbridge, S.J. Bame, and J.T. Gosling, Plasma and magnetic fields from the sun, to be published in the volume, The Physical Output of the Sun and Its Variation With Time, Proceedings of the International Symposium on Solar-Terrestial Physics, Boulder, CO, June 1977.

Forslund, D.W., R.L. Morse, and C.W. Nielson, Electron cyclotron drift instability, Phys. Rev. Lett., 25, 1266-1270 (1970).

Fowler, T.K., Thermodynamics of unstable plasmas, in Advances in Plasma Physics edited by A. Simon and W.B. Thompson, Wiley, New York, (1968).

Freidberg, J.P., and R.A. Gerwin, The lower hybrid drift instability at low drift velocities, Physics of Fluids, in press (1977).

Greenstadt, E.W., C.T. Russel, F.L. Scarf, V. Formisano, and M. Neugebauer, Structure of the quasi-perpendicular laminar bow shock, J. Geophys. Res.,80, 502-514 (1975).

Gary, S.P., and J.J. Sanderson, Longitudinal waves in a perpendicular collisionless plasma shock, I, J. Plasma Phys., 4, 739-751 (1970).

Gary, S.P., Longitudinal waves in a perpendicular collisionless plasma shock, II, J. Plasma Phys. 4, 753-760 (1970).

Gary, S.P., Longitudinal waves in a perpendicular collisionless plasma shock, III, J. Plasma Phys., 6, 561-566 (1971).

Gary, S.P., Longitudinal waves in a perpendicular collisionless plasma shock IV, J. Plasma Phys., 7, 417-425 (1972).

Gary, S.P., Long wavelength instability in a perpendicular shock, Plasma Physics, 15, 399-410 (1973).

Gladd, N.T., The lower hybrid dridt instability and the modified two stream instability in high density theta pinch experiments, Plasma Physics, 18, 27-40 (1976).

Hamasaki, S., R.C. Davidson, N.A. Krall, and P.C. Liewer, Stable sheath thickness in collisionless high-beta plasmas, Nucl. Fusion, 14, 27-33 (1974).

Huba, J.D., and C.S. Wu, Effects of a magnetic field gradient on the lower hybrid drift instability, 19, 988-994 (1976).

Keilhacker, M. and K.-H. Steuer, Time-resolved light-scattering measurements of the spectrum of turbulence within a high-β collisionless shock wave, Phys. Rev. Lett., 26, 694-697 (1971).

Krall, N.A., Drift Waves, in Vol. I Advances in Plasma Physics edited by A. Simon and W.B. Thompson, Wiley, New York, (1968).

Krall, N.A., and P.C. Liewer, Low-Frequency instabilities in magnetic pulses, 4, 2094-2103 (1971).

Krall, N.A. and J.B. McBride, Magnetic curvature and ion distribution function effects on lower hybrid drift instabilities, Science Applications Inc. report no. 76-618-LJ, (1976).

Krall, N.A. and A.W. Trivelpiece, Principles of Plasma Physics, McGraw-Hill, New York, 1973.

Lakhina, G.S., and A. Sen, Electromagnetic and ∇B-effects on the modified two stream instability, Nucl. Fusion, 15, 662-675 (1973).

Lampe, M., W.M. Manheimer, J.B. McBride, J.H. Orens, K. Papadopoulos, R. Shanny, and R.N. Sudan, Theory and simulation of the beam cyclotron instability, Phys. Fluids, 15, 662-675 (1972).

Lashmore-Davies, C.N., and T.J. Martin, Electrostatic instabilities driven by an electric current perpendicular to a magnetic field, Nucl. Fusion, 13, 193-203 (1973).

Lemons D.S., and S.P. Gary, Electromagnetic effects on the modified two-stream instability, J. Geophys. Res., 82, 2337-2342 (1977).

Lemons, D.S., and S.P. Gary, Current driven instabilities in a high beta, quasi-perpendicular shock, submitted to J. Geophys. Res., (1977B).

Liewer, P.C., and R.C. Davidson, Sheath Broadening by the lower-hybrid-drift instability in post-implosion theta pinches, Nucl. Fusion, 17, 85-100 (1977).

Manheimer, W.M. and J.P. Boris, Self-Consistent theory of a collisionless resistive shock, Phys. Rev. Lett., 659-662, 28, (1972).

Montgomery, M.D., J.R. Asbridge, and S.J. Bame, Vela 4 plasma observations near the earth's bow shock, J. Geophys. Res., 75, 1217-1231 (1970).

Morse, D.L., and E.W. Greenstadt, Thickness of magnetic structures associated with the earth's bow shock, 81, 1791-1793 (1976).

Muraoka K., E.L. Murray, J.W.M. Paul, and D.D.R. Summers, Anisotropy of turbulence in a collsionless shock, J. Plasma Phys., 10, 135-140 (1973).

McBride, J.B. and E. Ott, Electromagnetic and finite β_e effects on the modified two stream instability, Phys. Lett., 39A, 363-364 (1972).

McBride, J.B., E. Ott, J.B. Boris, and J.H. Orens, Theory and simulation of turbulent heating by the modified two-stream instability, J. Plasma Phys., 10, 135-140 (1973).

Paul, J.W.M., C.C. Daughney, and L.S. Holmes, Measurement of light scattered from density fluctuations within a collisionless shock, 223, 822-824 (1969).

Paul, J.W.M., and L.S. Holmes, M.J. Parkinson and J. Sheffield, Experimental observations on the structure of collisionless shock waves in a magnetized plasma, Nature, 208,133-135 (1965).

Priest, E.R., and J.J. Sanderson, Ion acoustic instability in collisionless shocks, 14, 951-958 (1972).

Rodriguez, P., and D.A. Gurnett, Electrostatic and electromagnetic turbulence associated with the earth's bow shock, J. Geophys. Res., 80, 19-31 (1975).

Rodriguez, P., and D.A. Gurnett, Correlation of bow shock plasma wave turbulelce with solar wind parameters, J. Geophys. Res., 81, 2871-2882 (1976).

Sanderson, J.J., Jump conditions across a collisionless, perpendicular shock, 9, 2327-2330 (1976).

Stix, T.H., The Theory of Plasma Waves, McGraw-Hill, New York, (1962).

Wong, H.V., Electrostatic electron-ion streaming instability, Phys. Fluids, 13, 757-760 (1970).

Wu, C.S., and R.W. Fredricks, Cyclotron drift instability in the bow shock, J. Geophys. Res., 77, 5585-5589 (1972).

X. VITA

Don Stephen Lemons was born in Oklahoma City, Oklahoma, on May 25, 1949. After attending public schools in Oklahoma and New Mexico he entered New Mexico State University in June of 1967. There his major field of study was physics. Upon graduating with a B.S. degree in June, 1972 he continued his study of physics at the College of William and Mary. Between terms of this university he spent three consecutive summers at Los Alamos Scientific Laboratory studying the application of theoretical plasma physics to space and laboratory plasmas. In August, 1977 he completed a dissertation titled "Cross Field Current Instabilities in a Vlasov Plasma" and submitted it in partial fulfillment of the requirements for the Ph.D. degree.